Process innovations for net-shaping of oxide ceramic composites and property enhancement by reinforcements

by

Pallagani Jeevankumar

Registration Number: 17PHPH20

A thesis submitted in partial fulfilmentfor the degree of

Doctor of Philosophy

in

Physics

Under the supervision of

Prof. V. Seshu Bai

&

Dr. A. Rajanikanth (co-supervisor)





School of Physics, University of Hyderabad Hyderabad – 500046, India May, 2024

To The condensed matter Community

Declaration

I, Pallagani Jeevankumar, hereby declare that this thesis entitled "Process innovations

for net-shaping of oxide ceramic composites and property enhancement by

reinforcements." submitted by me under the supervision of Prof. V. Seshu Bai and Dr.

Rajanikanth (co-supervisor), School of Physics, University of Hyderabad, Hyderabad is

a bonafied research work and also free from plagiarism. The work is original and has not

been submitted earlier as a whole or in part for the award of any degree/diploma to this

University or any other University / Institution.

Reg. No. 17PHPH20

Date: 18/05/2024

Place: Hyderabad

Certificate





This is to certify that the thesis entitled "Process innovations for net-shaping of oxide ceramic composites and property enhancement by reinforcements" bearing Reg. No. 17PHPH20, in fulfilment of the requirements for the award of Doctor of Philosophy in Physics is a bonafide work carried out by P. Jeevankumar under our supervision and guidance.

This thesis is free from plagiarism and has not been submitted earlier in part or in whole to this University or any other University/Institution for the award of any degree/diploma. Further, the student has the following publications before the submission of the thesis for adjudication.

Publications:

- 1. P. Jeevankumar, P. Rose, A. Rajanikanth, T. Rajasekharan, V. Seshu Bai, Netshaping of advanced ceramic composites by gelcasting into precision molds made by rapid-prototyping, Int. J. Appl. Ceram. Technol. 21, 664-674 (2024)
- 2. P.Jeevankumar, Poly Rose, Pawan Kumar Verma , Seshu Bai Vummethala, Rajasekharan Thankappan Pillai, Fabrication of $Ba_{0.5}\ Sr_{0.5}\ TiO_3$ components combining rapid prototyping with gelcasting using different gelling systems; Open Ceramics 17 (2024) 100512

Patent applied:

- 1. A Method for Fabricating a Component with Complex Geometry.
- 2. A Method Preparing Ceramic Components Comprising Alpha Alumina Platelets.

Further, the student has passed the following course towards the fulfilment of course work required for Ph.D.

S.No.	Course Code	Course Name	Credits	Result
1	PY801	Research Methodology	4	Pass
2	PY803	Advanced Experimental Techniques	4	Pass
3	PY851	Probes of Condensed Matter	4	Pass

V. Seshu Sai

Prof. V. Seshu Bai Supervisor School of Physics, University of Hyderabad, Hyderabad – 500046, India

Dr. V. Seshu Bai School of Physics University of Hyderabad Dr. A. Rajanikantl

Dr. A. Rajanikanth Co - Supervisor School of Physics, University of Hyderabad, Hyderabad – 500046, India

Dr. A. Rajani Kanth School of Physics University of Hyderabad Hyderabad-500 046, INDIA.

Dean

School of Physics,

University of Hyderabad, Hyderabad-500046, India

School of Physics University of Hyderabad HYDERABAD - 500 046

Acknowledgements

I deem it a proud privilege and pleasure in expressing my sincere gratitude to my thesis advisor, **Prof.**V. Seshu Bai School of Physics, University of Hyderabad, for her valuable guidance, support, encouragement and independence given to me during my research. She was always passionate and enthusiastic about her research projects, was very open to new ideas and showed me how exciting research can be. She has always been extremely generous with her time; knowledge and I was inspired by her dedication to science. Her careful planning coupled with a strong sense of duty, strictness and warmth of love had enabled me in the successful completion of this thesis.

I am deeply grateful to **Dr. A. Rajanikanth**, Assistant professor at the School of Physics, University of Hyderabad, my thesis co-supervisor, and a member of the Doctoral Committee, for his valuable guidance, support, and concern during my Ph.D. His insistence on excellence, discipline, and sincerity always influenced me towards new research ideas. His care, motivation, and kindness will be remembered forever.

I would like to thank **Prof. K.C. James Raju**, who has been there as my Doctoral Committee member, for his discussions and suggestions throughout my research work.

I am deeply grateful to **Dr. T. Rajasekharan**, for his invaluable scientific advice and insightful discussions, which have significantly contributed to the depth and quality of this thesis work. His expertise and guidance were helpful in shaping the direction of this study, and his generous sharing of knowledge has been an inspiration throughout this thesis work.

Further, I am grateful to the present Dean, School of Physics, Prof. K.C. James Raju and former Deans, Prof. V. Seshu Bai, Prof. Ashok Chatterjee and Prof. Bindu A. Bambah, for providing me with all the school level facilities.

I also thank all other faculty and the non-teaching staff of the School of Physics for their cooperation.

I thank University of Hyderabad for the financial assistance during my Ph.D. course also I acknowledge the Department of Science and Technology (DST), India for funding my research work and scholarship.

I thank Department of Science and Technology (DST/AMT) for funding the research project DST/TDT/AMT/2017/052/G. IoE –UoH for funding the trip to France to present my work at The XVIII Conference and Exhibition of the European Ceramic Society -2023 in Lyon, France.

I am grateful to the School of Engineering Sciences and Technology, UoH, for providing facilities for indentation studies and measurements of mechanical properties and thermal properties.

I am grateful to MSME-IIT, Hyderabad for images on the TEM facility and ASL and INSMART for collaborating in research work.

I would like to express my heartfelt gratitude to my fellow lab mates Mr. Pawan Kumar Verma, Poly Rose, Venkat, Akhil and Ms. Devaparana. Their camaraderie, unwavering support, and collaborative spirit have been invaluable throughout the course of this research. I am fortunate to have had the opportunity to work alongside such talented individuals. Their friendship and encouragement have made this journey not only academically rewarding but also personally fulfilling.

I am deeply grateful to my friends Supriya, Saineetha, Nagaraju, Venkata Ramaniah, Manga Babu, Anilkumar, Ajay, Navi gosh, Akum and Sridhar who have been a constant source of encouragement and understanding throughout the journey of completing this thesis. Their unwavering support, even during the most challenging times, has been a source of strength. I appreciate the laughter, camaraderie, and shared experiences that have enriched my life beyond the confines of academia.

I am grateful to my well-wishers, Dr. Sagar, Durgarao, Dr. Gautham and Dr. Raghunandan Ummethala for their inspiration and support.

I owe my gratitude to my family whose innumerable sacrifice, unconditional love and confidence have driven me this far.

Preamble

Ceramics find applications in several sectors due to their unique properties like high strength, hardness, resistance to oxidation at high temperatures, corrosion, erosion resistance, low density, chemical stability, and their relatively low cost [1,2].

Ceramic materials are classified as inorganic compounds. They have a crystalline structure, mainly composed of strong ionic or covalent bonds. These bonds formed when metals combine with oxygen, producing metal oxides such as alumina (Al₂O₃) and zirconia (ZrO₂). Ceramics include a broad spectrum of compounds such as borides, carbides, and nitrides, which offers a wide range of applications in various sectors.

Oxide, carbide, boride, and nitride ceramics have diverse applications. Oxide ceramics (like alumina and zirconia) are used for biomedical and high-temperature compatibility [3,4]. Carbide ceramics (such as silicon carbide and tungsten carbide) are valued for their hardness and wear resistance, ideal for cutting tools and armor applications [5,6]. Boride ceramics (like zirconium diboride and boron carbide) are known for their hardness and lightweight properties, suitable for armor and aerospace applications [7,8]. Nitride ceramics (such as silicon nitride and aluminum nitride) offer high-temperature stability, useful in gas turbines and electronics [9,10]. These ceramics are crucial for various technological advancements in demanding environments.

The inherent characteristics of ceramics, including high porosity, brittleness, and limited fracture toughness, pose challenges in their practical applications [11]. Additionally, machining processes for ceramics are often expensive due to their hardness and tendency to undergo fracture during shaping. To enhance the mechanical properties of ceramics, various methods such as reinforcements and process modifications have been explored [12]. Reinforcements involve incorporating secondary phase materials, such as particles, platelets, whiskers and fibres with suitable interfacial coating into the ceramic matrix to improve fracture toughness, wear resistance and other mechanical properties [13,14]. Process modifications encompass alterations in fabrication techniques, such as changing sintering conditions or introducing additives, to optimize microstructure and enhance mechanical performance [15]. These approaches aim to overcome the inherent brittleness and low fracture toughness of ceramics, thereby expanding their potential for various applications.

Traditionally, manufacturing complex shapes often involved significant material wastage and post-processing steps. Additive manufacturing allows for the fabrication of intricate near-net-shape parts with exceptional precision [16]. This minimizes material wastage and the need for extensive finishing, leading to a more efficient and generic process. Monolithic ceramics, while offering excellent high-temperature performance and chemical resistance, often exhibit drawbacks in mechanical properties

such as brittleness and low fracture toughness [17]. These characteristics limit their application in highstress environments where impact resistance and sustainability are essential. In contrast, ceramic matrix composites (CMCs) represent a significant advancement over monolithic ceramics due to their enhanced mechanical properties [18]. By incorporating fibres or particles as reinforcements into a ceramic matrix, CMCs can exhibit superior fracture toughness, tensile strength, and impact resistance compared to monolithic ceramics [19]. CMCs can withstand higher mechanical loads thus leading to increased demand in applications such as aerospace, automotive, and industrial manufacturing [20]. Conventional ceramic forming techniques use colloidal processing and consolidation in specially designed dies and are well established [21]. These techniques include die-casting, CIP-casting, and injection molding, each with its own merits and demerits [22]. Gelcasting and Rapid prototyping (RPT) offers a single-step solution for complex ceramic parts [23], but optimizing the process requires overcoming several problems. Selecting a suitable binder system is crucial [24]. Finding the optimal binder system and dispersant to get good solid loading of ceramic slurry and the resulting viscosity is another challenge. Higher solid loading produces a denser final part but can make filling the mold and removing air bubbles difficult. De-airing techniques like vacuum de-gassing become essential to eliminate these bubbles and ensure a uniform structure. Finally, the demolding process itself requires careful consideration. Mold design should facilitate easy release of the component to minimize the risk of cracking the fragile green body. 3D printing (additive manufacturing) offers a solution for fabricating intricate molds for near-net shaping of ceramics a major problem arises from the demolding process when using popular choices like Acrylonitrile butadiene styrene (ABS) and polylactic acid (PLA) filaments-based molds. and demolding process [25]. Traditional near-net shaping often relies on extended soaking times to dissolve the mold and release the fragile green ceramic part. This extended soaking time creates a potential threat. First, the mold removal solvents can slowly interact with the green body, causing unwanted interactions that can initiate defects in the final ceramic product [26]. Present work exploits the benefits of expanded polystyrene (EPS) and 3D-printed thin wall molds, by developing methods of eliminating the mold to green body interaction during the demolding process [27, 28].

The present work involves investigations on oxide ceramics derived from alumina and zirconia with a goal to develop methods for net shaping ceramic composites [29-31] with superior properties for high-performance in actual applications.

Chapter_1. Introduction and Motivation

This chapter briefly explains the importance of ceramics in general and gives an introduction to oxide ceramics and their applications. Reports in literature on the properties of oxide ceramics especially those derived from alumina and zirconia, with various reinforcements are reviewed. Present state of the art on net shaping of ceramics is narrated with a discussion on their merits and demerits.

The ceramic systems chosen for the present study are described, which include monolithic alumina, mixed oxides like barium strontium titanate with composition Ba_{0.5}Sr_{0.5}TiO₃ (BSTO), and composites of alumina and partially stabilized zirconia with 3 mol% yttria (3YPSZ), with an aim to develop methods of net shaping. Efficacy of reinforcements like alumina platelets and carbon short fibre to enhance mechanical properties of alumina and zirconia composites are explored, while enabling fabrication of complex shapes.

Chapter_2. Experimental and characterization techniques

This chapter presents all the experimental techniques used to characterize the powders, slurries, and the products. These include

X- ray diffraction studies to confirm the phase formation and to determine the lattice parameters.

Rheological characterization: Viscosity of the ceramic suspensions to identify suitable solid loading for casting.

CNC profile cutter and 3D printer for fabrication of expanded polystyrene (EPS) and ABS molds of requisite designs, respectively.

Temperature and humidity-controlled Ovens and various programmable high temperature furnaces for thermal processing at various stages of fabrication like drying, debindering (controlled removal of binders) and sintering in suitable atmospheres.

Archimedes technique for density measurement of ceramic compacts.

Vickers indentation method for hardness measurement.

Universal testing machine (UTM) for flexural strength and fracture toughness using 3-point bend test.

Dielectric spectrometer to measure Dielectric constant and dielectric loss of BSTO ceramics.

Optical microscopy, field emission scanning electron microscopy and transmission electron microscopy for microstructural and fractography analysis.

Chapter 3. Net shaping of ceramic composites

This chapter delves into the fabrication of ceramic components with complex geometries, combining the rapid prototyping and geleasting (RPGC) processes. In this process, suitable levels of solid loading are optimized measuring viscosity of the slurries. Various mold materials, mold removal processes, and precision mold fabrication techniques are explored. The focus lies on achieving near-net shaping of ceramic components with complex geometries. We examined two different mold materials. One of them is EPS molds, which were prepared by subtractive manufacturing technology, while the second one is ABS molds, prepared by additive manufacturing technology. These molds are designed to enable the fabrication of intricate shapes. Free-flowing ceramic suspensions were cast into the molds and were gelled. After mold removal, the green body was subjected to drying, debindering, and sintering to obtain dense ceramic components, whose physical, mechanical and microstructural features are studied. Initial experiments with alumina components served as a model system for process optimization, with insights applied to other material systems such as yttria stabilized zirconia (YSZ), barium strontium titanate (BSTO), and ZrB₂. In conclusion, this chapter provides a comprehensive exploration of near-net shaping of different ceramic components like alumina, BSTO and ZrB₂ with intricate geometries, offering valuable insights into optimizing ceramic component fabrication processes for various applications.

Chapter 4. Fabrication of alumina - α alumina composites

This chapter explores the fabrication process of alumina-alumina composites reinforced with second phase inclusions. In this work, we have chosen single-crystalline α-alumina platelets as a reinforcement. The experimental procedure involves preparing the α-alumina platelets with LaPO₄ as an interfacial coating. Composites with varying weight percentages (0, 1, 2, 3, 4, 5, 15, and 25%) of LaPO₄-coated platelets mixed with alumina powder and prepared from free-flowing composite slurries and cast into EPS molds, set, dried, debindered, and sintered to obtain final composites. Subsequently, the fabricated composites were characterized to evaluate density and mechanical properties such as hardness, flexural strength, and fracture toughness as per ASTM standards. Fractography analysis on fractured surfaces was conducted to gain an insight into the toughening mechanisms. Microscopy (FE-SEM) images reveal occurrence of crack deflection and crack bridging. A significant enhancement in fracture toughness was observed, increasing from 3 to 5.4 MPa√m. Alumina reinforced with α-alumina platelets (1 to 5wt%) showed enhancement in fracture toughness, compared to monolithic alumina. In conclusion, this chapter presents a systematic approach to fabricate and characterize aluminaalumina composites reinforced with LaPO₄-coated α-alumina platelets. These platelets were uniformly dispersed within the alumina matrix, resulting in significant enhancement in fracture toughness while enabling fabrication of complex shapes by combining the RPGC process (27). The preparation of

composites with varying reinforcement concentrations and subsequent evaluation of their physical and mechanical properties are discussed. Fractography analysis provides valuable insights into toughening mechanisms in the present composites.

Chapter 5. Fabrication of $3YPSZ - \alpha$ alumina composites

This chapter details the fabrication process of partially stabilized zirconia (3YPSZ) - alumina composites reinforced with nano-sized α -alumina platelets coated with LaPO₄, with an aim to enhance mechanical properties. Utilizing a combination of geleasting and rapid prototyping techniques, the composites were prepared with varying the LaPO₄-coated platelet content (0, 1, 5, 10, 15, and 25 wt%). Characterization of the composites includes density, hardness, flexural strength, and fracture toughness measurements, followed by fractography analysis to evaluate toughening mechanisms. X-ray diffraction (XRD) studies are carried out before and after stress application to determine if any phase transformations contribute to the toughening process. The fabrication process ensures the uniform distribution of reinforcement throughout the matrix. Fractography analysis identified features like crack deflection and crack bridging by platelet reinforcements within the matrix, that contribute to fracture toughness. A remarkable increase by 70 % in fracture toughness from 5 MPa \sqrt{m} is observed in YSZ reinforced with α -alumina platelets (x = 5 to 15 wt.%). This investigation reveals a significant increase in fracture toughness, that offers potential applications in biomedical and high-temperature sectors. PSZ exhibits good stability, but moisture can promote phase transformation at high temperatures.

Chapter 6. Fabrication of 3YPSZ – short carbon fibre composites

This chapter outlines the fabrication process of partially stabilized zirconia (3YPSZ) – short carbon fibre composites reinforced with lanthanum phosphate (LaPO₄)-coated fibres, aimed at enhancement of mechanical properties. LaPO₄ gel was prepared using a modified sol-gel process and coated onto short carbon fibres, which were then uniformly mixed with PSZ powder to prepare the composite suspensions. After casting into EPS molds and followed by gelling, drying, debindering, and sintering processes, the composites were characterized for density, hardness, flexural strength, and fracture toughness. Flexural strength and fracture toughness evaluations determined load-bearing capacity and resistance to crack propagation. Fractography analysis on fracture surfaces aimed at evaluating toughening mechanisms; fibre pullout was observed to be a prominent mechanism through microstructural examination. 3YPSZ – short carbon fibre (5 wt.%) composites exhibited 80 % increase in fracture toughness, which is a significant enhancement over 5 MPa√m of monolithic 3YPSZ [17].

Chapter 7. Summary and conclusions

The RPGC process has been demonstrated to be capable of yielding remarkable advancements in fabrication of complex-shaped ceramics products, simultaneously allowing for second phase additions as reinforcements to achieve high fracture toughness. Through innovative strategies, such as utilizing EPS and thin-walled ABS molds, the process has overcome challenges associated with mold removal, while ensuring quick and efficient procedures to obtain dense compacts.

Achieving uniform distribution of lanthanum phosphate-coated platelets into the matrix has led to significant improvements in fracture toughness. For instance, in alumina- α alumina composites, fracture toughness increased from 3 to over 5.4 MPa \sqrt{m} at the optimum α alumina content. Similarly, in 3YPSZ reinforced with α - alumina platelets, fracture toughness improved from 5 to more than 8.5 MPa \sqrt{m} . 3YPSZ composites with short carbon fibre reinforcement (5 wt.%) exhibit fracture toughness of 9.1 MPa \sqrt{m} .

Thus, successful net-shaping of oxide composites, with remarkable improvement in their properties, is achieved with RPGC process.

CONTENTS

Chapter I Introduction

Chapter II Experimental & Characterization techniques

Chapter III Net shaping of ceramic components

Chapter IV Alumina - α alumina platelet composites

Chapter V $3YPSZ - \alpha$ alumina platelet composites

Chapter VI Yttria stabilized zirconia (3Y-PSZ) composites

with short carbon fibre reinforcement

Chapter VII Summary and conclusions

Process innovations for net-shaping of oxide ceramic composites and property enhancement by reinforcements

Chapter I

Introduction

1.1 Ceramics and ceramic matrix composites (CMC)

Ceramics are utilized in various sectors because of their distinguishable characteristics such as exceptional strength, hardness, resistance to oxidation at elevated temperatures, corrosion and erosion resistance, low density, chemical stability, and comparatively affordable cost [1,2]. Ceramic materials are classified as inorganic compounds. They have a crystalline structure, mainly composed of strong ionic or covalent bonds. These bonds are formed when metals combine with oxygen, producing metal oxides such as alumina (Al₂O₃) and zirconia (ZrO₂) [3,4]. Ceramics include a broad spectrum of compounds such as borides, carbides, and nitrides, which offer a wide range of applications in various sectors [5,6,7]. Advanced ceramics are important in various industries, including energy, transportation, communication, military, and medical. Alumina, zirconia, carbides, and nitrides are ceramic materials most commonly used [3-7]. They can be customised them with functional characteristics that are suitable for a wide range of applications, including biomedical, mechanical, optical, electronic, electrical and magnetic fields. Figure 1.1 presents a categorization of advanced ceramics according to their uses and purposes. It provides information on the specific characteristics that these ceramics should possess and includes examples for each category.

Advanced ceramics can be classified into:

- 1) Oxide ceramics such as alumina and zirconia
- 2) Non-oxide ceramics including carbides, borides, nitrides and silicates
- 3) Composites which are a combination of oxides and non-oxides.

Advanced ceramic materials fall into four composition-based groups such as oxide, carbide, boride, and nitride. Ceramics made of oxides, such as zirconia and alumina, are utilized for their compatibility at high temperatures and biomedical applications [3,4]. Carbide ceramics, which include tungsten carbide and silicon carbide, are much valued for their exceptional hardness and remarkable resistance to wear. These characteristics make them an excellent choice for applications involving cutting tools and armor [8,9]. Boride ceramics, such as zirconium diboride and boron carbide, are well-known for

their hardness and lightweight qualities, making them excellent for applications in the aerospace and armor industries [10,11]. Nitride ceramics, which include silicon nitride and aluminium nitride, are advantageous in gas turbines and electronics due to their ability to maintain their stability at high temperatures [12,13]. Ceramic materials like the above are investigated essential for a wide range of technological improvements in conditions that are demanding.

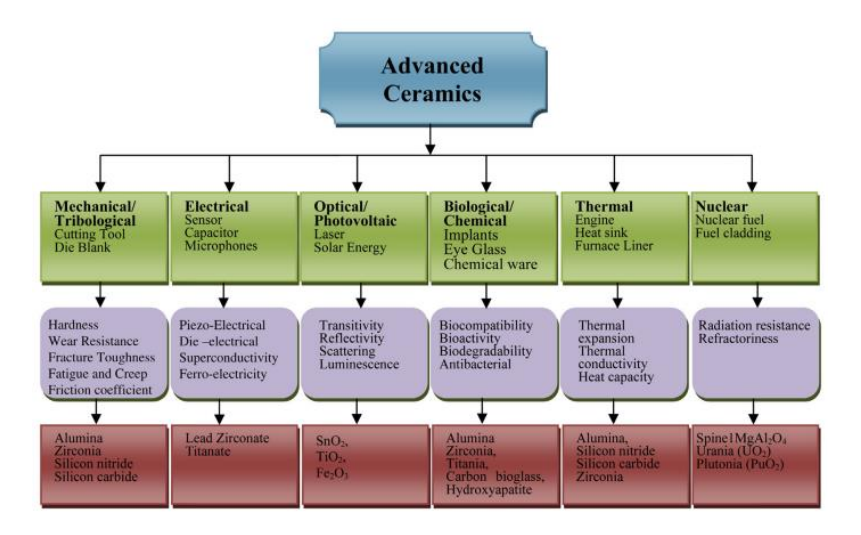


Fig.1.1. Shows the classification of advanced ceramics and their applications [7].

The ceramic business has become one of the most sought after and competitive sectors in the worldwide market. They are used in various sectors and industries, such as biomedical, energy storage, aerospace applications, automobiles (with spark plugs and ceramic engine components), and telecommunications infrastructure [14]. Ceramics are essential components in space shuttles, and aircraft (particularly in nose cones, jet vanes). watches (using quartz tuning forks for time keeping), snow skis (with piezoelectric ceramics that respond to applied voltage).

Monolithic ceramics, while offering excellent high-temperature performance and chemical resistance, often exhibit drawbacks in mechanical properties such as brittleness and low fracture toughness [15]. These characteristics limit their application in high-stress environments where impact resistance and sustainability are essential. In contrast, ceramic matrix composites (CMCs) represent a significant advancement over monolithic ceramics due to their enhanced mechanical properties [16].

Ceramic matrix composites

Ceramic Matrix Composite (CMC) is a composite material composed of a ceramic matrix and a dispersed phase containing ceramic particles, platelets, Whiskers and short fibers, and continuous fibers such as oxides or carbides [17-20]. Ceramic Matrix Composites are specifically engineered to enhance the mechanical properties like toughness and wear of monolithic ceramics, which are mainly constrained due to their brittleness.

Particulates reinforced ceramic matrix composites

Utilizing particles as a reinforcement in ceramics is a highly efficient method for enhancing fracture toughness. Under typical atmospheric conditions, ceramic matrix fractures mainly occur by cleavage [21]. Reinforced particles enhance fracture toughness by connecting the two sides of the crack and forming bridge along the fracture. When a crack encounters a cluster of densely packed particles, it initially infiltrates the space between them. This approach necessitates an extra force to create cracks, leading to an uneven dispersion of stress intensity along the propagation boundary [22]. This mechanism of arresting crack is called as trapping effect. Once the crack reaches a certain penetration depth, it can overcome the trapping effect through total particle-matrix bonding. Subsequently, the reinforced particle remains in place to build a bridge across the fracture side. Reinforced particles fracture when the applied stress is beyond the critical threshold.

Platelets reinforced ceramic matrix composites

Using platelets as reinforcement in ceramic matrix composites (CMCs) significantly improves mechanical characteristics [19,23]. The flat and broad shape of platelets efficiently obstructs the spreading of cracks within the ceramic matrix, leading to enhanced strength and toughness of the composite material. Moreover, platelets have a role in enhancing hardness and enhancing the composite's wear resistance [24]. Their arrangement and dispersion within the matrix improve the material's overall rigidity and dimensional stability. Specifically, platelet materials like alumina, silicon carbide and graphene or boron nitride can increase thermal conductivity, which is essential for applications needing effective heat dissipation [25]. Moreover, the thin and lightweight characteristics of platelets enhance the strength of the composite material without substantially adding to its overall weight, which is essential in situations where weight is a critical factor [26]. Platelets are significant in enhancing fracture toughness and averting catastrophic failure.

Whiskers reinforced ceramic matrix composites

Whisker-reinforced ceramic matrix composites are a versatile form of CMCs that can be used in several fields. Structural applications see substantial enhancements in their mechanical properties compared to monolithic ceramic matrix materials. Adding whiskers to a ceramic matrix enhances its strength, fracture toughness, thermal conductivity, thermal shock resistance, and resistance to high-temperature creep [27, 28]. Whiskers have a diameter that varies between 0.1 and 5 µm, with an aspect

ratio of 1 to 10. Their shape is needle-like or sharp pointed, with a discontinuous structure and a single crystal-like form. These materials differ from chopped or short fibrous materials which are polycrystalline or amorphous. Silicon carbide whiskers are widely used as a reinforcing component in commercial applications of ceramic matrices. CMCs consist of whiskers made from materials such as TiC, TiN, Al₂O₃, mullite, Si₃N₄, B₄C, and hollandite (Ba_{1.23} Al_{2.46} Ti_{5.54} O₁₆) [29,30]. The interaction between cracks and whiskers causes crack bridging and whisker pullout, as demonstrated by the substantial toughening behavior in CMCs reinforced with whiskers. The debonding along the crack deflection is commonly associated with the matrix-whisker interface [31].

Short fiber reinforced composites

Short-fiber composites, commonly called discontinuous composites, are produced using traditional ceramic methods. These composites consist of a ceramic matrix, such as alumina, zirconia, zirconium diboride or silicon carbide reinforced with chopped fibres made of crabon, alumina, zirconia, silicon carbide, titanium boride, aluminum nitride, and other ceramic fibres [20,32-34]. Most CMCs are strengthened with carbon, alumina and silicon carbide fibers because of their exceptional strength and stiffness (modulus of elasticity). Adding short-fiber to matrix, improves its toughness and resistance to fracture propagation by contributing to toughening mechanisms [35].

Long fiber reinforced composites

Long-fiber composites are strengthened by either long monofilament or long multifilament fibres. The most effective method of strengthening is achieved by using a dispersed phase in the form of continuous monofilament fibres [36]. These fibres are created by depositing silicon carbide onto a substrate consisting of either tungsten (W) or carbon (C) fibres using chemical vapour deposition (CVD) [37]. Monofilament fibres enhance the interfacial interaction with the matrix material, resulting in increased toughness. The matrix material options for long-fiber (continuous fibre) composite include silicon carbide, alumina (alumina-silica), zirconia, zirconium diboride or carbon [38].

- Silicon carbide matrix: Composites are produced by the process of chemical vapour
 infiltration or liquid phase infiltration of SiC matrix into carbon or silicon carbide fiber [39].
 Silicon carbide matrix composites are utilised in the production of combustion liners for gas
 turbine engines, hot gas re-circulating fans, heat exchangers, rocket propulsion components,
 filters for hot liquids, gas-fired burner parts, furnace pipe hangers, and immersion burner tubes.
- Alumina and alumina-silica (mullite) matrix composites: Composites are created via the sol-gel technique, direct metal oxidation, or chemical bonding. Alumina and alumina-silica

(mullite) matrix composites are utilised in the production of heat exchangers, filters for hot liquids, thermo-photovoltaic burners, burner stabilizers and combustion liners for gas turbine engines [40].

• Carbon-Carbon composites are produced by the process of chemical vapour infiltration or liquid phase infiltration, when a matrix material is infused into a preform made from carbon fibres. Carbon-Carbon Composites are utilised in the production of high-performance brake systems, refractory components, hot-pressed dies, heating elements, and turbojet engine components [41].

Table 1.1- Most commonly used fibre and their properties

Fibre type	Properties		
Carbon	Excellent fatigue and tensile strength, color is a major		
	limitation		
Glass	Good aesthetic properties, adequate mechanical and physical		
	properties		
Hydroxyapatite	Biocompatible, questionable fatigue properties		
Alumina	Rigid, High strength, Corrosion resistance, oxidative		
	resistance, Biomedical compatibility		
Zirconia	Higher fracture toughness, good thermal shock resistance,		
	lower density, Biomedical compatibility		
Silicon Carbide	High stiffness, high tensile strength, low weight, high chemical		
	resistance		

1.2 Shape forming of ceramics

Traditionally, ceramic fabrication employs three main processes, beginning with raw materials ground into a fine powder. These processes, are independent of the final purpose of the ceramic and focus on shaping the powder into the desired form.

- 1. Dry shaping technologies.
- 2. Wet shaping or suspension-based technologies.
- 3. Plastic shaping technologies.

The three traditional main routes are further divided by different shaping methods, as illustrated in Figure 1.2.

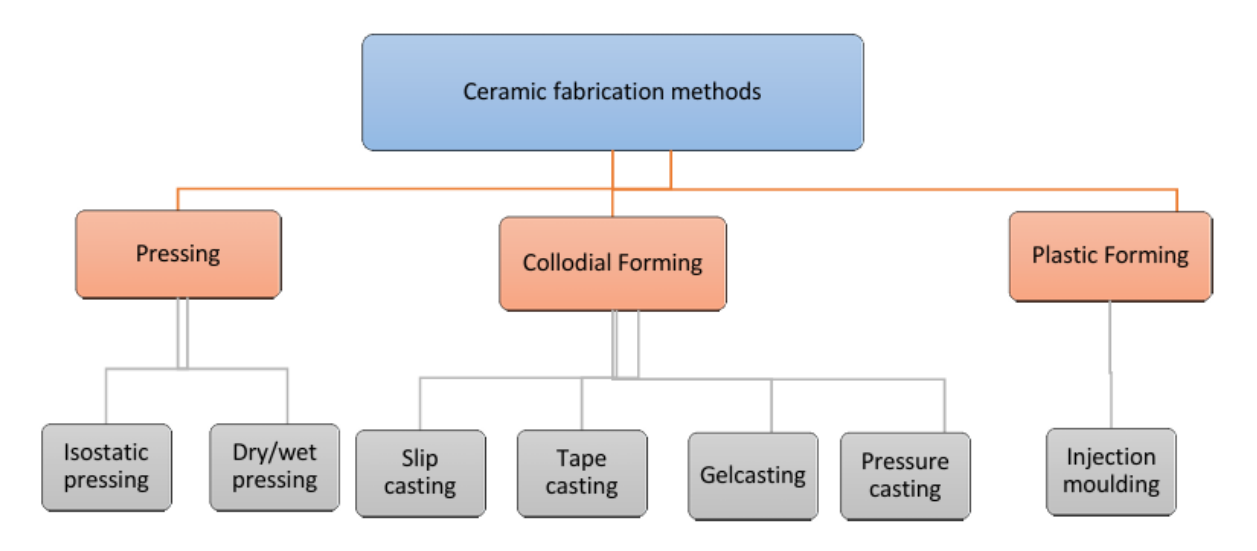


Fig. 1.2. Shape forming techniques of ceramics [42].

Several wet shaping techniques have been employed for the consolidation of ceramic powders. Before shaping, ceramic powders are combined with various processing additives such as binders, dispersants, deflocculants, plasticizers and water. After the powder preparation stage, the next step is the shape forming stage. Various techniques are used to shape ceramic powders into the desired form as discussed in Fig.1.2. Some relevant methods are discussed below -

- Tape casting
- Slip Casting
- Pressure casting
- Freeze casting
- Direct coagulation casting (DCC)
- Extrusion
- Gelcasting

Tape casting:

Tape casting is a technique employed in the production of thin sections, substrates and films made of ceramic or metallic materials. The process is applying a slurry or paste of the substance onto a flexible carrier film, typically made of plastic tape, in order to create a thin layer [43]. The slurry generally comprises the necessary material in powdered form, accompanied by binders, solvents, and additional additives for regulating viscosity and other characteristics. Using the Doctor-blade method, slot dies, or curtain coating technology, a watery or nonaqueous slurry is put on a tape during tape casting. Because they are made with organic binders and plasticizing chemicals, ceramic limb green tapes can be ruffled, coiled, or wrinkled. Using layered technology, green tapes are punched and glued together to make three-dimensional parts. Laminate Object Manufacturing (LOM) [44], a one-of-a-kind process for additive manufacturing, can use green ceramic tapes as half-products.

Slip casting and pressure slip casting:

Slip casting is a historic method used to shape ceramics and porcelain goods. This wet-shaping process begins with aqueous slurries injected into a plaster mold. The gypsum's porosity allows water to drain out through the capillaries of the mold [45]. Powder particles cannot enter pore channels, resulting in a solid layer on the mold surface. After increasing the layer thickness, the residual slurry is removed from the mold. After a short drying time, the mold is opened and the green components removed for further drying and sintering. Porous polymers can replace plaster molds for longer mold life for vacuum applications [46]. Wet-shaping technique allows for the production of intricately designed pieces. However, a single plaster mold can only produce a limited number of pieces. Pressure slip casting is commonly used for creating tableware, sanitary goods, and ceramic crucibles.

Freeze casting

Freeze-casting is a simple and cost-effective technique to create ceramic objects from powder particles. It's environmentally friendly and works with many materials [47]. However, understanding how different factors affect the final shape can take time and effort. The process has four main steps: Make a ceramic suspension in water or another solvent. Second, shape and solidify the suspension. Third, remove the solvent by sublimation [48]. Finally, sinter the resulting material, strengthening the ceramic walls while keeping the pore structure intact.

Direct coagulation casting (DCC)

The ceramics industry uses the Direct Coagulation Casting (DCC) process to fabricate intricate ceramic components with exceptional accuracy. Ceramic powder and a liquid binder, typically water or an organic solvent, combine to create the ceramic slurry which is cast into mold of required shape of component [49].

During the settling of the slurry in the mold, the binder undergoes coagulation, resulting in its solidification and forming a green body that maintains the mold's shape. It is called "direct coagulation casting" because the solidification process occurs immediately within the mold [50].

After the green body forms, it is delicately removed from the mold and it undergoes additional processing stages, such as drying and sintering. The DCC technique provides various benefits, such as its capability to create complex shapes with precise dimensions and the possibility of large-scale manufacturing. Moreover, it can be utilized with diverse ceramic materials, rendering it a highly adaptable choice for many applications across industries such as aerospace, automotive, and electronics.

Extrusion:

Extrusion can produce tubes, honeycomb or multichannel structures. It is one of the primary thermoplastic shaping procedures for ceramics, alongside injection molding. To shape the powders, they must first be combined with a thermoplastic organic binder. The mixture of powder and binder is termed feedstock [51]. This term refers to thermoplastic or plastic blends in powder processing, as well as ceramic additive manufacturing technologies [52]. Advanced ceramic materials require a feedstock as they are synthesized in high purity, unlike traditional ceramics that contain clay minerals. Feedstock preparation involves high shear forces to break down agglomerates and coat powder particles with a binder layer. Feedstock is prepared by mixer blender. Methylcellulose is commonly used as a binder in cold plastic extrusion feedstocks [53].

Extrusion is done using piston or vacuum screw extruders with a mouthpiece to control the final shape of the product [54]. The abrasive ceramic particles in the feedstocks require a costly hard metal mouthpiece. Extrusion is an effective way to make filtration membranes, catalyst supports, tubes, and diesel soot filters.

Gelcasting:

Ogbemi O. Omatete and his team developed gelcasting, a ceramic shape-forming technique, to fabricate ceramic components with uniform and high-quality ceramics in 1991, at Oak Ridge National Laboratory [55]. The procedure starts with creating a suspension using a ceramic powder and water-soluble organic material such as a monomer and a crosslinker. The ceramic powder is mixed with a polymer solution, and a suitable dispersant, and is allowed to tumble. Prepared slurry was then cast into a mold. An initiator and catalyst polymerize the slurry. The process involves removing the gelled part, followed by drying, binder removal, and sintering. Finally, thermal processes yield dense ceramic components [56-58]. The gelcasting method has been successfully applied to various ceramic powder systems, including alumina, zirconia, zirconium dibrode, tugstesten carbide, silicon carbide, boron carbide, aluminum nitride and silicon nitride [59]. Its suitability encompasses the production of large parts with simple shapes, such as toroidal rings, as well as small parts with intricate shapes.

1.3 Literature on different shape forming techniques of ceramics

M.V. Silva et al. [60] fabricated armor plates using alumina as the primary material, with different percentages of Al₂O₃ (92%, 96%, and 99%). The plates, with a thickness of 10mm, were fabricated by uniaxial pressing at a pressure of 110MPa and sintering at a temperature of 1600°C for 6 hours. Following the sintering process, evaluations were performed to measure the relative density,

Vickers hardness, and four-point flexural strength. The porosity level influenced the strength values, which varied between 210 and 300 MPa.

Sindi Sithembiso Ndinisa et al. [61] developed alumina ceramic components by combining gelcasting and 3D printing molds, they could create intricate ceramic parts cost-effectively. The team used 3D-printed ABS filament molds, which allowed for easy demolding through acetone dissolution. Their study focused on the impact of suspension's solid loading on the properties and microstructure of alumina parts. The ceramic components displayed impressive characteristics after sintering for 3 hours in the air. They achieved high densities of up to 99.0%, hardness measuring 18GPa, flexural strength of 374MPa, and fracture toughness of 3.8MPa \sqrt{m} . These results were consistent with previously published values, demonstrating the effectiveness of their manufacturing approach.

Murat Bengisu et al. [62] introduced a novel geleasting system utilizing a 1 wt% chitosan solution in diluted acetic acid, reacting with glutaraldehyde. This system achieved a 50 vol% loading of alumina slurry with optimized conditions. This system's key advantages include biopolymer chitosan, allowing for air drying of green parts and geleasting at ambient temperature.

M. Schumacher et al. [63] conducted a study on developing bone substitute materials using rapid prototyping (RPT) techniques. Their main focus was developing ceramic scaffolds with interconnected pores made from calcium phosphate ceramics such as hydroxyapatite and tricalcium phosphate. They utilized a negative-mold RPT technique to create scaffolds featuring a range of pore patterns, including round and square cross-sections and perpendicular and inclined orientations. The observed patterns led to macro porosity values ranging from 26.0% to 71.9% and pore diameters around $340~\mu m$. The compressive strength of the scaffolds varied between 1.3 to 27.6 MPa and was mainly affected by the phase composition and macro porosity.

T. Rajasekharan et al. [64] introduced a technique that combines rapid prototyping (RPT) and gelcasting to fabricate complex shapes of alumina components. At first, they utilized RPT to construct a mold directly from CAD files, employing layer by layer printing. Unlike conventional RPT methods that use lost-mold techniques, they developed a polymer mold that can accommodate larger samples, facilitate easy demolding, and fosters the formation of more intricate details in the component. The ABS polymer was used to create these highly effective molds. Then free-flowing water-based alumina slurry was prepared to achieve the desired solid loading and viscosity and was poured into the mold. After the slurry solidified, the mold was carefully removed and the green component was extracted which then went through drying, debindering and sintering processes. This approach presents a

potential method for creating intricately shaped alumina components with accuracy and uniformity, integrating the benefits of RPT and gelcasting techniques.

Xiaogang Xu, et al., [65] methyl cellulose (MC) as the gelation agent in the gel-casting process of γ -LiAlO₂. This choice was made because MC can create strong gels when heated. The researchers examined the thermal gelation characteristics of the MC solution by evaluating its apparent viscosity as it underwent temperature changes. Their study investigated how the concentration of MC solution and the amount of solid loading affect the rheological properties of γ -LiAlO₂ slurries. It was noted that all slurries had shear-thinning behavior, which is beneficial for the casting process.

Jung-Soo Ha et al., [66] conducted gelcasting experiments with Al₂O₃ in various atmospheric conditions: air, vacuum (38 torr), and N₂. They studied how the atmosphere affected the process. They discovered that atmospheres with oxygen, such as air and low vacuum (38 torr), didn't work well and that gelcasting in N₂ atmosphere reduced the problems like the bodies flaking off.

Qing Yao et al. [67] successfully used environmentally friendly gelcasting to produce transparent yttrium alumina garnet (YAG) ceramic. They used a water-soluble copolymer, isobam, as a dispersion and gelling agent. Their work methodically examined the rheological properties of slurries with different levels of solid loading and isobam concentrations. The slurry composition that yielded the best results consisted of 0.5 wt.% isobam and 68 wt.% solid loading. This composition had a low viscosity and excellent stability, which led to greater uniformity of the green body and enhanced optical quality of the transparent ceramics.

Jie Xu et al., [68] investigated a new, environmentally friendly gelcasting technology for alumina suspensions using curdlan as a gelling agent. The researchers examined curdlan suspensions' rheological and gelling properties throughout a temperature range of 10–85°C, observed changes during the heating and cooling processes. Their study also investigated the impact of curdlan concentration and solid loading on the alumina suspension's rheological characteristics and gelling behaviour. They successfully fabricated complex-shaped green bodies with a compressive strength of approximately 3.7 MPa.

1.4 Properties of ceramics and ceramic composites

Advanced ceramics made of oxides, such as alumina and zirconia, are utilized for their compatibility with high temperatures and biomedical applications [3,4]. A advanced ceramic materials such as silicon nitride and silicon carbide demonstrate high hardness, wear resistance, and thermal shock

resistance, making them suitable for demanding applications in aerospace, automotive, and military sectors [69,70].

Zirconium diboride has superior properties owing to their ability to maintain strength and toughness at elevated temperatures, making them ideal for use in high-temperature environments such as gas turbines, furnaces, and nuclear reactors [71,72].

Furthermore, advanced ceramic materials used in emerging electronics and energy storage sectors. For instance, fuel cells and lithium-ion batteries use ceramic materials like yttria-stabilized zirconia as solid electrolytes because of their high ionic conductivity and stability [73].

It is generally understood that ceramic matrix composites, are important materials for applications requiring high mechanical and thermal performance capabilities. Numerous characteristics that distinguish ceramics from other materials result from the ionic and covalent bonds between its constituents. Ceramics are inorganic, non-metallic, polycrystalline materials and can be natural or synthetic. CMCs have a wide variety of choices. The classification is often established based on the composition of the matrix and the type of reinforcement employed. C/SiC is a ceramic matrix composite composed of carbon fibres and a matrix composed of silicon carbide. Ceramic matrix composites are broadly categorized as oxide and non-oxide composites, in addition to the previously described categories of matrices and fiber materials. The primary categories of Ceramic Matrix Composites include C/C, C/SiC, SiC/SiC, and Ox/Ox, with Ox being one of the oxide elements [74]. Ceramic matrix composites reinforced with fibers like carbon or silicon carbide are also light and can withstand high temperatures. These composites are a good choice for brake systems, rocket nozzles, and airplane engines [75].

The extremely refractory transitional metal carbides and borides were chosen because they could withstand severe heating profiles in corrosive environments and heavy and variable mechanical loads. The low fracture toughness of UHTCs limits their use as single-phase monolithic structural components. UHTCMCs are mostly examined for aerospace applications, although their ability to withstand extreme environments makes them potential candidates for various high-temperature structural applications [76]. Material for fuel rod cladding, neutron absorbers, fusion first walls, and tokamak diverters in the nuclear energy industry is expected to have excellent neutronic properties. Reinforcement type affects mechanical properties, particularly fracture toughness and processing [77].

1.5 Fabrication of oxide and non-oxide ceramics

Ceramics can be mainly divided into two categories: oxide ceramics and non-oxide ceramics. The oxide ceramics are inorganic compounds of metals or metalloids with oxygen, such as alumina (Al₂O₃), zirconia (ZrO₂), silica (SiO₂), titania (TiO₂) etc. Non-oxide ceramics are compounds that are carbides, borides, nitrides and silicides of another element. Examples of these are tungsten carbide (WC), zirconium diboride (ZrB₂), boron carbide(B₄C), boron nitride (BN), titanium diboride (TiB₂) etc. Most of the oxide and non-oxide ceramics have a high melting temperature, which makes their shape-forming procedures are mainly based on powder metallurgical methods.

Several dry and wet shaping methods are popular in the shaping of ceramics, each having advantages and disadvantages. Dry processing techniques such as pressing are fast processing techniques, but they are not capable of producing complex shapes[78]. Wet shaping techniques like slip casting, injection molding, gelcasting, and direct coagulation techniques are suitable for making complex shapes, but these techniques involve several steps. The final properties also vary with the shape-forming procedure used. J.A. Lewis has reviewed different colloidal processing techniques based on their suspension rheology and consolidation techniques[79]. He categorised the wet forming process on the basis of consolidation techniques into three types: fluid removal, particle flow and gelation.

A. Krell and P. Blank studied the influence on the strength of alumina parts fabricated by uniaxial pressing, cold isostatic pressing, pressure filtration and gelcasting[80]. They found that wet forming techniques (Pressure filtration and gelcasting) have uniform density, resulting in better mechanical properties on the final parts. In 1996, O. Omatete et al. successfully developed the gelcasting procedure to fabricate complex alumina shapes from its powder [55]. This method has been later adapted to other oxide and non-oxide ceramics. Kia Liu et al. has gelcast zirconia using molds, printed using stereolithography for dental applications[81].

Traditional shape-forming techniques in ZrB_2 -based ceramics include die pressing, hot pressing and spark plasma techniques. Recent studies focus on wet forming techniques for easy consolidation and more dense products. J. Yin et al. have successfully gelcast ZrB_2 samples with 97.3 % density [82]. The final samples have a Vickers hardness of 13.1 ± 0.6 GPa and a fracture toughness of 2.5 ± 0.4 MPa \sqrt{m} . C. Tallon et al. fabricated ZrB_2 ceramics through slip casting and cold pressing and compared the densities. The samples prepared by slip casting possess a higher relative density (99.5 %) than the cold-pressed samples, when sintered by hot pressing at 2000°C in 40 MPa[83]. ZrB_2 -SiC ceramics were prepared using aqueous gelcasting by Rujie He et al[84]. Samples attained a relative density of 98 % when sintered at 2100°C without pressure. Flexural strength and fracture toughness of the final samples were 405 \pm 27 MPa and 4.3 \pm 0.3 MPa \sqrt{m} , respectively. ZrB_2 -based composites with various percentages of SiC were fabricated using hot pressing at 2000°C at a relatively low pressure of

10MPa[85]. With the addition of 30 vol% of SiC addition, samples attained 99.8 % of relative density with Vickers hardness of 21.3 GPa and fracture toughness of 4.7 MPa \sqrt{m} .

Other widely used non-oxide ceramics are carbides of tungsten, silicon, titanium etc. In the case of tungsten carbide shaping, traditional processes include cold pressing, powder injection molding (PIM), extrusion, etc. Cold pressing is involved in the production of most of the tool inserts while rods are made with extrusion[86]. Y. Li and Z.Guo has gelcast WC – 8 wt% Co with Hydroxyethyl methacrylate (HEMA) as a binder[87]. The samples have a transverse rupture strength of 2250 MPa and hardness of HRA90 when sintered at 1400°C. I. Azcona et al. has compacted ultrafine WC powder with 10 wt% Co using uni-axial pressing[88]. The compacted samples were sintered by using hot isostatic pressing (HIP) and vacuum sintering, and compared the properties of final samples. They were able to generate fully dense samples using HIP at low temperature of 1000°C. In recent years, additive manufacturing is also getting attention for the production of WC samples. Additive manufacturing techniques which are successful in making complex shapes of WC include selective laser melting (SLM), fused filament fabrication (FFF), 3D gel-printing (3DGP), Binder Jet Additive Manufacturing (BJAM), and direct ink writing (DIW)[89–93].

Silicon carbide, which is being used for structural applications at high temperatures are fabricated through both dry and wet processing routes. W. Si et al. has modified direct coagulation casting (DCC) method to fabricate SiC components[94]. By casting low viscous (<1–3 Pa.s) slurry, samples attained relative density above 98.7 % after sintering. Another popular SiC shaping procedure is slip casting. A. Gubernat et al. have made shapes out of SiC suspension using slip casting[95]. The slip cast samples of SiC exhibited excellent mechanical properties, fracture toughness, and hardness of 5 MPa \sqrt{m} and 18-19 GPa, respectively. I. Ganesh et al. have demonstrated geleasting of SiC samples using aqueous suspension. They were able to generate dense (97.5 % relative density) as well as porous (porosity >80%) fabricated, where the compressive strength of the sintered porous structures was > 16 MPa. K. Terrani et al. had successfully 3D printed complex geometries of SiC by combining binder jetting and chemical vapour infiltration process[96]. The printed sample has a thermal conductivity of 37 W·(m·K)⁻¹ and a flexural strength of 297 MPa.

Nitrides of silicon and boron are another important category of non-oxide ceramics which are widely used as structural materials in high temperature and corrosive environments. W. Zeng et al. have fabricated silicon nitride (Si₃N₄) ceramic parts using gelcasting technique with a slurry having a solid loading of 52 vol% [97]. when sintered at 1780°C, the samples attained a relative density of 97.8 %, with flexural strength and fracture toughness of 687 MPa and 6.5 MPa \sqrt{m} , respectively. Other than gelcasting, O. Penas et al. made silicon nitride shapes using slip casting[98], and tapes were developed through tape casting by B. Bitterlich et al[99]. Gelcasting was also used to fabricate porous Silicon Nitride-Boron Nitride composites by K. Liu et al [100].

1.6. Fabrication of molds and rapid prototyping techniques

Rapid prototyping (RPT) encompasses a variety of technologies capable of producing precise 3D models directly from computer-aided design (CAD) files, eliminating the necessity for mold or die manufacturing [58, 101]. Initially designed for model-making purposes, RPT has evolved to enable the fast production of functional items. People often use the term "solid freeform fabrication" (SFF) to emphasize the lack of tooling requirements. All RPT technologies share the standard approach of building 3D objects layer by layer [102], making them ideal for automated manufacturing and removing the need for molds or dies.

RPT can produce precise three-dimensional objects directly from CAD files, eliminating the need for complex tools, dies, or molds. This approach allows for creating physical models for intricate components with reduced investment in both time and money. When producing only a few ceramic prototypes or small batches of parts, traditional processing techniques for ceramics become expensive and time-consuming. In addressing these issues, researchers have explored alternative methods using the lost-mold technique. In mold shape Deposition Manufacturing (Mold SDM), developed at Stanford University [103], a wax mold is created and filled with a slurry containing the final part material in powder form. The wax mold is produced by decomposing the desired part geometry into machinable compacts and then building up the mold in layers by machining the wax or sacrificial support material.

The conventional techniques like injection molding and slip casting required the use of precise molding, resulting in increased expenses. In most circumstances, the cost of mold manufacture will drive the overall cost of a component. High-quality water-cooled dies are necessary for injection molding [104]. At the same time, these must be rapidly disassembled in order to remove the part. Slip casting requires the use of complex porous molds.

The process of traditional mold manufacturing is known for its time-consuming and labour-intensive nature, which frequently leads to significant delays in production. This method usually requires complex procedures, such as creating patterns, and assembling molds. New studies focus on investigating modern additive and subtractive manufacturing technologies, to simplify mold fabrication procedures and overcome the constraints linked to conventional methods [105,106].

The selection, fabrication, and exploitation of molds are key elements that significantly impact the effectiveness of gelcasting applications. Aluminum, glass, Polyvinyl Chloride (PVC), polystyrene, and

polyethylene are frequently used for molds [107]. Nevertheless, every material has its unique benefits and constraints. Aluminum molds, although they are resilient and extensively utilized, involve a laborious manufacturing procedure, especially for intricate forms. In addition, ceramic slurry can stick to aluminum surfaces, making demolding more difficult. Plastic and glass molds may not be appropriate for quick removal or breakdown. In addition, the breakdown of ABS/PLA molds created through rapid prototyping presents issues due to their interaction with the green body, which can prolong the disintegration process [108,61]. Although simple metal molds are frequently used, specific gelcasting applications may necessitate surface treatments or coatings to inhibit the attachment of gelcast components. The complexities of mold materials and their impact on gelcasting procedures is essential for attaining the best outcomes and reducing production difficulties.

Plaster molds are commonly employed in slip casting for ceramics. However, their use in gelcasting poses challenges due to pores on the plaster mold surface. These pores and capillary forces lead to rapid water removal from the gelcasting slurry, rendering plaster molds unsuitable for gelcasting applications. Glass typically has a smooth surface that facilitates easy removal of molds. However, machining glass to create intricate molds poses a significant challenge. Alternative molds, like wax, have been employed to address the challenge of removing the object from the mold, which can be accomplished by heating the mold to temperatures ranging from 90 to 120°C [109]. However, when temperatures exceed 120°C, the drying process initiates, and if the humidity is not regulated correctly, it can lead to formation of defects like cracks and warping.

Ndinisa et al., [61] discuss a study on creating intricate alumina parts using gelcasting on thick molds produced through 3D printing with ABS and PLA. These mold's dissolution is done by immersion in acetone for ABS mold and hot water for PLA mold. This approach of mold removal process is time-consuming and unwanted interaction of the green body with the immersion medium causes defects in final components.

1.7 Fabrication of ceramic matrix composites

1.7.1. Liquid phase methods for fiber reinforced CMC

Slurry infiltration: In this method, a ceramic matrix precursor is mixed with a preform made of reinforcing fibers. The ceramic matrix precursor is usually a slurry of ceramic particles suspended in a liquid. The slurry penetrates the gaps between the fibers, creating the structure during the curing and sintering processes that follow.

Xuewu Li et al.,[110] made an alumina fiber-reinforced zirconia composites by adding continuous alumina fibers to a yttria-stabilized zirconia (YSZ) matrix to make it stronger. They coated a layer of LaPO₄ onto the alumina fibers. They made a high-density composite material with excellent mechanical properties, such as a flexural strength of 277 MPa and an exceptional fracture toughness of 15.93 MPa \sqrt{m} .

Chemical vapour infiltration:

Chemical vapor infiltration (CVI) process, which significantly advanced materials manufacturing. This technique involves adding a powder slurry to reduce pore size effectively. CVI functions by thermally decomposing gaseous precursors at high temperatures inside a reactor. Subsequently apply the obtained solid components to the fiber preform, gradually building up to create the ceramic matrix.

Amirthan et al.,[111] investigated Si/SiC ceramic composite and its properties by adding liquid silicon to carbon preforms made from cotton fabric and phenolic resin. The composite was further processed using chemical vapor infiltration with methyl trichlorosilane as a precursor gas. The study aimed to investigate the impact of the duration of infiltration on the densification process and the resulting mechanical properties. The results showed a significant increase in density due to the closure of pores as the infiltration period increased.

Sol- gel process

Metal alkoxides react chemically with water in the sol-gel processing method to form a sol, which then turns into a gel, followed by drying and heating to form the ceramic matrix. This method allows for precise control over composition and morphology.

E.D. Rodeghiero [112] employed sol-gel processes for producing ceramic matrix composites with high-temperature resistance. These composites include Ni/a-Al₂O₃, Fe/a-Al₂O₃, Ni/ZrO₂, SiC (whisker)/a-Al₂O₃, and SiC (platelet)/a-Al₂O₃. Unlike most powder mixing methods, sol-gel procedures produced uniform microstructures that had good coherence between the matrix and reinforcing phases.

Liquid silicon infiltration (LSI)

LSI entails saturating a permeable preform with liquid silicon, which permeates the preform and chemically interacts with carbon-based materials within the preform, resulting in the formation of a silicon carbide (SiC) in the composite. This technique yields ceramic matrix composites that exhibit outstanding resistance to oxidation and exceptional stability at high temperatures. Researchers led by

Guoin Zheng et, al. [113] looked into how to make unidirectional carbon fiber-reinforced SiC composites (CF/SiC) using different kinds of carbon fibers: polyacrylonitrile-based high strength carbon fiber (HSCF), pitch-based high modiolus (HMCF) with a low degree of graphitization and pitch-based carbon fiber (CF70) with a high degree of graphitization.

1.7.2 Solid Phase methods:

Hot pressing-Hot pressing involves the application of both high temperatures and pressures to a combination of ceramic powder and fibre reinforcements. This method enhances the compactness and adhesion between the ceramic particles and fibres, leading to a solid composite structure with enhanced mechanical qualities.

Ultra-high-temperature ceramics pose a challenge due to their high sintering temperatures. By the application of pressure, composites can be densified at lower temperatures using hot isostatic press (HIP) [114].

Spark plasma sintering: Spark Plasma Sintering (SPS) is an efficient method of consolidating materials by applying a pulsed direct current through a powder compact. This causes localised heating as a result of Joule heating [115]. This technique facilitates rapid consolidation of ceramic powders while minimising the enlargement of grains, leading to the formation of fine-grained ceramic matrix composites with improved characteristics.

1.7.3 Polymer in filtration pyrolysis Prepeg impegration

This technique involves saturating fibre preforms with a polymer resin that contains ceramic precursors. The impregnated preforms are subsequently subjected to regulated heating settings to induce the pyrolysis of the polymer and the conversion of the precursors into a ceramic matrix, resulting in the formation of a composite structure.

Franziska Uhlmann et al. [116] investigated the thermo-chemical durability of PIP-Cf/SiC composites by altering the SiC matrix. To create Cf/SiC–ZrB₂–TaC composites, they included ZrB₂ and Ta powder in the pre-ceramic slurry. These composites have density (ranging from 2.39 to 2.72 g/cm3), porosity (ranging from 20.3 to 24.8 vol.%), and fiber volume content (ranging from 52 to 57 vol.%).

1.7.4 Hybrid methods: Combination of liquid phase and solid phase processes

CMCs can be fabricated using a combination of liquid and solid phase procedures to enhance their characteristics. As an illustration, a preform can undergo partial densification by hot pressing prior to being infiltrated with a ceramic slurry in order to get the intended matrix structure.

J. Magnant et al., [117] have fabricated CMCs reinforced by continuous carbon and silicon carbide

fibers using this method. The study used highly concentrated and well-dispersed aqueous colloid suspensions for slurry impregnation, ensuring uniform dispersion of ceramic materials within multidirectional fiber preforms. This is followed by Low-Pressure Spark Plasma Sintering (LP-SPS) as an efficient method for densifying fiber-reinforced ceramic matrix composites in hybrid approaches.

1.8 Mechanical, microstructural and fractography studies

Szutkowska's et al., [118] examined the fracture toughness of different alumina matrix composite materials fabricated by the Cold Isostatic Pressing (CIP) technique. Three different compositions are analyzed: monolithic Al₂O₃, Al₂O₃ with 10 wt% zirconia (ZrO₂), and Al₂O₃ with 10 wt% 3YSZ (Yttria-Stabilized Zirconia). The monolithic Al₂O₃ demonstrates a strength of 385 MPa and a fracture toughness of 3.75 MPa \sqrt{m} . By adding 10 wt% zirconia, the composite demonstrates an impressive strength of 377 MPa and a significantly improved fracture toughness of 4.68 MPa \sqrt{m} . Additionally, when 10 wt% 3YSZ is included, the material exhibits a strength of 379 MPa and a fracture toughness of 4.00 MPa \sqrt{m} .

Laurent et al., [119] explored the production and analysis of nanocomposites consisting of carbon nanotubes (CNTs), iron, and alumina. The composite consists of alumina (Al₂O₃) with 10 vol% multiwalled carbon nanotubes (MWNTs) fabricated using the Hot Isostatic Pressing technique. The study reports a fracture toughness of 4.2 MPa \sqrt{m} for the Al₂O₃ with 10 vol% MWNT composite. There has been a notable improvement in fracture toughness compared to monolithic alumina.

Volkmann et al., [120] studied the mechanical performance and effects of heat treatments on oxide/oxide ceramic matrix composites. The study offers valuable insights into the preparation and analysis of mullite ceramic composite reinforced with N720 alumina fibres. The composite exhibits a strength of 235 MPa and a fracture toughness of 3.3 MPa \sqrt{m} .

Paek et al.,[121] explore the preparation and fracture behavior of composites made from alumina platelets and alumina–monazite (LaPO₄). The composite system consists of Al_2O_3 with 25wt% LaPO₄ and Anorthite, strengthened with 5wt% α -alumina platelets. Fabrication is achieved using tape casting, a method renowned for its capability to create thin ceramic tapes with precise microstructures. The composite exhibits good mechanical properties, with a strength of 228 MPa and a fracture toughness of 3.48 MPa \sqrt{m} . The findings highlight platelet reinforcement's effectiveness in improving ceramic composites' mechanical performance.

Corrêa De Sá et al., [122] studied the mechanical properties of alumina-zirconia (Al₂O₃-ZrO₂) composites used for ceramic dental implants. The composite was made using the uniaxial pressing technique and consisted of partially stabilized zirconia (PSZ) with 3 mol% yittria and alumina

particulates. Their study found a maximum fracture toughness of around 4.57 MPa√m and a flexural strength of about 510 MPa for the PSZ composite.

Xuewu Lia et al.,[110] conducted a study on composites made of alumina fiber-reinforced yttria-stabilized zirconia (YSZ), focusing on achieving high density and toughness. The study reveals a clear understanding on the properties of PSZ composites. Monolithic PSZ, without addition of reinforcements, demonstrated a maximum fracture toughness of around 3.72 MPa√m and a flexural strength of about 1047 MPa. The mechanical properties of the composite were significantly enhanced when continuous uncoated alumina fibres were added to the PSZ matrix. The maximum fracture toughness reached around 6.89 MPa√m, while the flexural strength was approximately 296 MPa. This study demonstrates the positive impact of continuous fiber reinforcement on the toughness of PSZ composites. The mechanical properties of the PSZ composite were further improved by incorporating continuous fibers with a LaPO₄ coating. The fracture toughness reached a maximum of around 15.93 MPa√m, while the flexural strength measured approximately 277 MPa. The significant enhancement highlights the combined impact of fiber reinforcement and coating, leading to exceptional mechanical performance.

Navarro et al., [123] studied the preparation and evaluation of zirconia-based/Al₂O₃ composites for electrolytes in solid oxide fuel cell systems. The PSZ composite, fabricated using isostatic pressing, demonstrated a maximum fracture toughness of around 2.40 MPa \sqrt{m} and a flexural strength of about 300 MPa. Kailer et al,.[124] studied the potential of utilizing the Chevron Notch Beam method to assess fine-grained zirconia ceramics' fracture toughness. The monolithic zirconia, prepared by hot pressing exhibited a fracture toughness of around 6.22 MPa \sqrt{m} .

Chłędowska et al,. [125] studied the impact of adding aluminium oxide to 3 mol% yttria-stabilized tetragonal zirconia (3YSZ) for solid oxide fuel cells (SOFCs). They examined the effect of the dopant on the electrical and mechanical properties of the electrolytes. The PSZ composite, fabricated using gelatin method and containing 3 mol% zirconia particulates, demonstrated a fracture toughness of around 6.37 MPa√m.

The study conducted by M. Ruhle etal., [126] explores the role of tetragonal (t) and monoclinic (m) ZrO₂ phase in toughening ZrO₂-toughened Al₂O₃ ceramics. They found that both types of ZrO₂ phases contribute to toughening mechanisms, through different processes. In the stress field of propagating cracks, t-ZrO₂ phase undergo a stress-induced transformation to m-ZrO₂. This transformation helps in absorbing energy and slow crack propagation, thereby enhancing the material's toughness. On the other

hand, residual stresses around already-transformed m-ZrO₂ phsae can lead to microcracking, which can enhance the material's toughness.

1.9 Motivation of the Present work

Some of the conventional manufacturing methods result in significant material waste and require several additional steps to fabricate the desired final shape of components. This approach not only utilizes substantial resources but also contributes to the overall duration and expenses of manufacturing. Introduction of additive manufacturing (AM) has completely transformed the industry by providing a more efficient and simplified option. Additive manufacturing, or 3D printing, allows for the creation of complex objects with high accuracy, directly from computer aided design (CAD) files. Additive manufacturing adds layer by layer of the material to get the final component and eliminates the necessity for subtractive machining methods. In addition, additive manufacturing enables the creation of intricately designed and customized shapes that would be difficult or unattainable with traditional forming methods. The flexibility of AM technology allows for new opportunities in creative design and efficient product improvement in various sectors, including aerospace, automotive, healthcare, and consumer products. Moreover, additive manufacturing provides enhanced design flexibility, allowing engineers to rapidly and effectively fabricate throughout the product development phase. In summary, additive manufacturing is a notable progression in manufacturing technology, providing a more effective, environmentally friendly, and adaptable method for creating intricate components with excellent accuracy.

Gelcasting is a well-known ceramic shape forming process, which involves using methyl acrylamides (AM) to start the creation of a strong gel network within a slurry that contains ceramic powder particles. This procedure entails initiating free radical polymerization between acrylamide (the monomer) and methylene bisacrylamide (the crosslinker), with the use of initiators and catalysts. The gel structure that forms as a result effectively suspend the ceramic particles and evenly spread throughout the solution. This makes it easier to shape complex ceramic components. Nevertheless, the application of acrylamide in gelcasting is limited due of concerns over its neurotoxicity and vulnerability to oxygen inhibition. Therefore, ongoing research efforts in gelcasting are concentrated on investigating alternative technologies that provide safer and more environmentally sustainable choices. The available options consist of natural polymers such as agarose, gellan gum, and curdlan, as well as environmentally sustainable cross-linkable binder systems including Isobam, methylcellulose, and HMDA-paraformaldehyde. Researchers are exploring alternate approaches to address the limits of standard gelcasting technologies. Present research work aims to advance the development of safer, more sustainable, and diverse procedures for shaping ceramics.

The combination of gelcasting and rapid prototyping techniques is shown as a promising approach in the fabrication of ceramic components. Gelcasting, known for its ability to produce intricate shapes and near-net complex geometries, is coupled with rapid prototyping methods to streamline the manufacturing process and achieve superior control over the structure and characteristics of ceramic components.

The inherent characteristics of ceramics, including high porosity, brittleness, and limited fracture toughness, pose challenges in their practical applications. Additionally, machining processes for ceramics are often expensive due to their hardness and tendency to undergo fracture during shaping. To enhance the mechanical properties of ceramics, various methods such as reinforcements and process modifications have been explored. Reinforcements involve incorporating secondary phase materials, such as particles, platelets, whiskers and fibres with suitable interfacial coating into the ceramic matrix to improve fracture toughness, wear resistance and other mechanical properties. Process modifications include changes in fabrication techniques, such as fabrication of molds, alteration of sintering conditions or methods of introducing of additives, to optimize microstructure and enhance mechanical performance. These approaches aim to overcome the inherent brittleness and low fracture toughness of ceramics, thereby expanding their potential for various applications.

In the present study, we have chosen different ceramic systems to investigate different techniques of forming shapes. These systems include monolithic alumina, mixed oxides like barium strontium titanate with a composition of $Ba_{0.5}$ $Sr_{0.5}TiO_3$ (BSTO) and ZrB_2 . Additionally, composites made of alumina and zirconia which is partially stabilized with 3 mol% yttria (3Y-PSZ), are investigated in detail. The main goal is to evaluate the effectiveness of reinforcements, such as α - alumina platelets and carbon short fibers, in improving the mechanical properties of alumina and zirconia composites. The work investigates the efficacy of these reinforcements to improve the mechanical performance of the ceramics, while simultaneously exploring to create complex shapes that may have been difficult to obtain using conventional methods. The outcome of the present investigation of net shaping and reinforcing approaches demonstrates enhanced performance of the oxide ceramic materials studied and promises potential applications in diverse fields, like aerospace and automotive sectors for structural components, biomedical implants and in electronic devices.

References:

1. <u>Davis, Karen</u>, Material Review: Alumina (Al₂O₃). International Journal of Advance Research and Innovative Ideas in Education. 2010; 2: 109-114.

- 2. A. M. Abyzov; Aluminum Oxide And Alumina Ceramics (Review). Part 1. Properties Of Al₂O₃ And Commercial Production Of Dispersed Al₂O₃; Scientific Research And Development. 2019; 60: 16-23.
- 3. Adebayo Y. Badmos, Douglas G. Ivey, Characterization of structural alumina ceramics used in ballistic armour and wear applications. Journal of Materials Science. 2001; 36: 4995 5005.
- 4. Paolo Francesco Manicone, Pierfrancesco Rossi Iommetti, Luca Raffaelli, An overview of zirconia ceramics: Basic properties and clinical applications. Journal of Dentistry, 2007; 35: 819-26.
- 5. Jialin Sun, Jun Zhao, Zhifu Huang, Ke Yan, Xuehui Shen, Jiandong Xing, Yimin Gao, Yongxin Jian, Hejie Yang, Bo Li. A Review on Binderless Tungsten Carbide: Development and Application. Nano-Micro Letters. 2020; 12: 1-37
- 6. Yamada, K., Mohri, M. Properties and Applications of Silicon Carbide Ceramics. Springer Dordrecht. 1991; 1:13-44.
- 7. Manju Kurian, Smitha Thankachan, Introduction: ceramics classification and applications. Ceramic catalysis. 2023,1-17.
- 8. Sun, J., Zhao, J., Huang, Z. et al. A Review on Binderless Tungsten Carbide: Development and Application. Nano-Micro Letters. 2020;12: 1-37.
- 9. Man Xu, Yarabahally R. Girish, Kadalipura P. Rakesh, Piye Wu, Honnayakanahalli M. Manukumar, Shayan M. Byrappa, Udayabhanu, Kullaiah Byrappa. Recent advances and challenges in silicon carbide (SiC) ceramic nanoarchitectures and their applications. Materials Today Communications 2021; 28; 1-24.
- 10. Monteverde F, Guicciardi S, Bellosi A. Advances in microstructure and mechanical properties of zirconium diboride based ceramics. Material Science Engineering A 2003;346:310–319.
- 11. Wei Zhang, A novel ceramic with low friction and wear toward tribological applications: Boron carbide-silicon carbide. Advances in Colloid and Interface Science. 2022; 301: 1-22.
- 12. S. Hampshire, Silicon nitride ceramics review of structure. Processing and Properties. 2007; 24: 1-8.
- 13. W. Werdecker and F. Aldinger, "Aluminum Nitride-An Alternative Ceramic Substrate for High Power Applications in Microcircuits. *IEEE Transactions on Components, Hybrids, and Manufacturing Technology.* 1984; 7: 399 404.
- 14. Jürgen Rödel, Alain B.N. Kounga, Marion Weissenberger-Eibl, Daniel Koch, Antje Bierwisch, Wolfgang Rossner, Michael J. Hoffmann, Robert Danzerf, Gerhard Schneider. Development of a roadmap for advanced ceramics: 2010–2025. Journal of the European Ceramic Society 2009; 29: 1549–1560.
- 15. George A. Gogotsi, Fracture toughness of ceramics and ceramic composites; Ceramics International. 2003; 29: 777 84.
- 16. Donald, I.W., McMillan, P.W. Ceramic-matrix composites Journal of Materials Science. 1976; 11: 949–72.
- 17. Oriol Gavalda Diaza, Gonzalo Garcia Lunaa, Zhirong Liaoa, Dragos Axinte. The new challenges of machining Ceramic Matrix Composites (CMCs): Review of surface integrity. International Journal of Machine Tools and Manufacture. 2019; 139: 24–36.
- 18. E. Volkmann, K. Tushtev, D. Koch, C. Wilhelmi, J. Göring, K. Rezwan, Assessment of three oxide/oxide ceramic matrix composites: Mechanical performance and effects of heat treatments. Composites Part A: Applied Science and Manufacturing publishes. 2015; 68: 19-28.
- 19. S.R. Choi*, N.P. Bansal, Mechanical behavior of zirconia/alumina composites. Ceramics

- International. 2005; 31: 39-46.
- 20. Sufyan Garoushi, Enas Mangoush, Pekka Vallittu and Lippo Lassila. Short Fiber Reinforced Composite: a New Alternative for Direct Onlay Restorations. The Open Dentistry Journal, 2013; 7: 181-185.
- 21. I. A. Ibrahim, F. A. Mohamed, E. J. Lavernia, Particulate Reinforced Metal Matrix Composites A Review. Journal Of Materials Science. 1991; 26: 1137 1156.
- 22. A.Thirumoorthy, T. V. Arjunanb, K. L. Senthil Kumar. Latest Research Development in Aluminum Matrix with Particulate Reinforcement Composites A Review. Materials Today: Proceedings. 2018; 5; 1657–1665.
- 23. A. N. Norris. The Mechanical Properties Of Platelet Reinforced Composites. International Journal Of Solids And Structures. 1990;26: 663-674.
- 24. Lorenz J. Bondere, Kirill Feldman, Ludwig J. Gauckler, Platelet-reinforced polymer matrix composites by combined gel-casting and hot-pressing. Part I: Polypropylene matrix composites. Composites Science and Technology. 2010; 70;1958–1965.
- 25. Shuang Li a, *, Xudong Luo b, Chuncheng Wei a, Peiling Gao a, Peng Wang a, Lijuan Zhou. Enhanced strength and toughness of silicon carbide ceramics by graphene platelet-derived laminated reinforcement. Journal of Alloys and Compounds. 2020; 834: 1-7.
- 26. Linan An, Suxing Wu, Helen M. Chan, And Martin P. Harmer, David G. Brandon. Alumina Platelet Reinforced Reaction Bonded Aluminum Oxide Composites: Textured And Random. Journal of Materials Research. 1997;12: 3300-3306.
- 27. Tiegs T, SiC whisker reinforced alumina. In: Handbook of ceramic composites. Springer, NY, USA, 2005; 307–323
- 28. Becher PF, Wei GC) Toughening Behavior in Sic-Whisker-Reinforced Alumina. Jornal of European Ceramic Society. 19846; 7:267–269.
- 29. Lansmann V, Jansen. M Application of the glass-ceramic process for the fabrication of whisker reinforced celsian-composites. Journal of Material Science. 2001; 36:1531–1538.
- 30. Lin X, Darrell Ownby P. Pressureless sintering of B₄C whisker reinforced Al₂O₃ matrix composites. Journal of Material Science. 2000; 35: 411–418.
- 31. Boccaccini AR, Winkler V Fracture surface roughness and toughness of Al2O3-platelet reinforced glass matrix composites. Composites Part A: Applied Science Manufacturing. 2002; 33:125–131.
- 32. HeX, GuoY, YuZ, Zhou Y, Jia D. Study on microstructures and mechanical properties of short-carbon-fiber-reinforced SiC composites prepared by hot-pressing. Material Science Engineering A. 2009;527:334–338.

- 33. Yang F, Zhang X, Han J, Du S. Processing and mechanical properties of short carbon fibers toughened zirconium diboride-based ceramics. Materials Design. 2008; 29:1817–1820.
- 34. Zhang Y, Li S, Han J, Zhou Y. Fabrication and characterization of random chopped fiber reinforced reaction bonded silicon carbide composite. Ceramic International. 2012; 38:1261–1266.
- 35. Xia Z, Riester L, Curtin WA, Li H, Sheldon BW, Liang J, Chang B, Xu JM. Direct observation of toughening mechanisms in carbon nanotube ceramic matrix composites. Acta Materials. 2004: 52:931–944.
- 36. C. Kaya, F. Kaya, E.G. Butler, A.R. Boccaccini, K.K. Chawla, Development and characterisation of high-density oxide fibre-reinforced oxide ceramic matrix composites with improved mechanical properties. Journal of the European Ceramic Society. 2009; 29: 1631–39.
- 37. Cao X, Lin B, Zhang X) Investigations on grinding process of woven ceramic matrix composite based on reinforced fiber orientations. Composites Part B Engineering. 2015; 71:184–192.
- 38. Renjith Devasia, Anil Painuly, Deepa Devapal, K.J. Sreejith, Continuous fiber reinforced ceramic matrix composites. Fiber Reinforced Composites 2021;669-751. https://doi.org/10.1016/B978-0-12-821090-1.00022-3.
- 39. Roger R. Naslain, SiC-Matrix Composites: Non brittle Ceramics for Thermo-Structural Application. Int. J. Appl. Ceram. Technol., 2 [2] 75–84 (2005).
- 40. J. Wu, M. Chen, F.R. Jones and P.F. James, Mullite and alumina-silica matrices for composites by modified sol-gel processing. Journal of Non-Crystalline Solids162 (1993)197-200.
- 41. Yu. S. Virgil'ev and I. P. Kalyagina, Carbon–Carbon Composite Materials. Inorganic Materials. 40 (2004) 33–49.
- 42. Sindi Sithembiso Ndinisa, Development of Complex Shaped Alumina Parts by Gelcasting And Additive Manufacturing. University of the Witwatersrand, Johannesburg. 2019.
- 43. M. Jabbari, R. Bulatova, A.I.Y. Tok, C.R.H. Bahl, E. Mitsoulis, J.H. Hattel. Ceramic tape casting: A review of current methods and trends with emphasis on rheological behaviour and flow analysis. Materials Science and Engineering B. 2016; 212: 39–61.
- 44. Y. Zhang, X. He, J. Han, S. Du and J. Zhang. Al2O3 Ceramics Preparation by LOM (Laminated Object Manufacturing). International Journal of Advanced Manufacturing Technology. 2001; 17:531–534
- 45. Carolina Tallon ^a, Monika Limacher ^{a b}, George V. Franks. Effect of particle size of shaping of ceramics by slip casting. Journal of European ceramic society. 2010;30: 2819-2826.
- 46. Yasumasa Takao, Tadashi Hotta, Kenji Nakahira, Makio Naito, Nobuhiro Shinohara, Masataro Okumiya, Keizo Uematsu. Processing defects and their relevance to strength in alumina ceramics made by slip casting. Journal of the European Ceramic Society. 2000; 20:389-395.
- 47. H. Lu, Z. Qu, Y. C. Zhou, Preparation and mechanical properties of dense polycrystalline hydroxyapatite through freeze-drying. Journal Of Materials Science: Materials In Medicine.1998; 9: 583 587.
- 48. Stephen W. Sofie and Fatih Dogan, Freeze Casting of Aqueous Alumina Slurries with Glycerol. Journal of American Ceramic. Society. 2001;84: 1459–64.
- 49. Wei Li, Hongxiang Zhang, Yanping Jin, Mingyuan Gu, Rapid coagulation of silicon carbide slurry via direct coagulation casting. Ceramics International. 2004; 30: 411–416.
- 50. Wenjie Si, Thomas J. Graule, Felix H. Baader, and Ludwig J. Gauckler, Direct Coagulation

- Casting of Silicon Carbide Components. Journal of American Ceramic Society. 1999;82: 1129–36.
- 51. Chen Jinsong, Bao Enquan, Huang Dazhi, Ding Yunfei and Qiu Xuhui, Extrusion Freeforming-Based 3D Printing of Ceramic Materials. Materials Transactions. 2020; 61:2236 2240.
- 52. Kedarnath Rane Matteo Strano, A comprehensive review of extrusion-based additive manufacturing processes for rapid production of metallic and ceramic parts. Advances in Manufacturing. 2019; 7:155–173.
- 53. Xin Wu and I-Wei Chen, Hot Extrusion of Ceramics. Journal of American Ceramic Society. 1992; 75: 1846-53.
- 54. M. Faesa, H. Valkenaersa, F. Vogelera, J. Vleugelsb, E. Ferraris, Extrusion-based 3D printing of ceramic components. Procedia CIRP. 2015; 28: 76 81.
- 55. Janney MA, Omatete OO, Walls CA, Nunn SD, Ogle RJ, Westmoreland G. Development of low-toxicity gelcasting systems. Journal of American Ceramic Society. 1998; 81:581–91.
- 56. Jinlong Yang, Juanli Yu, Yong Huang, Recent developments in gelcasting of ceramics. Journal of the European Ceramic Society. 2011;31: 2569–2591.
- 57. Albert C. Young, Ogbemi. Ornatete, Mark A. Janney, and Paul A. Menchhofer, Gelcasting of Alumina. Journal of American Ceramic Society. 1991; 74: 31612-18.
- 58. R. GilissenU, J.P. Erauw, A. Smolders, E. Vanswijgenhoven, J. Luyten, Gelcasting, a near net shape technique. Materials and Design. Materials and Design. 2000; 21: 251 257.
- 59. V. G. Babashov, N. M. Varrik, Gel Casting Method For Producing Ceramic Materials: A Review. Glass And Ceramics. 80; 2023: 9-16.
- 60. M.V.Silva,1 D. Stainer,2 H. A. Al-Qureshi,1 O. R. K. Montedo,3 and D. Hotza1, Alumina-Based Ceramics for Armor Application: Mechanical Characterization and Ballistic Testing; Volume 2014, Article ID 618154, 6 pages http://dx.doi.org/10.1155/2014/618154
- 61. Sindi Sithembiso Ndinisa, David James Whitefield and Iakovos Sigalas, Ceramics International, https://doi.org/10.1016/j.ceramint.2019.10.021.
- 62. Murat Bengisua, Elvan Yilmazb, Gelcasting of alumina and zirconia using chitosan gels; Ceramics International 28 (2002) 431–438
- 63. M. Schumacher U. Deisinger R. Detsch G. Ziegle, Indirect rapid prototyping of biphasic calcium phosphate scaffolds as bone substitutes: influence of phase composition, macroporosity and pore geometry on mechanical properties; J Mater Sci: Mater Med (2010) 21:3119–3127
- 64. Rajasekharan T, Swaroop Raju PM, Pandey RK, Seshu Bai V, Pradyumna R, Baig MAH. Complex-shaped alumina products through rapid prototyping. Metals Materials and Processes. 2007; 19:41–46
- 65. Xiaogang Xu, Zhaoyin Wen*, Jiu Lin, Ning Li, Xiangwei Wu, An aqueous gel-casting process for g-LiAlO2 ceramics, X. Xu et al./Ceramics International 36 (2010) 187–191; 10.1016/j.ceramint.2009.07.017
- 66. Jung-Soo Ha, Effect of atmosphere type on gelcasting behavior of Al2O3 and evaluation of green strength Ceramics International 26 (2000) 251±254
- 67. Qing Yao, Le Zhang, Zhigang Jiang, Guocan Huang, Tianyuan Zhou, Yue Ben, Shuai Wei, Rong Sun, Hao Chen and Yun Wang, Isobam assisted slurry optimization and gelcasting of

- transparent YAG ceramics, Ceramics International, https://doi.org/10.1016/j.ceramint.2017.10.098
- 68. J. Xu, et al., A novel gelcasting of alumina suspension using curdlan gelation, Ceramics International (2015), http://dx.doi.org/ 10.1016/j.ceramint.2015.04.144
- 69. Nikkisha S, Rohan. S, Pragyan Pattanaik, Ankit Kumar Mishra, Dheva Darshini, Review Study on Mechanical and Thermal Properties of Ceramic Materials for Future Aerospace Applications. Materials and its Characterization. (2) 2022; 1 107-113.
- 70. Ojo Jeremiah Akinribide Gadifele Nicolene Mekgwe, Samuel Olukayode Akinwamide, Fehmi Gamaoun, Chamil Abeykoon, Oluwagbenga T. Johnson, Peter Apata Olubambi, A review on optical properties and application of transparent ceramics. Journal of Materials Research and Technology.2022;21:712-738
- 71. F. Monteverde, A. Bellosi, S. Guicciardi, Processing and properties of zirconium diboride-based composites. Journal of the European Ceramic Society. 2002; 22: 279–288.
- 72. C.R.D. Ferreira, A.A.G. Santiago, R.C. Vasconcelos, D.F.F. Paiva, A.A. Araújo, F.V. Motta, M.R.D. Bomio. of microstructural, mechanical, and biomedical properties of zirconia/hydroxyapatite ceramic composites. 2022;48: 12376-12386.
- 73. Safari, A., & Ghazvini, M. Advanced ceramic electrolytes for solid oxide fuel cells: A review. Journal of the European Ceramic Society. 2020; 40: 693-718.
- 74. Nathan S. Jacobson, Elizabeth J. Opila, Kang N. Lee, Oxidation and corrosion of ceramics and ceramic matrix composites. Current Opinion in Solid State and Materials Science. 2001; 5: 301–309.
- 75. George Karadimas and Konstantinos Salonitis, Ceramic Matrix Composites for Aero Engine Applications—A Review. Applied sciences. 2023; 13: 1-42.
- 76. Jon Binner, Matt Porter, Ben Baker, Ji Zou, Vinothini Venkatachalam, Virtudes Rubio Diaz, Andrea D'Angio, Prabhu Ramanujam, Tailin Zhang & T. S. R. C. Murthy (2019): Selection, processing, properties and applications of ultra-high temperature ceramic matrix composites, UHTCMCs a review, International Materials Reviews, DOI: 10.1080/09506608.2019.1652006.
- 77. Luca Zoli, Francesca Servadei a, Giada Bassi, Arianna Rossi, Monica Montesi, Antonio Vinci, Diletta Sciti, Silvia Panseri. From outer space to inside the body: Ultra-high temperature ceramic matrix composites for biomedical applications. Journal of the European Ceramic Society. 2024; 44: 729–737.
- 78. M. Aminzare, F. Golestani-fard, O. Guillon, M. Mazaheri, H.R. Rezaie, Sintering behavior of an ultrafine alumina powder shaped by pressure filtration and dry pressing, Materials Science and Engineering: A 527 (2010) 3807–3812. https://doi.org/10.1016/J.MSEA.2010.03.051.
- 79. J.A. Lewis, Colloidal Processing of Ceramics, Journal of the American Ceramic Society 83 (2000) 2341–2359. https://doi.org/10.1111/J.1151-2916.2000.TB01560.X.
- 80. A. Krell, P. Blank, The Influence of shaping method on the grain size dependence of strength in dense submicrometre alumina, J Eur Ceram Soc 16 (1996) 1189–1200. https://doi.org/10.1016/0955-2219(96)00044-1.
- 81. K. Liu, K. Zhang, D.L. Bourell, F. Chen, H. Sun, Y. Shi, J. Wang, M. He, J. Chen, Gelcasting of zirconia-based all-ceramic teeth combined with stereolithography, Ceram Int 44 (2018) 21556–21563. https://doi.org/10.1016/J.CERAMINT.2018.08.219.
- 82. R. He, X. Zhang, P. Hu, C. Liu, W. Han, Aqueous gelcasting of ZrB2–SiC ultra high temperature ceramics, Ceram Int 38 (2012) 5411–5418. https://doi.org/10.1016/J.CERAMINT.2012.03.051.
- 83. C. Tallon, D. Chavara, A. Gillen, D. Riley, L. Edwards, S. Moricca, G. V. Franks, Colloidal processing of zirconium diboride ultra-high temperature ceramics, Journal of the American Ceramic Society 96 (2013) 2374–2381. https://doi.org/10.1111/JACE.12383.

- 84. R. He, X. Zhang, P. Hu, C. Liu, W. Han, Aqueous gelcasting of ZrB2–SiC ultra high temperature ceramics, Ceram Int 38 (2012) 5411–5418. https://doi.org/10.1016/J.CERAMINT.2012.03.051.
- 85. M.S. Asl, M.G. Kakroudi, S. Noori, Hardness and toughness of hot pressed ZrB2–SiC composites consolidated under relatively low pressure, J Alloys Compd 619 (2015) 481–487. https://doi.org/10.1016/J.JALLCOM.2014.09.006.
- 86. H. Nie, T. Zhang, Development of manufacturing technology on WC–Co hardmetals, Tungsten 1 (2019) 198–212. https://doi.org/10.1007/s42864-019-00025-6.
- 87. Y. Li, Z. Guo, Gelcasting of WC–8wt%Co tungsten cemented carbide, Int J Refract Metals Hard Mater 26 (2008) 472–477. https://doi.org/10.1016/J.IJRMHM.2007.11.003.
- 88. I. Azcona, A. Ordóñez, J.M. Sánchez, F. Castro, Hot isostatic pressing of ultrafine tungsten carbide-cobalt hardmetals, J Mater Sci 37 (2002) 4189–4195. https://doi.org/10.1023/A:1020048105585/METRICS.
- 89. X. Zhang, Z. Guo, C. Chen, W. Yang, Additive manufacturing of WC-20Co components by 3D gel-printing, Int J Refract Metals Hard Mater 70 (2018) 215–223. https://doi.org/10.1016/J.IJRMHM.2017.10.005.
- 90. W. Lengauer, I. Duretek, M. Fürst, V. Schwarz, J. Gonzalez-Gutierrez, S. Schuschnigg, C. Kukla, M. Kitzmantel, E. Neubauer, C. Lieberwirth, V. Morrison, Fabrication and properties of extrusion-based 3D-printed hardmetal and cermet components, Int J Refract Metals Hard Mater 82 (2019) 141–149. https://doi.org/10.1016/J.IJRMHM.2019.04.011.
- 91. H. Kim, J. Il Kim, Y. Do Kim, H. Jeong, S.S. Ryu, Material extrusion-based three-dimensional printing of WC–Co alloy with a paste prepared by powder coating, Addit Manuf 52 (2022) 102679. https://doi.org/10.1016/J.ADDMA.2022.102679.
- 92. C.L. Cramer, N.R. Wieber, T.G. Aguirre, R.A. Lowden, A.M. Elliott, Shape retention and infiltration height in complex WC-Co parts made via binder jet of WC with subsequent Co melt infiltration, Addit Manuf 29 (2019) 100828. https://doi.org/10.1016/J.ADDMA.2019.100828.
- 93. A. Domashenkov, A. Borbély, I. Smurov, Structural modifications of WC/Co nanophased and conventional powders processed by selective laser melting, Materials and Manufacturing Processes 32 (2017) 93–100. https://doi.org/10.1080/10426914.2016.1176195.
- 94. W. Si, T.J. Graule, F.H. Baader, L.J. Gauckler, Direct coagulation casting of silicon carbide components, Journal of the American Ceramic Society 82 (1999) 1129–1136. https://doi.org/10.1111/J.1151-2916.1999.TB01886.X.
- 95. A. Gubernat, Ł. Zych, W. Wierzba, SiC Products Formed by Slip Casting Method, Int J Appl Ceram Technol 12 (2015) 957–966. https://doi.org/10.1111/IJAC.12359.
- 96. K. Terrani, B. Jolly, M. Trammell, 3D printing of high-purity silicon carbide, Journal of the American Ceramic Society 103 (2020) 1575–1581. https://doi.org/10.1111/JACE.16888.
- 97. W. Zeng, X. Gan, Z. Li, K. Zhou, The preparation of silicon nitride ceramics by gelcasting and pressureless sintering, Ceram Int 42 (2016) 11593–11597. https://doi.org/10.1016/J.CERAMINT.2016.04.040.
- 98. O. Penas, R. Zenati, J. Dubois, G. Fantozzi, Processing, microstructure, mechanical properties of Si_3N_4 obtained by slip casting and pressureless sintering, Ceram Int 27 (2001) 591–596. https://doi.org/10.1016/S0272-8842(01)00006-2.
- 99. B. Bitterlich, J.G. Heinrich, Aqueous tape casting of silicon nitride, J Eur Ceram Soc 22 (2002) 2427–2434. https://doi.org/10.1016/S0955-2219(02)00029-8.
- 100.K. Liu, C. Zhang, B. Li, S. Wang, F. Cao, Synthesis of porous silicon nitride-boron nitride composites by gel-casting and PIP, J Mater Eng Perform 23 (2014) 2829–2833. https://doi.org/10.1007/S11665-014-1064-Y/FIGURES/4.

- 101.Rolf Janssen*, Sven Scheppokat1, Nils Claussen, 2Tailor-made ceramic-based components—Advantages by reactive processing and advanced shaping techniques. Journal of the European Ceramic Society. 2008; 28: 1369–1379.
- 102.Lin T, Liu S, Ji Z, Shao H, Hao J. Vitrified bond diamond grinding wheel prepared by gel-casting with 3Dprinting molds. Diam Relat Mater. 2020; 108:1–7
- 103. Mark R. Cutkosky, Fritz B. Prinz, A Manufacturing Interface for 3D Design, NSF MIP-9617994, MIP-9618050. Stanford University. 1999;1-26.
- 104.P P Zhou, G QWu, Y Tao, X Cheng, J Q Zhao and H Nan, Optimization of the injection molding process for development of high-performance calcium oxide -based ceramic cores. Mater. Res. Express 2018; 5: 1-11.
- 105. Adrian Benitez Lozano, Santiago Henao Álvarez, Carlos Vargas Isaza and Wilfredo Montealegre-Rubio, Analysis and Advances in Additive Manufacturing as a New Technology to Make Polymer Injection Molds for World-Class Production Systems. Polymers. 2022; 14: 1-20.
- 106.Ognen Tuteski, Atanas Kočov, Mold Design And Production By Using Additive Manufacturing (Am) Present Status And Future Perspectives. International Scientific Journal "Industry 4.0". 2018;3: 82-85.
- 107. A. G. Cooper, S. Kang, J. Stampfl and F. B. Prinz, "Fabrication of ceramics parts for a miniture jet engine application using mold., Ceramic Transactions. 2000; 108:389-398.
- 108.K. Liu, C. Zhou, F. Chen, H. Sun, K. Zhang, Fabrication of complicated ceramic parts by gelcasting based on additive manufactured acetone-soluble plastic mold, Ceramics International. 2020; 46: 25220-25229.
- 109. Norrul Hafizan, Ab Wahab, Nor Hayati Saad, Norazne Nasi, Abdul Rahim Mahamad Sahab, Plaster Mold Selection for Ceramic Slip Rotary Molding System (CSRM). Journal of Mechanical Engineering. 2017; 4: 109-120,
- 110. Xuewu Lia, Xiaohui Fana, *, Na Nib,c, *, Xiaofeng Zhaoa, Chuanwei Lid, Ping Xiao, Continuous alumina fiber-reinforced yttria-stabilized zirconia composites with high density and toughness; as: Xuewu Li, et al., Journal of the European Ceramic Society https://doi.org/10.1016/j.jeurceramsoc.2019.12.041.
- 111.G. Amirthan ^a, A. Udayakumar ^b, V.V. Bhanu Prasad ^c, M. Balasubramanian ^a Properties of Si/SiC ceramic composite subjected to chemical vapour infiltration 2009 35 2601-2607
- 112.E.D. Rodeghiero et al. / Materials Science and Engineering A244 (1998) 11–21 Materials Science and Engineering A244 (1998) 11–21.
- 113. Guoin ZHENG, Hideaki SANO, Yasuo UCHIYAMA, Kazuo KOBAYASHI, Kunio SUZUKI and Huiming CHENG* Preparation and Fracture Behavior of Carbon Fiber/SiC Composites by Multiple Impregnation and Pyrolysis of Polycarbosilane, Journal of the Ceramic Society of Japan 106 [12] 1155-1161 (1998).
- 114.S.V. Raj, Development and characterization of hot-pressed matrices for engineered ceramic matrix composites (E-CMCs). Ceramic International. 2019;45: 3608-3619.
- 115.S. D. Oguntuyi· O. T. Johnson· M. B. Shongwe, Spark Plasma Sintering of Ceramic Matrix Composite of ZrB2 and TiB2: Microstructure, Densification, and Mechanical Properties—A Review. Metals and Materials International. 2021;27:2146–2159.
- 116.F. Uhlmann, et al., Preparation and characterization of ZrB2 and TaC containing Cf/SiC composites via Polymer-Infiltration-Pyrolysis process, J Eur Ceram Soc (2017), http://dx.doi.org/10.1016/j.jeurceramsoc.2016.12.048
- 117. J. Magnant a, R. Pailler a, Y. Le Petitcorps a, L. Maillé a,*, A. Guette a, J. Marthe a, E. Philippe b [117] Fiber-reinforced ceramic matrix composites processed by a hybrid technique based on

- chemical vapor infiltration, slurry impregnation and spark plasma sintering. Journal of the European Ceramic Society. 2013; 33:181–190.
- 118.M. Szutkowska, Fracture toughness of advanced alumina ceramics and alumina matrix composites used for cutting tool edges. Journal of Achievements in Materials and Manufacturing Engineering. 2012; 54: 202-10.
- 119.Laurent, Ch., Peigney, A., Dumortier, O. & Rousset, A. Carbon nanotubes—Fe—alumina nanocomposites. Part II: Microstructure and mechanical properties of the hot-pressed composites. Journal of the European Ceramic Society. 1998;18: 2005–13.
- 120. E. Volkmann, K. Tushtev, D. Koch, C. Wilhelmi, J. Göring, K. Rezwan; Assessment of three oxide/oxide ceramic matrix composites: Mechanical performance and effects of heat treatments. Composites Part A. 2015; 68:19–28
- 121. Yeong-Kyeun Paek, Ender Suvaci and Gary L. Messing, Preparation and Fracture Behavior of Alumina Platelet Reinforced Alumina–Monazite Composites. Materials Transactions. 2002; 43: 3262 65.
- 122. M.C. Corrêa De Sá, B. De Moraes, C.N. Elias, J.D. Filho, L. Guimarães De Oliveira, Mechanical properties of alumina-zirconia 643 composites for ceramic abutments, Materials Research. 7(2004) 643-649. https://doi.org/10.1590/S1516-14392004000400021.
- 123.L.M. Navarro, P. Recio, J.R. Jurado, P. Duran, Preparation and properties evaluation of zirconia-based/Al₂0₃ composites as electrolytes for solid oxide fuel cell systems Part III Mechanical and electrical characterization, J Mater Sci 30(1995) 1949-1960. https://doi.org/10.1007/BF00353015.
- 124. A. Kailer, M. Stephan, On the feasibility of the Chevron Notch Beam method to measure fracture toughness of fine-grained zirconia ceramics, Dental Materials. 32 (2016) 1256–1262. https://doi.org/10.1016/j.dental.2016.07.011.
- 125.130. J. Chłędowska, J. Wyrwa, M. Rękas, T. Brylewski, Effects of Aluminum Oxide Addition on Electrical and Mechanical Properties of 3 mol% Yttria-Stabilized Tetragonal Zirconia Electrolyte for IT-SOFCs, Materials. 15 (2022). https://doi.org/10.3390/ma15062101.
- 126. M. RÜHLE, N. CLAUSSEN, A. H. HEUER, Transformation and Microcrack Toughening as Complementary Processes in ZrO₂-Toughened Al₂O₃. Journal of the American Ceramic Society. 1986; 69: 195-97.

Chapter II

Experimental & Characterization techniques

This chapter presents characterization techniques used for the evaluation of various ceramic systems studied in terms of phases present, their microstructures, physical properties and mechanical properties.

2.1 Powder characterization: X- ray diffraction study - determination of structure

X-ray Diffraction (XRD) is an essential analytical method in material science, providing information about the crystallographic structure and chemical composition of materials. It involves directing a monochromatic X-ray beam onto a sample and measuring the diffracted X-rays to obtain information about its atomic and molecular structure. The diffraction pattern produced by XRD is a unique identifier for each material, analogous to a fingerprint's uniqueness to an individual. These patterns, characterized by distinctive peaks and troughs, indicate the material's internal crystal lattice and can reveal the existence of different phases, the size of crystallites, and the level of crystallinity. The ability of XRD to detect subtle variations in atomic arrangements is particularly valuable for the study of polycrystalline materials.

A standard X-ray Diffraction (XRD) apparatus comprises of an X-ray generator, a sample holder at the centre of the setup, optics to direct the X-rays, and a detector arranged in a concentric configuration.

Bragg's Law:

Bragg's Law is a fundamental principle governing X-ray diffraction, providing a mathematical relationship that explains the conditions for constructive interference of X-rays scattered by a crystal lattice.

The mathematical expression for Bragg's Law is:

 $n\lambda = 2d\sin\theta$ -

Here,

- *n* is an integer representing the order of reflection,
- λ is the wavelength of the incident X-rays,
- d is the spacing between atomic planes in the crystal lattice, and
- θ is the angle of incidence.

When monochromatic X-rays with a wavelength (λ) strike a crystal lattice, they interact with the electron cloud surrounding the nucleus of atoms within the lattice, leading to scattering. According to

Bragg's Law, constructive interference—where waves reinforce each other—occurs when the path difference between X-rays scattered by adjacent atomic planes is an integer multiple of the wavelength. This constructive interference results in distinct bright spots on a diffraction pattern.

Figure 2.1 illustrates the schematic of Bragg's Law. In this phenomenon, monochromatic X-rays with a wavelength (λ) and planar wave characteristics are incident upon crystal planes having Miller indices (hkl). The crystal lattice, composed of atomic planes, reflects these incident X-rays at the same angle. The scattered X-rays undergo constructive and destructive interference, depending on the path difference between X-rays scattered from adjacent atomic planes. Constructive interference occurs when the path difference is an integer multiple of the X-ray wavelength, forming diffracted X-rays.

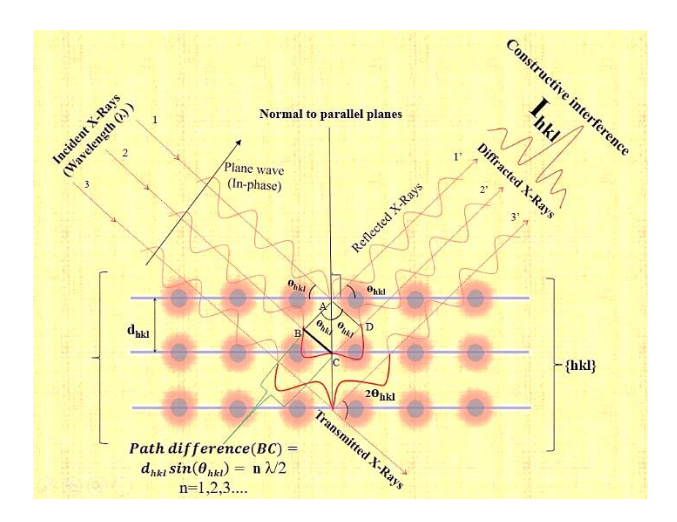


Fig.2.1. Schematic representation of Bragg's Law [1].

Applications of XRD:

XRD is widely used for various materials science, chemistry, biology, and engineering applications. Some of the applications include:

- ✓ Identifying and characterizing crystalline phases in materials
- ✓ Determining the crystal structure of materials
- ✓ Quantifying the phase composition of materials
- ✓ Studying the orientation and texture of materials
- ✓ Measuring the strain and stress in materials
- ✓ Analyzing the microstructure of materials
- ✓ Studying the thermal and mechanical properties of materials
- ✓ Identifying and characterizing defects in materials

2.3 Rheological characterization: Rheology of ceramic suspensions and viscosity

Viscosity in a fluid is caused by the internal friction between different layers of the fluid as they move past each other. This friction is due to the molecular interactions between the particles in the fluid. The stronger the interactions, the higher the viscosity of the fluid. Fluids, whether they are liquids or gases, consist of molecules that are in constant motion. In a liquid, the molecules are relatively close together and have strong intermolecular forces, allowing them to maintain a more ordered arrangement compared to gases. These intermolecular forces, such as van der Waals forces or hydrogen bonding, play a key role in determining a fluid's viscosity. When a force is applied to a fluid, such as when it is flowing or when an object is moving through it, the molecules in the fluid start to move. However, due to the intermolecular forces, the molecules tend to resist this motion and exert a drag force on each other. This internal friction between adjacent layers of the fluid results in the resistance to flow, which we perceive as viscosity. To visualize this, imagine a stack of playing cards. If you slide one card over another, there is some resistance due to the friction between the cards. Similarly, in a fluid, adjacent layers of molecules experience resistance as they slide past each other.

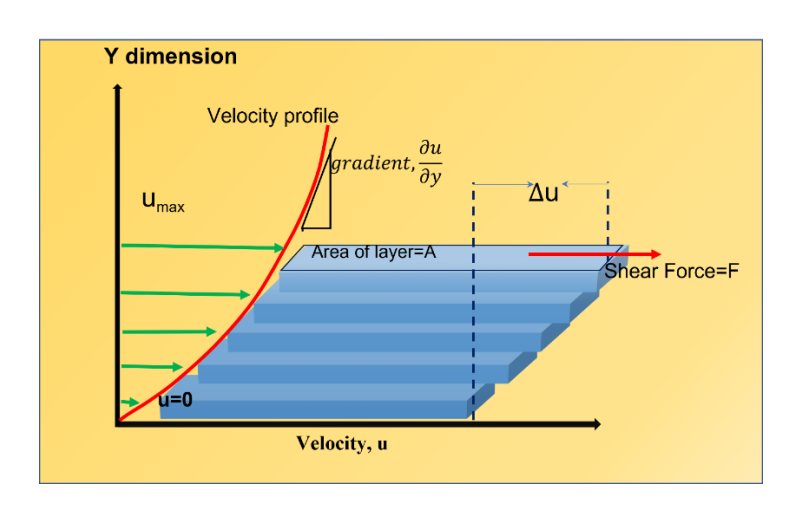


Fig.2.2. Visualization of viscosity of fluid [2].

The magnitude of this resistance or internal friction depends on various factors. One important factor is the strength of the intermolecular forces. Liquids with stronger intermolecular forces tend to have higher viscosities because the molecules are more strongly held together and require more energy to move past each other. Temperature also plays a significant role in determining viscosity. As the temperature of a fluid increases, the molecules gain more kinetic energy and move more rapidly. This increased motion disrupts the intermolecular forces, reducing the internal friction and decreasing the viscosity. For example, honey is more viscous at room temperature but becomes less viscous when heated. Additionally, the shape of the molecules and their size can affect viscosity. Long, tangled

molecules or large particles in a fluid can hinder the flow and increase viscosity. This is why substances like honey or molasses, which have complex molecular structures or larger particles, are more viscous than simple liquids like water.

The general formula for viscosity is expressed using Newton's law of viscosity, which relates the shear stress (τ) to the velocity gradient (du/dy) in a fluid. The equation is as follows:

$$\tau = \mu * (du/dy)$$

In this equation:

 τ represents the shear stress, which is the force per unit area (F/A) acting parallel to the direction of flow. μ (mu) is the dynamic viscosity of the fluid, which is a measure of the fluid's resistance to flow. (du/dy) represents the velocity gradient, which is the change in velocity (u) with respect to the distance (y) perpendicular to the direction of flow.

Essentially, the equation states that the shear stress in a fluid is directly proportional to the dynamic viscosity and the velocity gradient. The dynamic viscosity is a property of the fluid, and it determines how easily the fluid flows and how resistant it is to deformation. It's important to note that the equation assumes that the fluid behaves in a linear, Newtonian manner, where the shear stress is directly proportional to the velocity gradient. However, some fluids, known as non-Newtonian fluids, do not follow this relationship and have more complex viscosity behavior. Viscosity can be divided into two types: dynamic viscosity and kinematic viscosity. These two types are based on different properties and provide different insights into the flow behavior of fluids.

Dynamic Viscosity (μ):

Dynamic viscosity, denoted by the symbol μ (mu), is a measure of a fluid's resistance to shear or tangential stress when an external force is applied. It quantifies the internal friction within the fluid as adjacent layers slide past each other. Higher dynamic viscosity indicates greater resistance to flow. Mathematically, dynamic viscosity is related to the shear stress (τ) and the velocity gradient (du/dy) through Newton's law of viscosity:

$$\tau = \mu * (du/dy)$$

The SI unit for dynamic viscosity is the pascal-second (Pa·s), but other common units include poise (P) and centipoise (cP).

Ceramics processing relies heavily on the flow behavior of slurries in various stages of production. Understanding the viscosity of these slurries is essential for achieving the desired material properties and product quality. In 3D printing, the flow characteristics of the ceramic material directly impact the printing process and the final structural integrity of the printed objects. Fluids, as a broad category, can be classified into two main types: Newtonian and Non-Newtonian. The distinction lies in how these fluids respond to applied forces, particularly with changes in shear rate. Newtonian fluids, such as water and motor oil, adhere to Newton's Law of Viscosity, maintaining a constant viscosity regardless of variations in shear rate.

On the other hand, non-Newtonian fluids exhibit a more diverse behavior, with their viscosity changing in response to alterations in shear rate. Slurries, common in various industrial processes, fall under the umbrella of non-Newtonian fluids. The viscosity of slurries is influenced by factors such as particle size, shape, concentration, pH and the nature of the suspending liquid. Within the non-Newtonian category, there are several subtypes, each characterized by unique rheological properties: This diverse category includes several subtypes, each characterized by unique rheological properties:

- **Plastic:** These fluids exhibit a constant viscosity up to a certain shear stress, beyond which they start to flow.
- **Pseudoplastic (Shear-Thinning)**: Also known as shear-thinning fluids, these substances experience a decrease in viscosity as shear stress increases. Tomato ketchup serves as a classic example of a pseudoplastic fluid.
- **Rheopectic:** In contrast to pseudoplastic fluids, rheopectic fluids become more viscous over time when subjected to constant shear stress.
- **Thixotropic:** These fluids, like some paints, become less viscous when agitated or sheared, only to gradually regain their viscosity when left undisturbed.
- **Dilatant (Shear-Thickening):** The viscosity of dilatant fluids, such as a mixture of cornstarch and water, increases with shear rate, resulting in a thicker consistency.

The rheological characteristics of slurries can vary, and they often demonstrate non-Newtonian behaviour [16], particularly exhibiting shear-thinning or shear-thickening properties depending on their composition and conditions. Understanding these rheological nuances is essential in optimizing the handling and processing of slurries across diverse industrial applications.

The ability to finely tune these rheological properties not only enables the production of high-quality ceramic objects with intricate geometries but also opens up new possibilities for the integration of ceramics in a wide range of industrial and technological applications. As advancements in rheological

control continue to evolve, the potential for leveraging ceramics in additive manufacturing and beyond becomes increasingly promising.

2.4 CNC profile cutter and 3D printer: EPS and ABS molds preparation

The subtractive manufacturing process of EPS molds utilizes a specialized machine known as a CNC 3D profiler cutter for EPS (Expanded Polystyrene) molding. EPS, commonly known as Styrofoam, is a lightweight and versatile material often used in packaging, insulation, and construction. According to computer-generated designs, the CNC profiler cutter precisely carves EPS foam blocks into intricate shapes and molds. Using computer numerical control (CNC) technology, the profiler cutter follows a programmed path to carve the EPS foam block layer by layer, creating highly accurate and detailed three-dimensional shapes. The machine typically employs a rotating cutting tool, such as a hot wire or router, to remove material from the foam block. One of the key advantages of using a CNC 3D profiler cutter for EPS molding is its ability to produce complex and customized molds quickly and efficiently. Traditional methods of carving EPS foam by hand are time-consuming and labor-intensive, often resulting in inconsistencies and inaccuracies.



Figi. 2.3. CNC-3D profile cutter (SVP laser technologies, India)

3D printing is an additive manufacturing process that creates a physical object from a three-dimensional digital model or computer-aided design (CAD), typically by laying down thin layers of material in liquid or powdered form, such as plastic, metal, or cement, followed by fusing the layers successively. Each layer represents a horizontal cross-section of the final product, thinly deposited. Each technique offers access to different materials as well. While metals, optically transparent materials, and rubber-like items can be 3D printed, plastics are the most commonly used material.

Unlike traditional subtractive manufacturing techniques, which involve cutting or machining the object out of a larger block, 3D printing produces complex shapes with less material.

Fused filament fabrication (FFF) is one of the most popular and accessible methods of 3D printing, particularly for plastic materials. This process, often referred to as fused deposition modeling (FDM), involves the extrusion of thermoplastic filament through a heated nozzle, which then deposits the material layer by layer to create the desired object [5]. In an FFF 3D printer, the filament is typically housed on a spool and fed through a heated extruder assembly. The extruder heats the filament to its melting point, allowing it to flow smoothly through the nozzle. As the nozzle moves along predefined paths, controlled by the 3D model, it deposits the molten plastic material onto a build platform or previous layers, where it quickly solidifies.



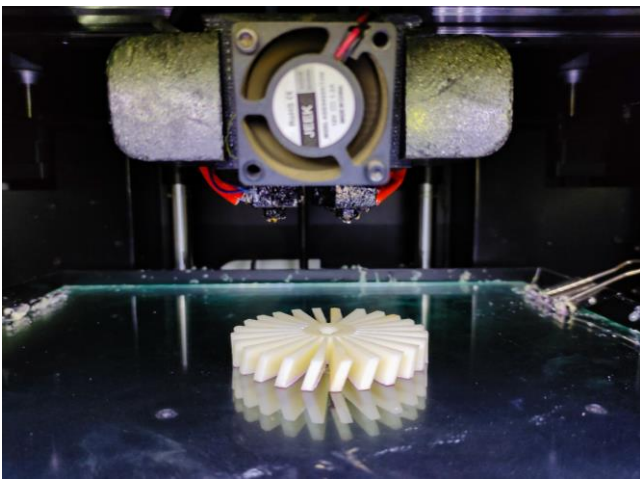


Fig. 2.4. 3D printer

Fig. 2.5. Printing process

Layer thickness and X-Y resolution are expressed in dots per inch (dpi) or micrometers (μ m) as printer resolution. Approximately 100 μ m (250 dpi) is the typical layer thickness. A few devices are capable of printing layers as thin as 16 μ m (1600 dpi). The particles have a diameter of around 50 to 100 μ m (510 to 250 dpi). One of the critical advantages of FFF 3D printing is its versatility in material selection. Many thermoplastic filaments are available, each with unique properties and applications. Common materials include PLA (polylactic acid), ABS (acrylonitrile butadiene styrene), PETG (polyethylene terephthalate glycol), TPU (thermoplastic polyurethane), and more. These materials offer varying levels of strength, flexibility, temperature resistance, and surface finish, allowing diverse parts and prototypes to be produced.

Tools and Technology used for 3D Printing

Different Software packages can aid in each different stage of the design process; from CAD design, to STL files preparation. Some of the best software for CAD modeling include:

- 1. Solidworks
- 2. Rhinoceros
- 3. Fusion 360
- 4. Onshape
- 5. Tinker CAD STL

Some of the popular slicing softwares are:

- 1. Cura
- 2. Simplify3D

The utilization of 3D printing technology for creating plastic molds has brought about a significant transformation in the manufacturing process. This innovation provides a quicker and more economical option than conventional mold production methods. By employing fused filament-based plastic materials, it is possible to create complex mold designs with great accuracy and quickly. This method facilitates expedited prototype and iteration, enabling manufacturers to evaluate and enhance their designs effectively. In addition, 3D-printed plastic molds are well-suited for small-scale production, offering versatility for customized or low-volume manufacturing requirements.

2.5 Furnaces: Heat treatments

High-temperature furnaces for binder removal and sintering ceramics are important in manufacturing, providing controlled environments for precise thermal treatments. These furnaces can ramp from room temperature (RT) to 1750°C at a rate of 0.5°C per minute, allowing for gradual heating to prevent thermal shock and ensure uniform binder removal. Following binder removal, these furnaces are used in sintering, where ceramic green bodies are heated to elevated temperatures to fuse particles and achieve densification. The sintering temperature depends on the specific ceramic material and desired properties but typically ranges from several hundred to several thousand degrees Celsius. High-temperature furnaces offer the necessary temperature control and stability to achieve optimal sintering conditions, resulting in important, dense ceramic components with enhanced mechanical properties.



Fig. 2.6. High Temperature tube Furnace for sintering up to 1750 °C in Inert gas

2.6 Archimedes technique: Density measurement

Based on Archimedes' Principle, the Water Displacement Method is a simple approach used to calculate the density of solid objects. In this procedure, the object being evaluated for density is immersed in a vessel that is filled with water. When the object moves through the water, it increases the water level. By precisely measuring the change in water level prior to and following the submersion of the object, one can ascertain the volume of water displaced. The density of an object can be estimated by applying the formula after the volume of water displaced and the object's mass are known

$$Density = \frac{Mass ext{ of Object}}{Volume ext{ of Water Displaced}}$$

This method is beneficial for irregularly shaped objects or those with complex geometries, where direct volume measurement may be challenging. The Water Displacement Method offers a simple yet effective means of density determination by relying on the principle that the buoyant force experienced by the object equals the weight of the water displaced. Firstly, the specimen is weighed in the air (Wa) to obtain its mass. Then, the specimen is submerged in distilled water at 24°C, and its weight underwater (Ww) is recorded. According to Archimedes' principle, the difference between the two weights (Wa - Ww) represents the weight of the water displaced by the volume of the solid specimen.

The specific gravity (SG) and density of the specimen can be calculated using the following formulas:

$$SG = rac{W_a}{W_a - W_w} imes SG_{ ext{of water}}$$

$$ho = rac{W_a}{W_a - W_w} imes
ho_L$$

Where

W_a= mass of the sample in air,

W_w= mass of the sample in water

SG= Specific Gravity of the immersing fluid

 ρ_L = density of water (1g/cc)

2.7 Vickers indentation: Hardness measurement

Vickers Microhardness Test:

In materials science, hardness refers to a material's resistance to localized deformation or indentation, such as scratches. It is a key property indicating a material's ability to withstand mechanical forces without permanent deformation or fracture. The American Society for Metals (ASM) defines hardness as a material's resistance to permanent indentation or penetration by a harder body, highlighting its significance in assessing material durability and wear resistance. Harder materials typically exhibit greater wear resistance, and hardness often correlates with tensile strength in metals.

The Vickers hardness test method uses a diamond indenter shaped like a right pyramid with a square base and an angle of 136 degrees between opposite faces, subjecting the material to a load ranging from 1 to 100 kgf. This full load is typically applied for 10 to 15 seconds. Post-removal of the load, the two diagonals of the indentation on the material's surface are measured using a microscope, and their average is calculated. The Vickers hardness is then determined by dividing the load (in kgf) by the indentation's area (in square mm).

This approach offers precise measurements and is versatile and applicable to a broad range of materials, including metals, plastics, and ceramics. Additionally, Vickers hardness can be estimated by evaluating the projected area of the impression, a process achievable through image analysis. Although studies on this are limited, measuring diagonals remains the preferred method for assessing hardness, even with distorted indents.

The Vickers hardness test encompasses two distinct force ranges: "Microindentation Vickers" (10g - 1kg) and "Macroindentation Vickers" (1 - 100kg), tailored to varying testing needs. Despite the differing force ranges, both categories utilize the same indenter, ensuring a continuous Vickers hardness scale across the complete range of metal hardness (usually HV100 – HV1000).

This indentation technique maintains a nearly constant HV value across diverse test loads, proving statistically precise under varying conditions, provided the specimen exhibits reasonable homogeneity. This consistent performance across different load settings ensures reliability in hardness values, enhancing its usefulness in material analysis and testing. The Vickers hardness test allows for

39

evaluations at different scales, including macro, micro, and nano indentations, enabling comprehensive hardness characterization in ceramics.

A schematic illustrating the Vickers indentation is depicted in Figure 2.7. This diagram displays the square pyramid-shaped diamond indenter tip used in the Vickers test and the diagonals of the indentation it leaves on the sample. Various types of indentation tests categorized based on the test force and the indenter type are illustrated in the flow chart depicted in Figure 2.7 for easy visualization.

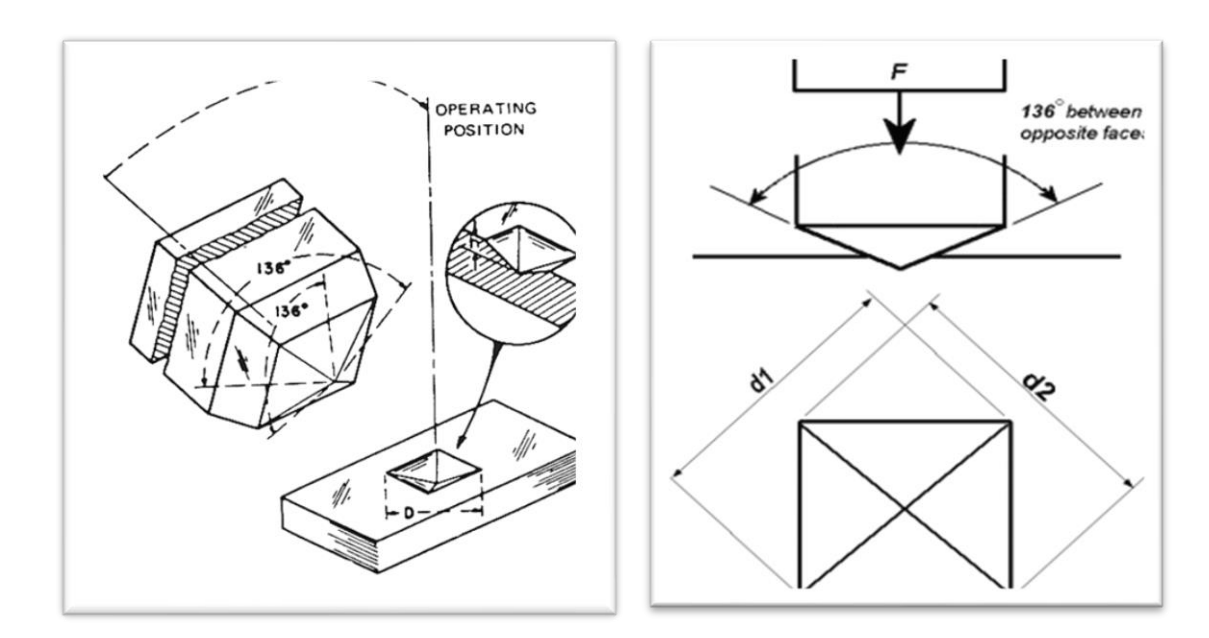


Fig. 2.7. Schematic illustrating the Vickers diamond pyramid indenter and the indentation produced [13].

The Vickers hardness number (HV) is calculated using a formula correlating the applied load to the surface area of the indentation.

$$HV = \frac{Applied\ force\ F\ in\ kgf}{Surface\ area\ the\ indentation\ in\ mm^2} = \frac{2F\ Sin\left(\frac{a^0}{2}\right)}{d^2} = 1.8544\frac{F}{d^2}$$

Where:

- F represents the applied load in kgf (kilogram-force).
- d denotes the arithmetic mean diagonal of the indentation in millimeters ((d1+d2)/2).
- α^0 signifies the angle between opposite faces of the square-based pyramid (136 degrees).

The Vickers hardness values are typically reported as, for instance, "300 HV/10," indicating a Vickers hardness of 300 attained using a 10 kgf test force.

2.8 Universal testing machine (UTM): Flexural strength and fracture toughness

The Universal Testing Machine (UTM) performs material testing, including the three-point bend test, which assesses flexural strength and fracture toughness. By subjecting specimens to bending stress until fracture, this method yields essential data for evaluating material behavior and fracture resistance, which is crucial in industries like aerospace and automotive for ensuring structural integrity.





Fig. 2.8. Universal texting machine (INSTRON 5982 UTM)

Flexural strength(σ):

Flexural strength was determined from the measured force on the 2 kN load cell. Cross head speed of 0.5mm/min was used. Flexural strength was calculated from the formula as per ASTM C1161-13 standard.

$$\sigma = \frac{3FL}{2BD^2}$$

 σ = Flexural strength (MPa), F = Load (N), L = Supporting span (mm), B = Width of test beam (mm) and D = Depth or thickness of test beam (mm).

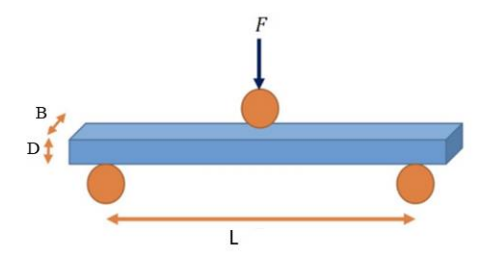


Fig. 2.9. 3-point bend test specimen

Fracture toughness(K_{Ic}):

Fracture toughness is measured by the direct crack method. The pre-cracked beam notch (pb notch) was cut with a precision diamond saw (Buehler ISOMET 4000) and a low diamond content metal bound wafering blade (Buehler series 7LC; 76mm 0.15mm). The revolution and cutting speed were 100 rpm and 1 mm/min. Following the initial cut, a saw with a razor blade mounted on it was used to make a sharp cut while applying diamond paste to ensure that the final pb notch geometry complied with ASTM C1421–10 standard

$$K_{Ipb} = g \left[\frac{P_{max} S_0 10^{-6}}{BW_2^3} \right] \left[\frac{3[a/W]^{1/2}}{2[1-a/W]^{3/2}} \right]$$

And

$$g = g(a/W) = A_0 + A_1(a/W) + A_2(a/W)^2 + A_3(a/W)^3 + A_4(a/W)^4 + A_5(a/W)^5$$

 K_{Ipb} measures fracture toughness (K_{Ic} as per ASTM standard) (MPa \sqrt{m}), g = g(a/W) = function of the ratio a/W for three-point flexure, $P_{max} =$ maximum force (N), $S_0 =$ span length (mm), B = side to side dimension of the test specimen perpendicular to the crack length (depth) (mm), W = top to bottom dimension of the test specimen parallel to the crack length (depth) (mm), and W = crack length (mm).

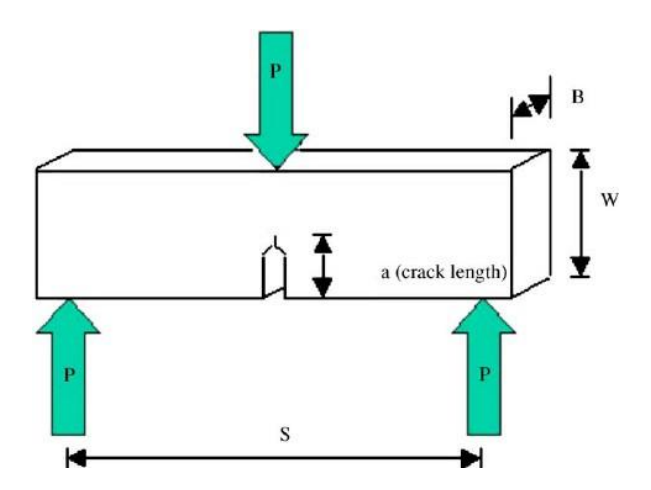


Fig. 2.10. Precracked beam specimen

To meet the requirements of ASTM C1421–10 [25] standard for a three-point flexure test, the pb notches' geometry parameters are chosen to be close to the upper limits in $5 \le S_0/W \le 10$, $0.35 \le a/W \le 0.60$, with a maximum error of 1.5%, while avoiding overcuts.

These parameters can ensure that the tests are carried out with high accuracy and precision, while also meeting the requirements of the ASTM C1421-10 standard.

2.9 Dielectric spectroscopy: Dielectric constant and dielectric loss

Introduction

For many electronic applications, a measurement of the dielectric materials can yield vital design parameter information. Its dielectric qualities can be connected to, for instance, the frequency of a dielectric resonator, the impedance of a substrate, or the loss of a cable insulator. Enhancing ferrite, absorber, and package designs can also benefit from the information. Knowledge of dielectric characteristics has also been found to be beneficial for more contemporary uses in the food, medical, automotive, and aerospace sectors.

Dielectric constant

If a material can retain energy in the presence of an applied external electric field, it is categorized as dielectric. When a parallel plate capacitor is exposed to a DC voltage source, the presence of a dielectric substance between the plates stores more charge than the absence of any material, or vacuum, between the plates. Because the dielectric material balances the charges at the electrodes, the capacitor's storage capacity is increased. The dielectric constant is correlated with the capacitance of the dielectric substance. A parallel plate capacitor stores more charge when a dielectric substance (a vacuum) is present between the plates than when a DC voltage source V is positioned across it. The dielectric constant, often known as relative static permittivity, is denoted by ε_r . $\varepsilon_r = \varepsilon/\varepsilon_0$, where ε_0 is the electric permittivity of empty space (=8.854x10⁻¹² F/m) and ε is the material's static permittivity.

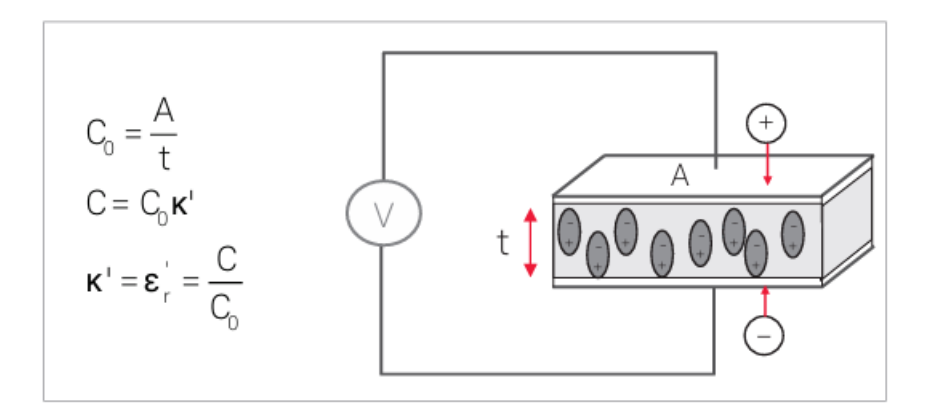


Figure 2.11. Parallel plate capacitors, DC case [16].

where C and $C_{0 \text{ are}}$ capacitance with and without dielectric, $\kappa' = \epsilon_r$ is the original dielectric constant or permittivity. 'A' is the area of the capacitor plates and 't' is the distance between them. By neutralizing charges at the electrodes that would otherwise contribute to the external field, the dielectric material enhances the capacitor's storage capacity. The above-mentioned equations show how the dielectric material's capacitance and dielectric constant are connected.

Dielectric loss/ Tangent loss

The loss of energy required to heat a dielectric substance in a fluctuating electric field is known as dielectric loss. In alternating field, electric permittivity is a complex quantity with in-phase (ϵ_r) and out of phase (ϵ_r) components. The dielectric material and frequency are usually the primary determining factors. The Loss of Tangent, also known as tan delta $(\tan \delta)$, is used to assess dielectric loss.

$$\tan \delta = \epsilon_r''/\epsilon_r'$$
 (6)
= energy lost per cycle / energy stored per cycle

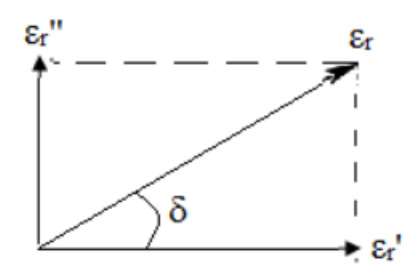


Figure 2.12. Loss tangent vector diagram [16].

2.10 Microstructural and Fractography analysis: Optical microscopy, field emission scanning electron microscopy and Transmission Electron microscopy

Filed emission Scanning electron microscopy

Electron microscopes were developed in the 1930s to overcome the limitations of optical microscopy and provide significantly greater magnification and resolution, surpassing that of optical instruments. When it comes to analysing and interpreting the microstructures of materials, scanning electron microscopy (SEM) is a potent technology widely utilized in material science. In the case of a Field Emission Scanning Electron Microscope (FE-SEM), a field-emission cathode in the electron gun of a SEM provides narrower probing beams at low as well as high electron energy, resulting in both improved spatial resolution and minimized sample charging and damage. The FE SEM interacts with an incoming electron beam and a solid sample. Electron bombardment of the specimen can generate diverse emissions, such as backscattered electrons, secondary electrons, Auger electrons, X-rays, visible photons, and more.

Secondary electrons occur when an incident electron collides with an electron in a sample atom. This collision causes the electron to be knocked out of its orbital shell, which can be used for image formation. It is capable of producing magnified images in the range of 10-100 nm. Back-scattered electrons (BSE) refer to electrons in a beam that are reflected from the material due to elastic scattering.

This scattering is mainly influenced by the atomic number, which provides more information about the distribution of elements in the sample.

The interaction of the incident electron beam with a material's surface results in X-ray generation within the material. When electrons are rearranged to fill vacant spaces in an atom's shell, the extra energy produced can be released as an X-ray rather than an Auger electron. This is similar to the procedure that is used to generate Auger electrons. X-rays have a unique energy specific to the element from which they originate to determine the composition of a sample.

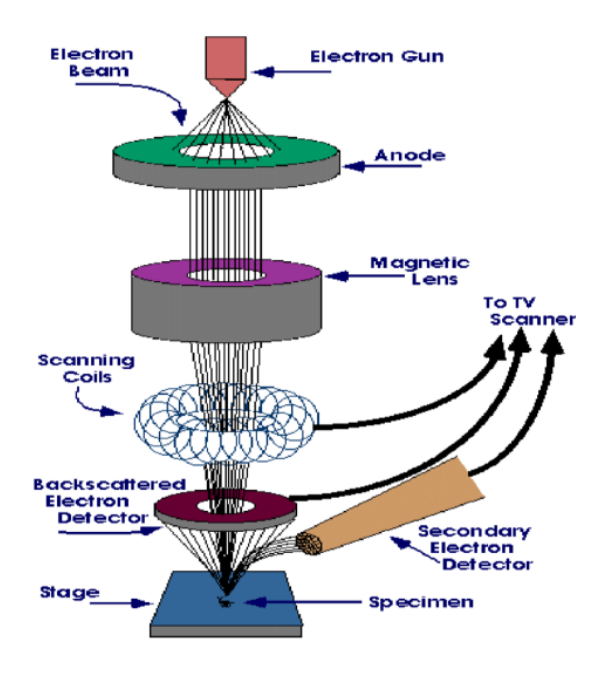


Fig.2.14. Schematic Diagram of FESEM [19].

A JEOL SEM 5600 LV and a JEOL FESEM 6330 FEG are the scanning electron microscopes (SEM) utilized in this work. A picture of the JEOL FESEM 6330 FEG is displayed in Figure 2.14. The sample used for scanning electron microscopy observation was sputtered with approximately 15 nanometres of gold to minimize the influence of charges.

Microstructures of the samples were studied using optical and FESEM images.

Transmission Electron Microscopy (TEM)

The transmission electron microscope (TEM) functions based on a concept that closely resembles that of the light microscope. The primary difference lies in the fact that light microscopes employ light beams to concentrate and form an image, whereas transmission electron microscopy (TEM) utilizes a beam of electrons to focus on the object and produce an image. Electrons have a comparatively shorter wavelength than light, which possesses a somewhat longer wavelength. The operation of a light microscope is based on the principle that an enhancement in resolution capability leads to a decrease

in the wavelength of light. Conversely, the transmission electron microscope (TEM) operates by illuminating the specimen with electrons, which enhances the resolution power and leads to a larger wavelength of electron transmission. Given that the electron's wavelength is around 0.005 nm, which is 100,000 times smaller than the wavelength of light, it follows that the transmission electron microscope (TEM) achieves a resolution roughly 1000 times greater than that of a light microscope. Research has demonstrated that the transmission electron microscope (TEM) can effectively observe incredibly particles, particles. the internal structures small such as virus

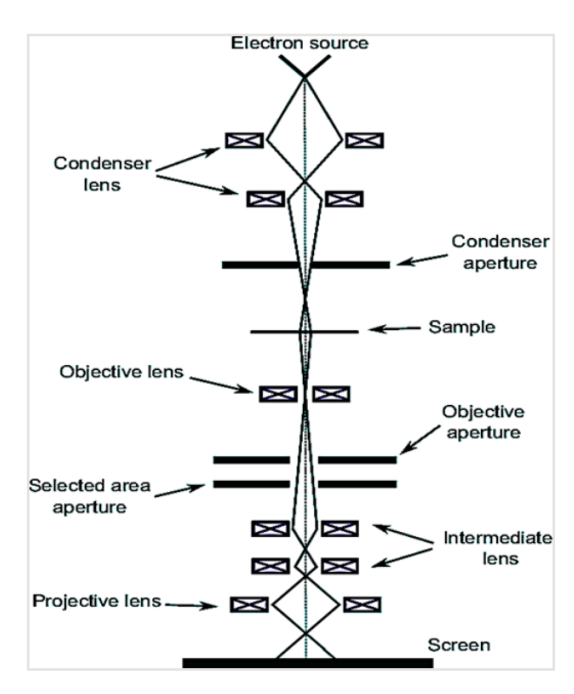


Fig..2.15. Instrumentation of the Transmission Electron Microscope [21].

Working principle of TEM

A TEM operates similarly to a slide projector. The projector produces light that passes through the slide. The structures and objects on the slide change the light as it moves through. This prevents the light beam from fully traversing the slide, resulting in obstruction. Directing the beam of light onto a surface creates a magnified version of the slide. Below is a comprehensive explanation of how a typical Transmission Electron Microscope works:

- The electron gun positioned in the upper part of the microscope generates a continuous flow of electrons with the same wavelength.
- Condenser lenses 1 and 2 concentrate the flow into a slender and unified beam. The first lens establishes the dimensions of the focused area of the electron beam on the sample. The

- second lens focuses the light to a precise point on the sample, converting it from a wide, dispersed area.
- The Condenser aperture restricts the electron beam by deflecting electrons that have high angles of incidence (those that are far from the optic axis, represented by the dotted line in the middle).
- A portion of the beam that makes contact with the specimen is transmitted.

 The objective lens focuses the transmitted part into a picture.
- Optional objective and focus Metal apertures constrain the beam, with the goal aperture increasing contrast by removing high-angle diffracted electrons and the chosen area aperture allowing users to evaluate regular electron diffraction by atom configuration.

The intermediate and projection lenses gradually magnify the image along the column. The operator's is illuminated by image beams hitting the phosphor picture screen. A wide spectrum of radiation from the electron beam's interaction with specimen electrons can reveal a lot about the sample. Elastic scattering and diffraction patterns do not lose energy. The transmission electron intensity may fluctuate due to the electron beam's inelastic interaction with electrons at dislocations, grain boundaries, and second-phase particles in the material. Both elastic and inelastic scattering can reveal much about the sample. Voltage boosts the TEM instrument's lateral spatial resolution. At 400 kV, TEM equipment has point-to-point resolutions exceeding 0.2 nm. High-voltage TEM equipment has stronger electron penetration because high-energy electrons interact less with matter. TEMs with high voltage handle thicker samples. Low TEM depth resolution. The TEM pictures depict electron scattering from a three-dimensional sample to a two-dimensional detector.

References:

1. J. Epp, X-ray diffraction (XRD) techniques for materials characterization

Materials Characterization Using Non-destructive Evaluation (NDE) Methods, 2016; 81-12

- 2. Richard R. Eley, Rheology and Viscometry, 2012; 1-37.
- 3. Sukhdeep Kaur, Manjit Sandhu, Jaipreet Kaur, Dielectric theory and its properties(IJETER), 2016; Volume 4, Issue 3
- 4. Shengting Fan, Physical properties and basic theory of dielectric, *IOP Conf. Ser.: Earth Environ. Sci,* 2021; 692 022122
- 5. N. Shahrubudin, T.C. Lee, R. Ramlan, An Overview on 3D Printing Technology: Technological, Materials, and Applications, Procedia Manufacturing, 2019; Volume 35: Pages 1286-1296
- 6. Chetan M. Thakar, Shailesh S. Parkhe, Ankit Jain, Khongdet Phasinam, G. Murugesan, Randy Joy Magno Ventayen, 3d Printing: Basic principles and applications, Materials today proceedings, 2022; Volume 51, Part 1: Pages 842-849
- 7. Alexander Ya. Malkin, Svetlana R. Derkach, Valery G. Kulichikhin, Rheology of Gels and Yielding Liquids, *Gels*, 2023; *9*(9): 715

- 8. Lafleur, P. G., & Vergnes, B. Polymer extrusion, 2014; page count- 352
- 9. Amar Kouadri, Embarek Douroum, Ahmed Ridha El
- Ouederni , Abdelylah Benazza , Samir Laouedj , Sofiane Khelladi, Assessment of mixing behaviors of non-Newtonian pseudoplastic fluids in short microdevices, International Communications in Heat and Mass Transfer, 2024; Volume 155: 107500
- 10. A.E. Giannakopoulos, P.-L. Larsson, R. Vestergaard, Analysis of Vickers Indentation, International Journal of Solids and Structures, 1994; Volume 31, Issue 19:Pages 2679-2708
- 11. B Daemi, <u>R Tomkowski</u>, <u>A Archenti</u>, High precision 3D evaluation method for Vickers hardness measurement, CIRP annals, 2020; Volume 69, Issue 1: Pages 433-436
- 12. Surya R. Kalidindi, Shraddha J. Vachhani, Mechanical characterization of grain boundaries using nanoindentation, Current Opinion in Solid State and Materials Science, 2014; Volume 18, Issue 4:Pages 196-204
- 13. J.M Antunes, A Cavaleiro, L.F Menezes, M.I Simões, J.V Fernandes, Ultra-microhardness testing procedure with Vickers indenter, Surface and Coatings Technology, 2002; 149: 27-35.
- 14.Standard Test Method for Flexural Strength of Advanced Ceramics at Ambient Temperature 1. https://doi.org/10.1520/C1161-13.
- 15. Standard Test Methods for Determination of Fracture Toughness of Advanced Ceramics at Ambient Temperature. https://doi.org/10.1520/C1421-10.
- 16. M.S. Venkatesh, G.S.V. Raghavan, An overview of dielectric properties measuring techniques, Canadian Biosystems Engineering, 2005; 47: 1-10.
- 17. Boris Mahltig, Thomas Grethe, High-Performance and Functional Fiber Materials—A Review of Properties, Scanning Electron Microscopy SEM and Electron Dispersive Spectroscopy EDS, *Textiles*, 2022; 2(2): 209-251
- 18. Taryl L. Kirk, Chapter Two A Review of Scanning Electron Microscopy in Near Field Emission Mode, Advances in Imaging and Electron Physics, 2017; Volume 204: Pages 39-109
- 19. Weilie Zhou, Robert Apkarian, Zhong Lin Wang & David Joy, Fundamentals of Scanning Electron Microscopy (SEM), Springer, New York, NY, 2006; page 1-40
- 20. Kalsoom Akhtar, Shahid Ali Khan, Sher Bahadar Khan, Abdullah M. Asiri, Scanning electron microscopy: principle and applications in Nanomaterials characterization Handbook of Materials Characterization. Springer, Cham, 2018
- 21. C.Y. Tang, Z. Yang, Chapter 8 Transmission Electron Microscopy (TEM) Membrane Characterization, 2017; Pages 145-159.
- 22. <u>Jian Guo Wen</u>, Sardela, M. (eds), Transmission Electron Microscopy, Practical Materials Characterization. Springer, New York, NY, 2014
- 23. David B. Williams, C. Barry Carter, Transmission Electron Microscopy, (2009)

- 24. T.Y. Kam, C.M. Chen, S.H. Yang, Material characterization of laminated composite materials using a three-point-bending technique, Composite Structures, 2009; Volume 88, Issue 4: Pages 624-628
- 25. Sebastian Huayamares , Dominik Grund , Iman Taha, Comparison between 3-point bending and torsion methods for determining the viscoelastic properties of fiber-reinforced epoxy, Polymer Testing, 2020; Volume 85: 106428

Chapter III

Net shaping of ceramic components

Introduction

Ceramics are used in various specialised fields due to its exceptional properties such as high strength, hardness, resistance to oxidation at high temperatures, resistance to corrosion, low density, chemical stability, and erosion resistance. Additionally, ceramics are relatively inexpensive. Owing to their hardness and high melting temperatures and the challenges associated with shaping them into final products [1,2].

The conventional method of producing ceramics utilising colloidal processing techniques and consolidating them in specifically prepared dies is widely recognised and established. The manufacturing processes of die-casting, slip-casting, and injection molding have been evaluated to determine their advantages and disadvantages [3-5]. We understand the necessity to enhance the existing powder processing methods in order to manufacture complex ceramic components with intricate geometries, while minimising expenses. The rapid prototyping (RPT) approach has been developed global interest due to its ability to rapidly refine designs and efficiently integrate systematic enhancements at each stage [6]. Many additive manufacturing (AM) processes include fabricating the desired product layer by layer using a computer-aided design (CAD) file [7]. This allows for easy and fast design modifications, if necessary, at a relatively low expense. Selective laser sintering (SLS) and three-dimensional (3D) printing techniques have been investigated as powder processing methods for creating solid components from ceramics and metals [8]. These techniques, complications arise when additional phases need to be incorporated into the matrix phase in order to produce a product with a consistent microstructure and enhanced properties. One additional challenge with the aforementioned methods is that when the ceramic part is constructed layer by layer, there is a high probability of weak regions forming at the connections between the layers [9]. Gelcasting is a method that involves creating easily free-flowing slurries of ceramic or metal powders and cast them into molds that can be discarded. This technology is becoming more significant alternative SLS direct 3D to or printing methods. We have developed a technique, rapid prototyping and gelcasting (RPGC) that allows for the production of relatively big and intricate components in a cost-effective manner, typically in a single step [6]. More details are given in section 1.6 in chapter 1.

3.1 Preparation and characterization of ceramic suspensions

3.1.1 Ceramic slurry preparation by gelcasting

Materials:

• Monomer: Methacryalmide (MAM)

• Cross linker: Methylenebisacrylamide (MBAM)

Dispersant: Darvan 821-A

• Initiator: N, N, N', N'-tetramethylene-1,2-diamine (TEMED)

• Catalyst: Ammonium persulfate (APS)

Alumina powder

To achieve a free-flowing suspension with a solid loading of 40 to 55%, the process involves several steps combining rapid prototyping and gelcasting techniques (RPGC). Initially, we prepared an organic premix solution by dissolving monomer (MAM) and cross-linker (MBAM) in deionized water at a weight ratio of 33:6:1 [10,6]. We then added Darvan 821-A, a dispersant for alumina (1-2 wt% as per solid loading), to the premix solution to disperse the ceramic powder. Next, we incorporate the calculated amount of alumina powder into the solution to ensure uniform dispersion. To achieve homogeneity, we then tumble this ceramic slurry for 24 hours at 15 rpm, using alumina balls as the mixing media. After mixing, the slurry is de-aired in a vacuum desiccator to remove trapped air bubbles [11]. Once de-airing is complete, the slurry is ready to cast into RPT molds coated with wax. We then allowed it to gel at 60 °C for 6 hours, followed by mold removal, drying, debindering, and sintering the product. The combination of rapid prototyping and gelcasting techniques allows for the precise shaping of alumina components, ensuring high dimensional accuracy and mechanical properties. Figure 3.1 illustrates the sequential steps in this net shaping process, for the RPGC process.

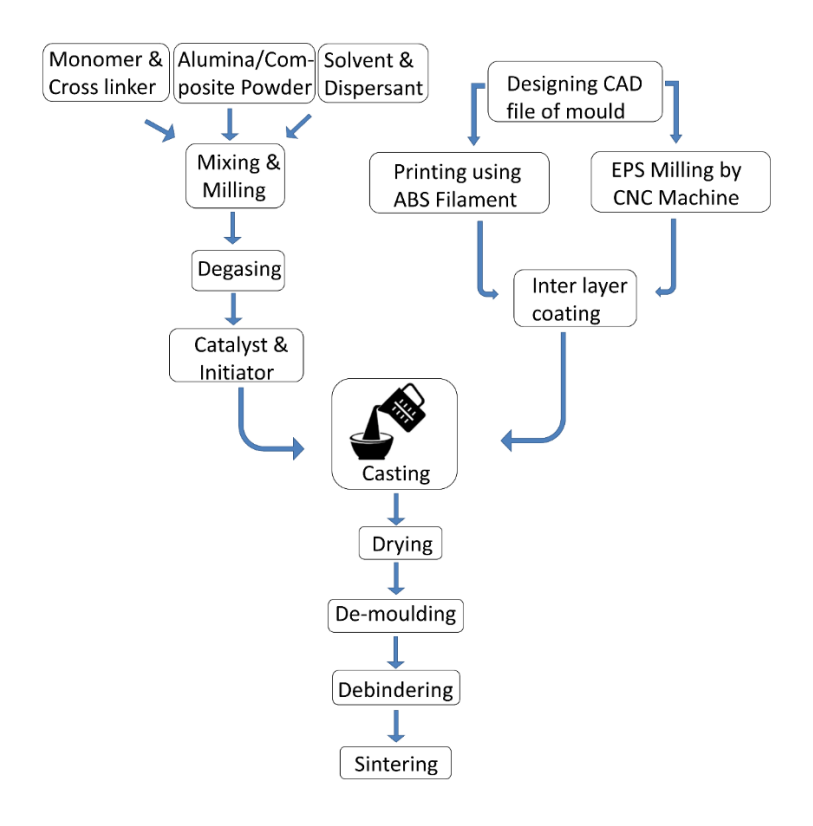


Fig 3.1. Flow chart showing the steps involved in net shaping of components from alumina/YSZ ceramics using RPGC process.

3.1.2 Viscosity of alumina slurries

The solid loading of a suspension is a key parameter in the casting process, as it needs to optimize the viscosity of slurries to flow freely and cast into molds whit good solid loadings to produce dense ceramic products. Optimal viscosity control, about 1 Pa.s is optimal for geleasting because it directly affects the characteristics of the sintered pieces. In our work, we measured the viscosities of alumina slurries at three different solid loading: 45%, 50%, and 55%. Figure 3.2 shows a direct proportional increase in the viscosity of the alumina slurry with increasing solid loading. Surprisingly, when the solid content reaches 55%, the viscosity reaches its highest point at 700 mPa.s., within the ideal range (< 1 Pa.s.) for casting [12]. From viscosity curves indicates that the alumina slurry with a 55% solid loading is highly suitable for casting.

Further increases in solid loading resulted in a viscous slurry that does not flow freely and impairs deairing. This would result in defects like voids in the final product that negatively affect the mechanical properties [11]. Therefore, we selected slurries with 50% solid loading levels for the component geleasting process. It provides optimal flowability and good solid loading combination, resulting in dense products with desirable qualities after sintering.

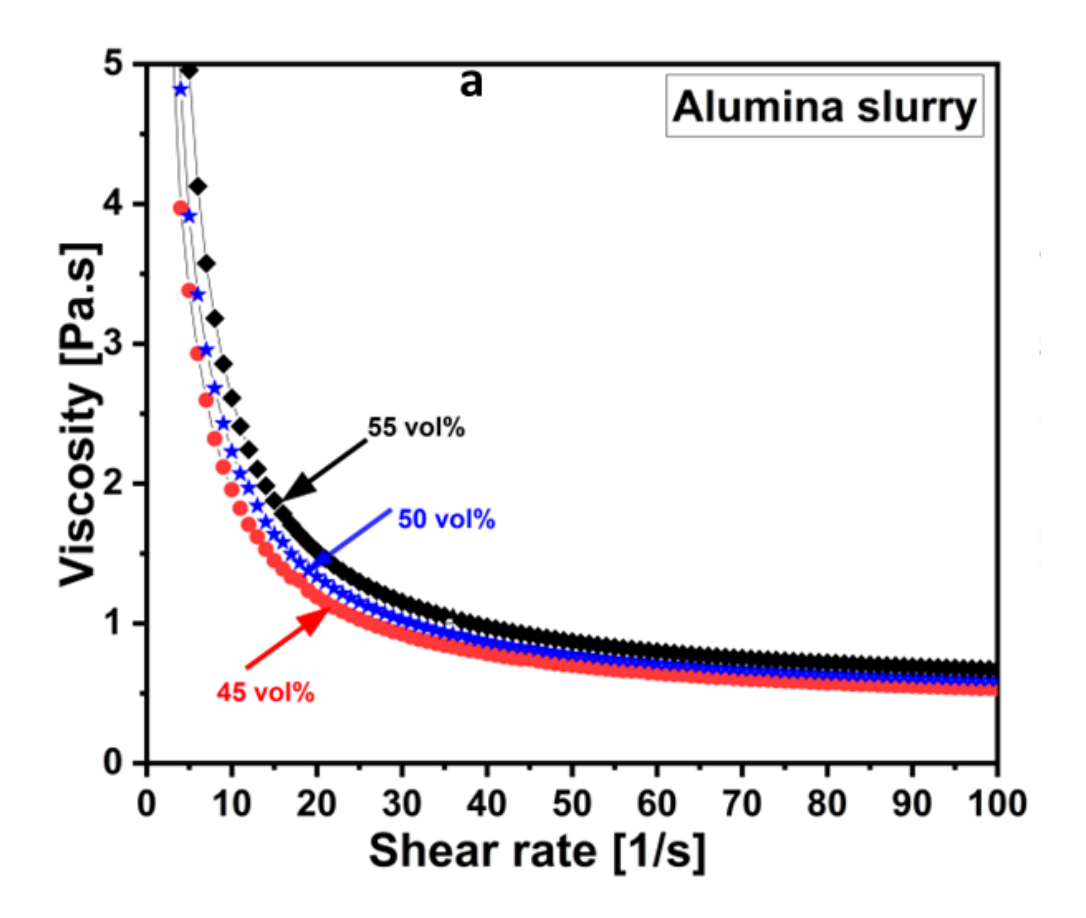


Fig.3. 2. Shear rate dependence of viscosity of a) alumina slurry with three levels of solid loading (45, 50 & 55%)

Entrapped air bubbles are a typical concern with solvent-based processing methods as they have a negative impact on the density and mechanical properties of the components produced. Prior to casting, the slurry was subjected to ultrasonication followed by degassing through vacuum. Ultrasonic vibration leads to degassing by causing the entrapped air bubbles to escape from the slurry. This was followed by vacuum degassing process [11] to reduce the pressure, causing the entrapped air bubbles to expand and eventually escape from the slurry. Combination of these approaches could remove entrapped air successfully yielding higher densities for the end products.

3.1.3 Rapid protyping – EPS and thin ABS molds preparation by subtractive and additive manufacturing

The criteria followed for mold fabrication are that

- 1. the mold is a replica of the component required,
- 2. the mold is non-porous,
- 3. the demolding process does not damage the green body, and
- 4. demolding should be easy and less time-consuming to avoid damage to the green body.

CAD tools created several solid models of the component replicas based on their required geometries. 3D printing creates the commonly used molds from ABS, PLA, or PVA, allowing easy removal using solvents like acetone and hot water [9,11,13]. The mold removal process typically takes a few hours, during which the green body may sustain some damage from soaking. Hence, looking for alternative approaches that enable mold removal in shorter durations is necessary. In this direction, we have made significant innovations in fabricating thin-walled ABS molds for easy dissolution. EPS molds have an advantage over ABS because they dissolve instantaneously in acetone, avoiding damage to the green body. However, EPS molds have the drawback of being porous, requiring subtractive manufacturing to shape them. In this work, we have addressed these aspects. There are no reports of EPS molds being used for component net shaping. The fabrication of ABS and EPS molds used for casting the slurries in the present work is discussed below.

a) EPS mold fabrication by 3D profile cutting

EPS is a relatively inexpensive polymer for commercial use. We fabricated molds from EPS block using a 3D profile-cutting CNC machine (SVP Laser Technologies, Chennai, India). First, a CAD design of the shape is created using Solid Works software, and the CAD file is then converted to G-codes by multi-CNC to be fed as input into a CNC machine for 3D profile cutting. The polystyrene EPS molds were created by removing layer by layer (subtractive manufacturing) from the EPS block as per the design. Figure 3.4 shows a typical CAD design and the corresponding EPS mold to fabricate an alu mina cup. In the case of a mold for complex shapes like rocket thrust nozzle, subtractive manufacturing requires the design of the mold to be divided into many parts. EPS molds of different parts were fabricated individually and assembled using synthetic glue (Fevicol). We used low-density polystyrene to fabricate various EPS molds, with a wax coating to make the internal surface non-porous.

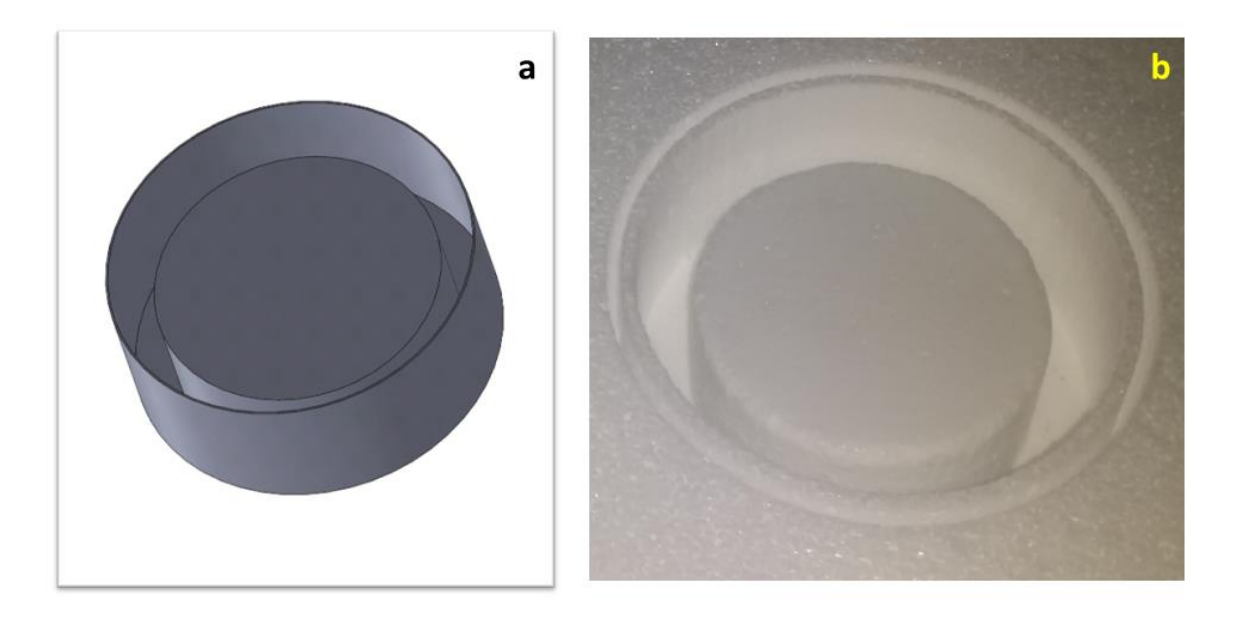


Fig.3. 4. a) CAD design of a mold and b) expanded polystryrene (EPS) mold fabricated by CNC 3D profile cutting, as a replica of a cup-shaped component.

b) ABS mold fabrication by 3D printing

The ABS molds were printed layer by layer (AM) per digital design using a 3D printer (AHA-3D make, India), extruding an ABS filament through a heated nozzle and depositing it on a base. A Cura 3Dslicing software was used to slice the model and make the negative, which served as the mold pattern. The printing parameters optimized for the ABS mold preparation are 30 mm/s printing speed and 30% filling density to achieve a high degree of forming accuracy and good sealing performance [14].

The CAD design and the mold used to fabricate an alumina component in the shape of a rocket thrust nozzle by gelcasting are shown in Figure 3.4. The wall thickness of the mold was kept to a minimum of 0.3 to enable easy mold removal at a later stage.

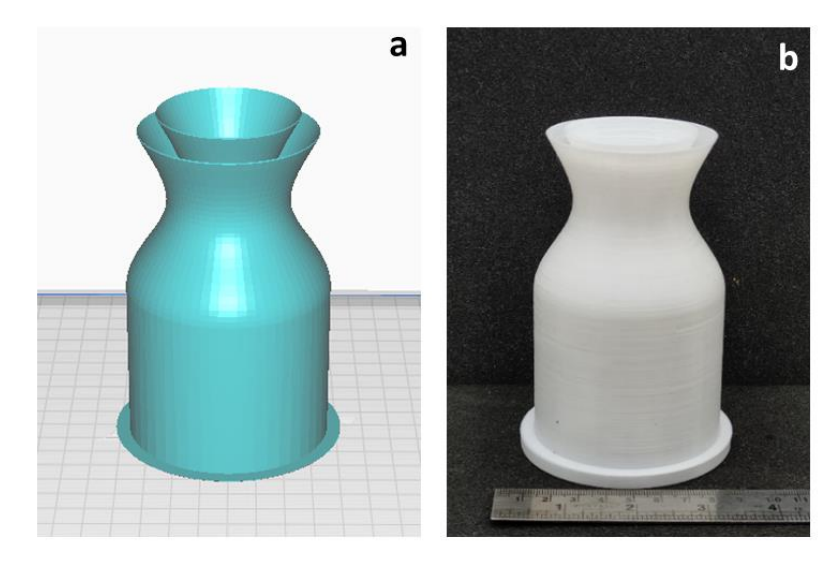


Fig.3. 4. a) CAD design for a Rocket thrust nozzle and b) Negative of the nozzle printed using ABS from the CAD design by a 3D printer.

3.2 Near -net shaping of alumina ceramic components by RPT and gelcasting

3.2.1 Fabrication of alumina green bodies

In the fabrication process, the free-flowing alumina slurry was cast into molds made of either ABS and EPS materials. These molds provide the desired shape and structure for the components being produced. Subsequently, the filled molds are subjected to a polymerization process by heating them in an oven set at 60°C for a duration of 6 hours. During this time, the polymerization reaction takes place, transforming the ceramic slurry into solid green bodies with the desired shape and dimensions.

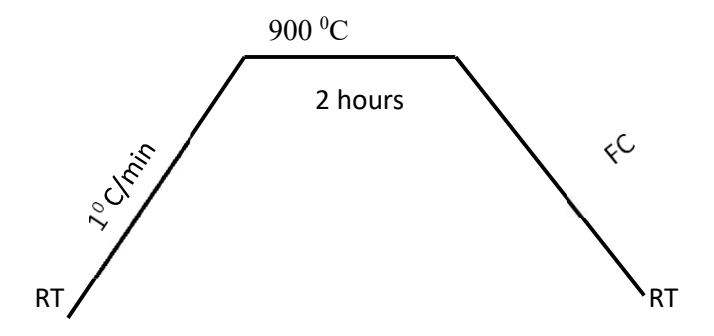
Once the gelling process is completed, the solid green bodies are carefully removed from the molds. This is achieved by dissolving the molds in acetone, which effectively dissolve the ABS and EPS material, releasing the solidified green body of the components. The use of acetone as a solvent allows for the easy and efficient extraction of the green bodies without causing damage to their structural integrity or shape. Overall, this method provides a straight forward and effective way to produce solid green bodies from the free-flowing slurry, enabling the fabrication of intricate ceramic components with precise geometries.

3.2.2 Mold removal, drying, debindering and sintering of alumina ceramics

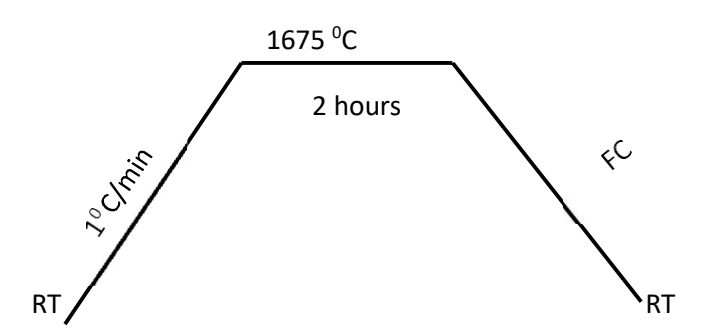
The dissolution is almost instantaneous for EPS molds. On the other hand, in the case of ABS molds, the colorless and transparent acetone solution gradually transformed into a turbid liquid in a few minutes. After two hours of immersion in acetone, the outer parts of the mold were dislodged, but the part of the mold buried in the green body remained intact. In the case of thin-walled molds, we found that it takes an hour for the mold to collapse and disintegrate entirely on its own after immersion in acetone. To speed up the experiment and to prevent the green body from getting damaged due to

acetone penetration, the mold was manually removed after softening. The green body was then immersed once more in fresh acetone to remove residues of the mold material before processing further. The green bodies were dried in an environmental chamber with a humidity control of 90% relative humidity (RH)and a temperature of 50 °C for four days. The binders in the dried green bodies were then removed by heating them to 900 °C for two hours in a tube furnace. The debindered compacts of alumina then sintered in air at 1675 °C for two hours.

a) Debindering of alumina green bodies in air atmosphere



b) Sintering Heat Profile: in air atmosphere Sintering heat profile for Alumina components:



To demonstrate the efficacy of the method, several components of different shapes and sizes were fabricated from alumina using the RPGC process, which are shown in Figure 3.5(a-d). In the case of the thrust nozzle, the EPS mold was designed in parts that were fabricated and assembled. Alumina components fabricated by gelcasting into 3D printed ABS molds, made by AMare shown in Figure 3.6 (a-d).

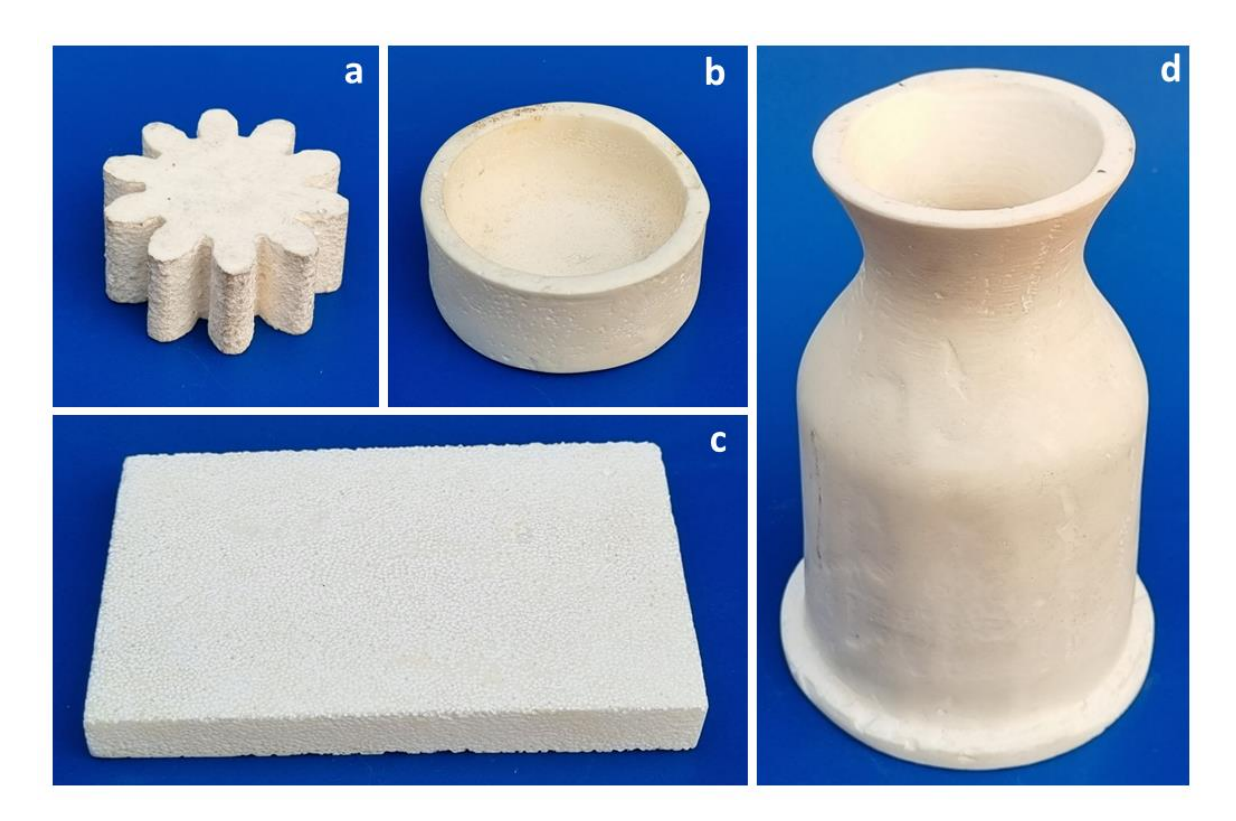


Fig.3. 5. (a-d). Alumina components fabricated by gelcasting into CNC 3D profile cut EPS molds, made by subtractive manufacturing. The components in Fig.3.5 are: a) a gear of maximum diameter 50 mm x height 23 mm, b) a cup of 70 mm OD x 30 mm height, c) a rectangular block of 92 mm x 60 mm x 8 mm, and d) rocket thrust nozzle of complex shape with maximum diameter 68 mm x height 102 mm.



Fig. 3.6.(a-d). Alumina components fabricated by gelcasting into 3D printed ABS molds, made by additive manufacturing. The components in Fig.3.6 are: a) a cup of OD 82 mm x height 38 mm, b) hollow cylinder of OD 82 x thickness 38 mm, c) rocket thrust nozzle of complex shape with maximum diameter 48 mm x height 70 mm, and d) rectangular tray of size 134 mm x 65 mm x 25 mm.

3.3 Physical, mechanical properties and microstructural characterization of alumina components

The Archimedes technique was used to determine the density and porosity of the components after they are sintered as discussed in section 2.1, We have also determined the uniformity in the density across the height, the long dimension of the thrust nozzle, as shown in Figure.3 7. The density of the components is nearly 99 % of the theoretical density and is quite uniform.



Fig.3.7. Variation in relative density measured along the long dimension of alumina thrust nozzle. The measurements were done on samples cut out of another nozzle.

The hardness of the samples is measured using Vickers indentation method. Indentations were made at 20 kgf load, applied for 15 seconds and the hardness was determined from the average value of the diagonals measured across the indentations. Data for 5 indentations at different places are used to find the average value.

We determined the flexural strength and fracture toughness using a 3-point bend test on a specimen cut to $3.0 \times 4.0 \times 45.0$ mm dimensions, as per ASTM C1161–13 [15] standard and fracture toughness as per ASTM C1421–10 standard [16], discussed in detail in section 2.8, chapter 2.

Table 3.1. Properties of alumina compacts

Sample	Sintering	Relative	Vicker's	Flexural	Fracture
	Temperature (°C)	Density (%)	Microhardness	Strength	toughness
	@ 2 hrs		HV (GPa)	σ	K _{Ic}
				(MPa)	(MPa √m)
Al ₂ O ₃	1675	99	22.5	389	3.01

Microstructural studies

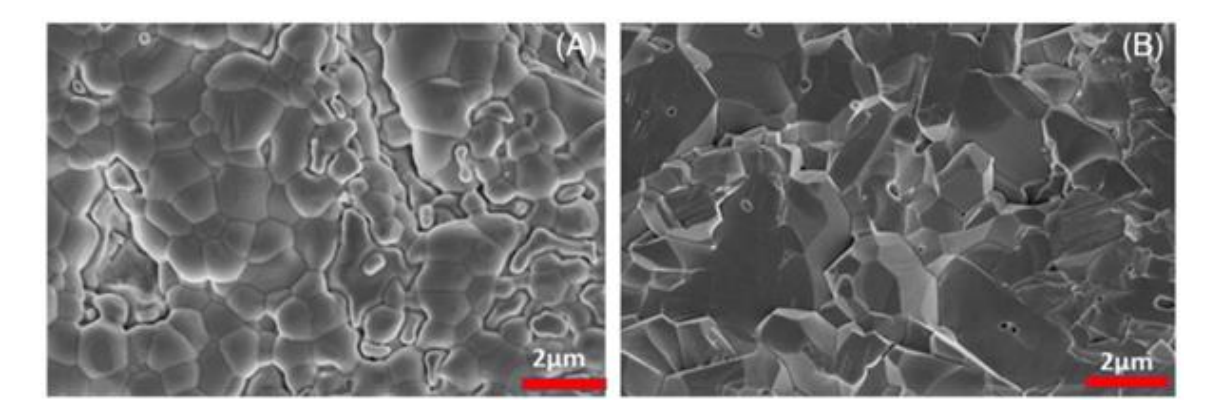


Fig.3.8. FESEM images recorded in (A) pure alumina sample (polished and thermally etched). (B) pure alumina fractured surface.

FESEM images recorded in various compacts are shown in Figure 3.8. Figure 3.8A shows the micrographs recorded in pure alumina specimen after polishing and thermal etching at 1350 °C for two hours [17]. The grains are densely packed, and porosity was not observed. Figure 3.8B shows images recorded on a fractured surface. The starting alumina powderwasof size \sim 700nm. Micrographs show grains of 1–3 µm size revealing that some grain growth has taken place.

Summary

Gelcasting and RPTs were used to fabricate complex shaped components of ceramic composites. Molds were designed using Solid works software. 3D printed ABS molds and 3D profile cut EPS molds of desired shapes were fabricated by RPT and free flowing slurries of sus pended ceramic

powders were cast into them. Demolding was done by dissolving the mold material in acetone which took about 60 min for ABS molds, and 30–60 s for EPS molds, based on the design. Design and fabrication of molds with a minimum possible thickness of ~0.3 mm for ABS molds and providing internal coating for the easily dissolvable EPS molds (to eliminate the problems associated with the porosity of the mold) and efficient de airing process before casting are some of the innovative developments in the present work. With a solid loading of about 55% in alumina slurry, the final products were of density close to 99%. Mechanical properties of final components are comparable or superior to reports in the literature. Flexural strength of 388MPa and fracture toughness of 3 MPa√m were recorded from measurements.

The present process has the advantage of enabling redesigning of molds to correct for shrinkages that occur during debindering and sintering. This technique is generic, reproducible,

is of low cost, and is extendable to fabricate components of requisite complex shapes from powders of various ceramic and metal systems, using slurry-based techniques. The RPGC method is aptly suited for the net-shaping of large and complex-shaped components with second-phase additions, with good microstructures and properties. The process innovations in mold fabrication open up a scope for designing large and complex molds that enable production of high-value components for medical, automotive, and aerospace applications

3.4 Fabrication of barium strontium titanate (BSTO) components by using different gelcasting systems and RPT molds

Barium strontium titanate (BSTO) is a ceramic that finds application as a high-storage capacitor, sensor, detector, transducer, in-tuneable microwave device, and filter [18,19]. This work discusses the synthesis of slurries with suspended particles and fabrication of Ba_{0.5} Sr_{0.5} TiO₃ components of different shapes and dimensions using environmentally friendly gelling systems like Isobam and methylcellulose, and also the widely used but toxic methyl acrylamide system [20-22]. Suitable molds made of acrylonitrile butadiene styrene (ABS) and expanded polystyrene (EPS) are fabricated by rapid prototyping and a concentrated slurry of the required ceramic is set in it by gelcasting; the process is referred to as the RPGC process [6,23]. The green body is further processed to obtain a density higher than 98 %. The sintered products are evaluated by measuring density, microstructure, and dielectric properties. This work opens up the possibility of adopting the versatile RPGC process with non-toxic organics for applications by industries.

3.4.1 Viscosity of BSTO slurries with different gelling systems

BSTO powder was synthesized by solid-state reaction in a two- step process [20,24]. The raw materials, BaCO₃, SrCO₃, and TiO₂, weighed out in stoichiometric ratio, were mixed well by tumbling

the powders in a turbo mixer for a duration of 12 hours, during which tungsten carbide (WC) balls were added to aid in uniform mixing. The initial heat treatment involved calcining the powders at 930 $\,^{\circ}$ C for a duration of 2 hours. This was followed by dry ball-milling for 4 h. This milling step helps in further homogenizing the mixture and reducing the particle size and enhances the reactivity of the reactants in the next step. The resultant ingot was then subjected to a second heat treatment at a higher temperature of 1100 $\,^{\circ}$ C for 2 hours. This step was essential to complete the reaction and ensure the formation of the desired Ba_{0.5} Sr_{0.5} TiO₃ compound.

To achieve a free-flowing suspension with 50 vol% solid loading, the amount of BSTO powder required is calculated and added to a measured quantity of organic premix solution. The solution was prepared by dissolving monomer (MAM) and cross-linker (MBAM) in deionized water (deionized water:MAM: MBAM = 33:6:1, by weight), to which Darvan C–N (1–2 wt%, based on the solid loading) was added as a dispersant. In the Isobam (IB) and methylcellulose (MC) systems, to make the premix solution, Isobam (2 wt%) or methylcellulose (2 wt%) was dissolved in distilled water, and 1 wt% of dispersant was added. Slurries with a solid loading of 50 vol% were prepared in each case by incorporating the BSTO powder into the corresponding premix solutions. The resultant ceramic slurries were tumbled for 24 h at 15 rpm with WC balls as mixing media to achieve uniformity. The slurries were then de-aired in a vacuum desiccator to remove any trapped air before casting into molds. Figure 3.9 shows the steps involved in the net shaping of BSTO components by the RPGC process [6,23]. We refer to the methacrylamide system as AM, the Isobam system as IB, and the methylcellulose system as MC.

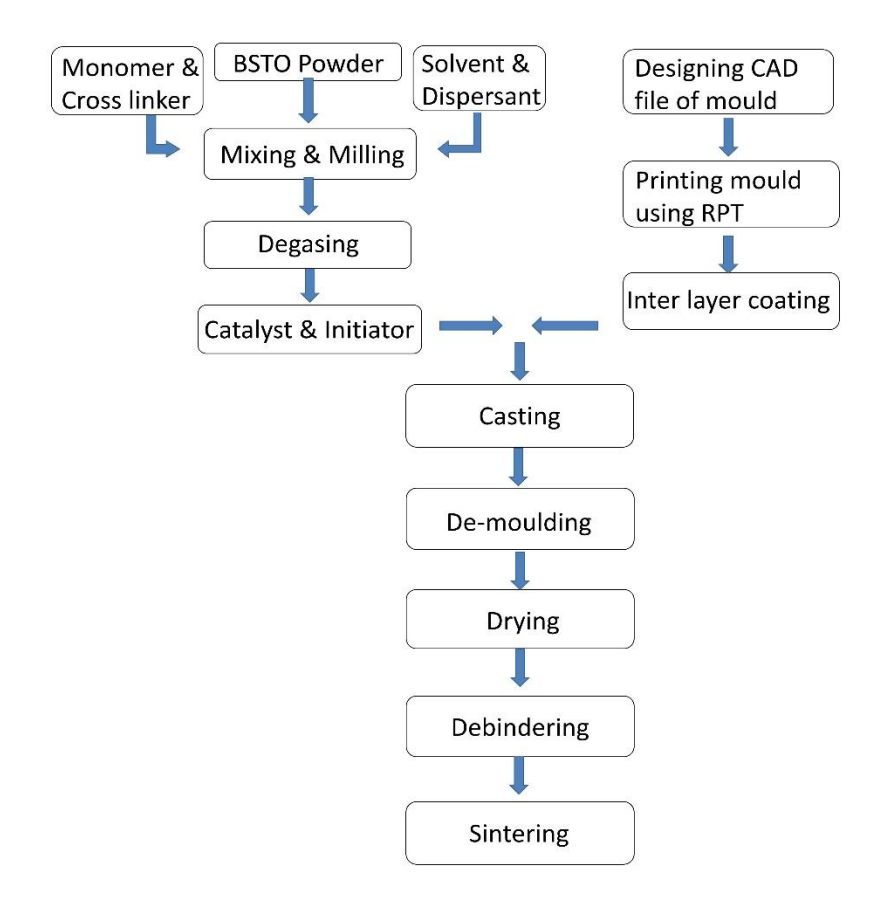


Fig.3. 9. Flow chart indicating the steps involved in net shaping of BSTO components by RPGC technique.

Fine particles can help stabilize the suspension. The data in Figure 10a shows that the BSTO powder consists of particles ranging from 0.3 μm to 0.7 μm. These particles can stabilize the system by preventing larger particles from settling. This ensures that the slurry remains uniform, preventing agglomeration and settling. The study focused on investigating and optimizing the rheological behavior of gelcast slurries by varying the binder content. The AM slurry's viscosity is slightly lower than the IB and MC slurries. Figure 3.10b demonstrates that the viscosity of BSTO slurry reaches its lowest point, averaging around 1-2 Pa.s, when subjected to shear rates of 50 to 100 s⁻¹. Which is suitable choice for casting, especially with a solid loading of 50 vol%.

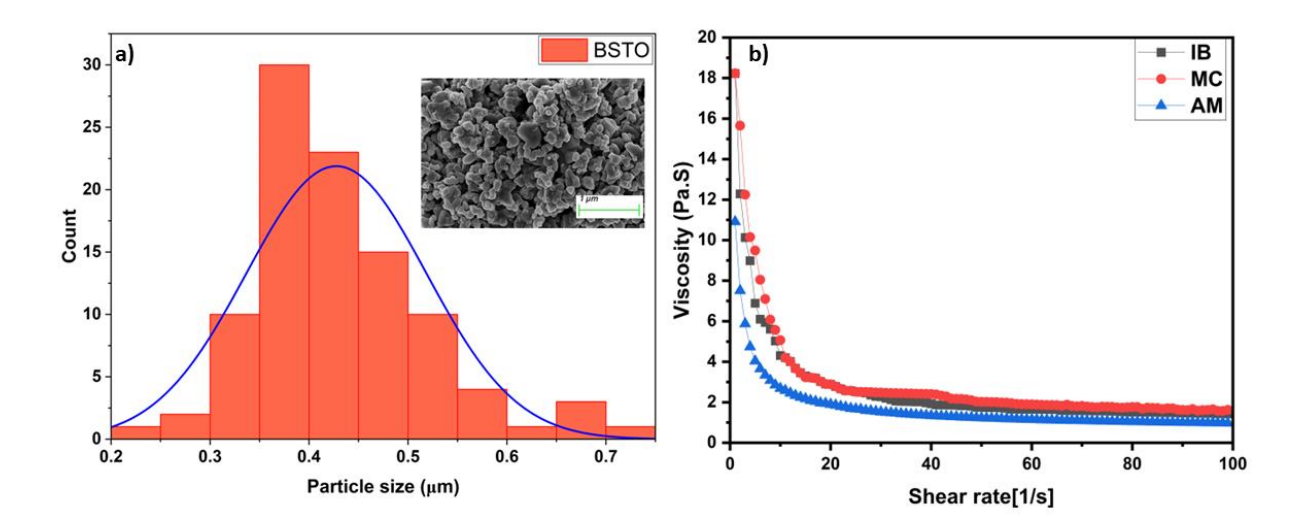


Fig.3. 10(a) Particle size distribution of BSTO powder (b) Shear rate dependence of viscosity of BSTO slurries prepared in AM, IB and MC gelcsating systems.

3.4.2 Fabrication Process

Figure 3.11 shows the process steps involved in the shape forming of BSTO components.

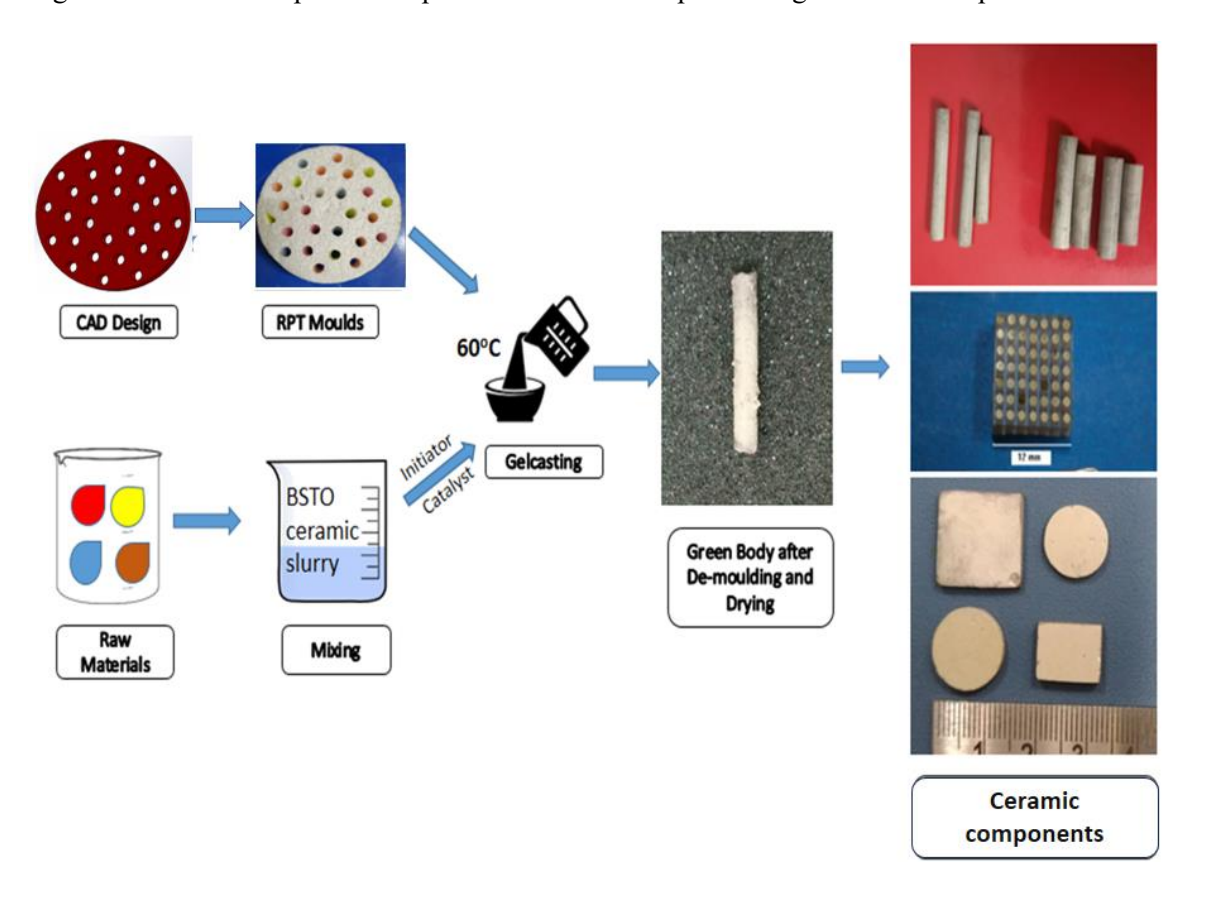


Fig. 3.11. Process steps in shape forming of BSTO ceramics.

3.4.3 Fabrication of Molds

a) ABS Mold fabrication by 3D printing

Using a 3D printer (AHA-3D create, India), the ABS molds were additively manufactured layer by layer according to the digital design by extruding an ABS filament through a heated nozzle and depositing it on a base. The model was cut using a slicing program (Ultimaker Cura), and the resulting negative served as the mold pattern. In order to obtain a high level of forming accuracy and good sealing performance, the printing parameters are set to a printing speed of 30 mm/s and a filling density of 30 % [23]. Figure 3.12 shows the CAD design and the mold used to create BSTO components by gelcasting. The mold's wall thickness was kept to a minimum of 0.3 mm for easy removal. Depending on the height of the product required, the extent of filling of the slurry was adjusted.

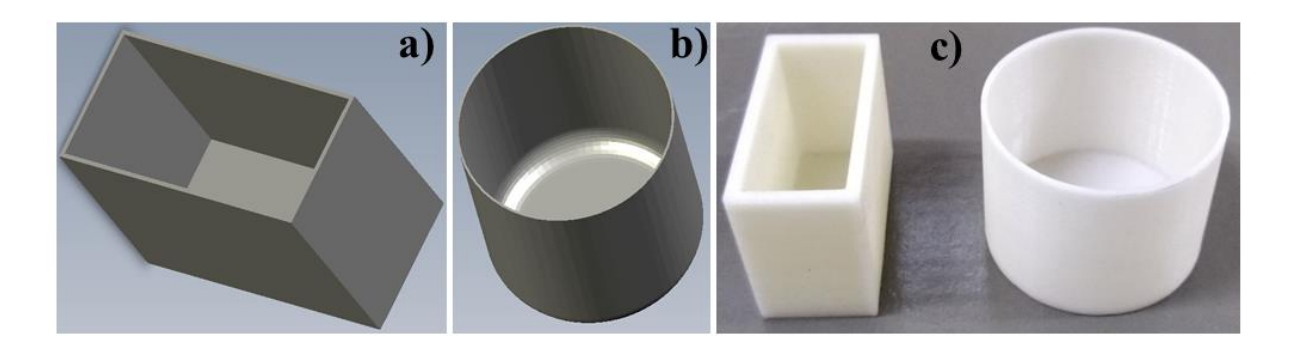
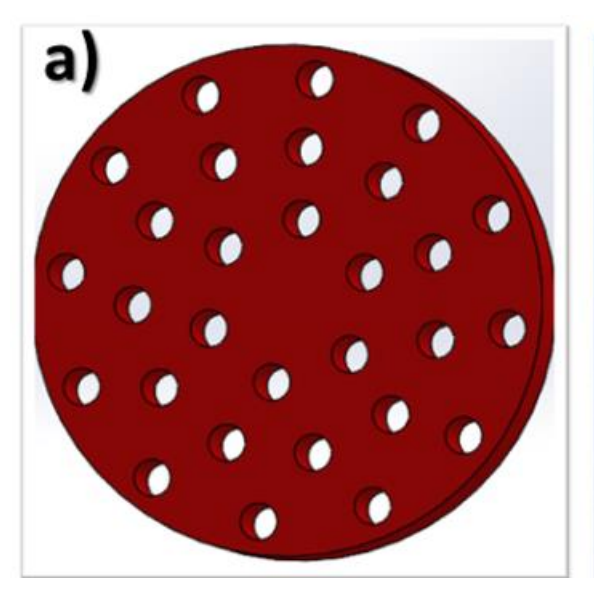


Fig.3.12. (a & b) Typical CAD designs for molds and (c) ABS molds for fabricating components of rectangular and circular cross-sections.

b) EPS mold fabrication using 3D profile cutting

Figure 3.13 shows a typical CAD design and an EPS mold created, to fabricate BSTO rods. and a wax coating.



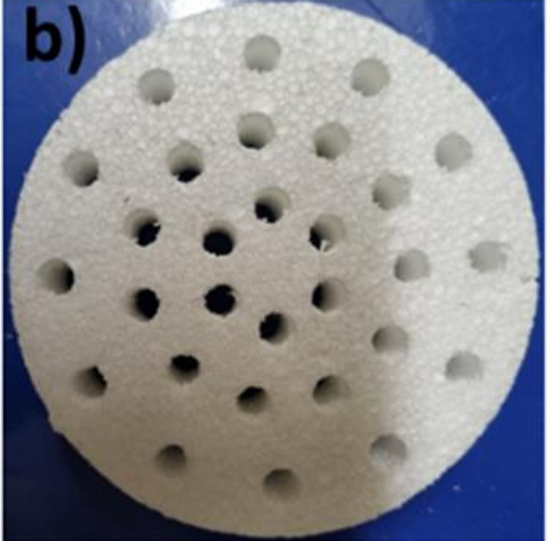


Fig. 3.13. (a) Typical CAD design for mold fabrication and (b) an EPS mold used to fabricate BSTO rods.

3.4.4 Mold removal and further processing of green bodies to realize components

The free-flowing slurry of the chosen system was cast into ABS or EPS molds and polymerized by heating at 60 °C in an oven for 6 hours. After completion of the gelling process, the solid green bodies were removed by dissolving the molds in acetone. The dissolution is almost instantaneous for EPS molds. In the case of thin-walled ABS molds, we found that it takes an hour for the mold to collapse and disintegrate entirely on its own after immersion in acetone. To speed up the experiment and to prevent the green body from getting damaged due to acetone intraction, the mold was manually removed after softening. The green body was then immersed in fresh acetone to remove residues of the mold material before processing further.

The green bodies were dried in an environmental chamber at 90% relative humidity (RH) and a temperature of 50 °C for four days. The dry green bodies' binders were then removed by heating them to 900 °C for 2 hours in a tube furnace. The debindered ceramic parts were then sintered in air at 1350 °C for 2 hours, and the furnace cooled to obtain the final BSTO compacts showed in figure 3.14.

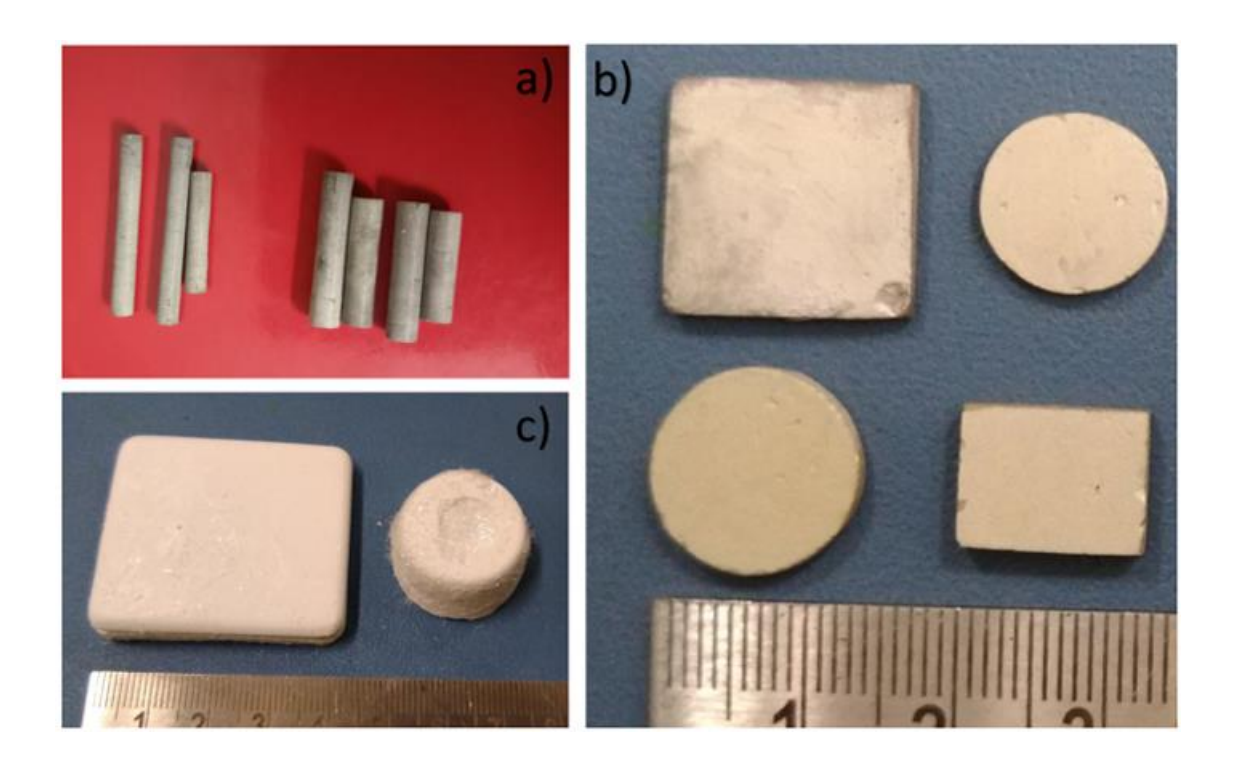


Fig.3. 14. (a) BSTO rods of different lengths (up to 10 mm) and diameter (2–4 mm), (b and c) BSTO components of different shapes fabricated by the RPGC process.

3.4.5. Physical, dielectric properties and microstructural studies of BSTO components

XRD analysis

The indexed X-ray diffraction (XRD) pattern for Ba_{0.5}Sr_{0.5}TiO₃ (powder and components) shown in Figure 3.15. The analysis on XRD confirms the formation of a single phase Ba_{0.5}Sr_{0.5}TiO₃ for both powders annealed at 1100 °C and components sintered at 1350 °C with cubic perovskite structure.

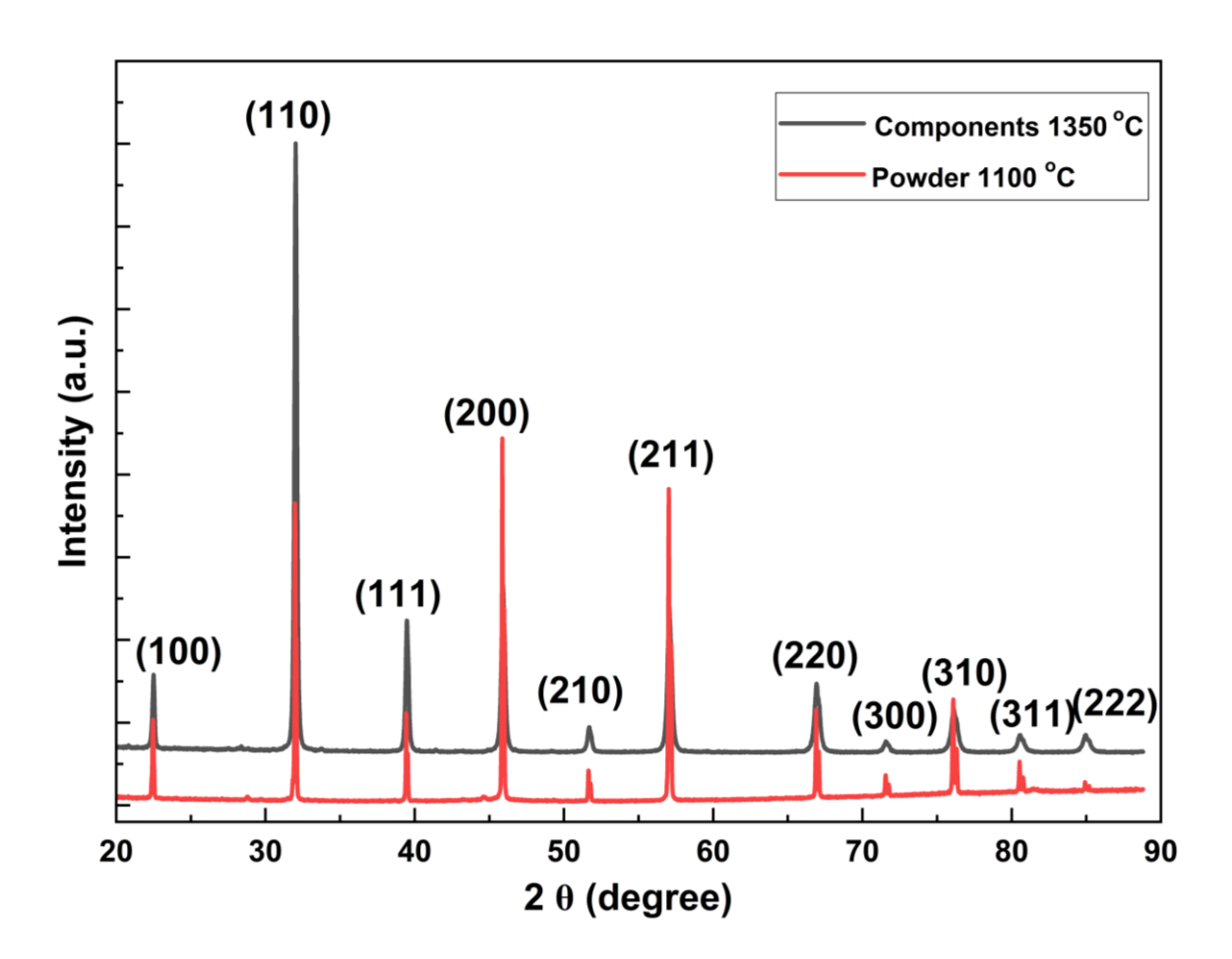


Fig.3.15. Indexed XRD patterns recorded for $Ba_{0.5}Sr_{0.5}TiO_3$ (BSTO powder and components) using CuK_{α} radiation

Density and hardness

The densities of the sintered samples were determined using Archimedes' principle, utilizing glycerine as the medium for immersion. Table 3.1 provides the relative densities (the ratio of measured and theoretical density) for BSTO components that were manufactured utilizing 3 different gelcasting systems. The relative densities of all these samples are approximately equal, and nine samples were used to measure density.

The hardness of BSTO components was evaluated using Vickers's indentation method. The hardness was determined by calculating the average value of the diagonals measured across the indentations after applying an indentation force of 0.5 kg for 15 seconds. The average value is determined using

data from five indentations conducted at various positions on the polished materials. The subsequent equation is employed to ascertain hardness.

Table 3.1: Sintering temperature, Relative density (%), and hardness for BSTO composites fabricated using AM, IB, and MC gelcasting systems.

Gelcasting System	Sintering Temp. (°C)	Relative Density (%)	Hardness (GPa)
AM	1350	98.5 ± 0.01	4.52 ±1.25
IB	1350	98.0 ± 0.01	4.33 ±1.14
MC	1350	97.5 ± 0.01	4.28 ±1.21

The BSTO ceramics made with the AM gelcasting system has the highest density and hardness, followed by those made with the Isobam and MC systems. These can be attributed to different viscosities of the slurries; the AM system gave rise to a slurry of marginally lower viscosity than IB and MC systems, resulting in slight variations in densities and hardness.

Microstructural Studies

The FESEM images of BSTO components, obtained after polishing and thermal etching at a temperature of 1100 °C for 2 hours [17], are displayed in Figure 3.16. The grains exhibit a high level of compaction, with no visible porosity or cavities. The mean diameter of the grains is 6.0 μm. The microstructural characteristics of the BSTO components produced utilising additive manufacturing (AM), injection molding (IB), and machining (MC) processes exhibit significant similarities. Therefore, one can anticipate similar characteristics in the items produced using the three procedures.

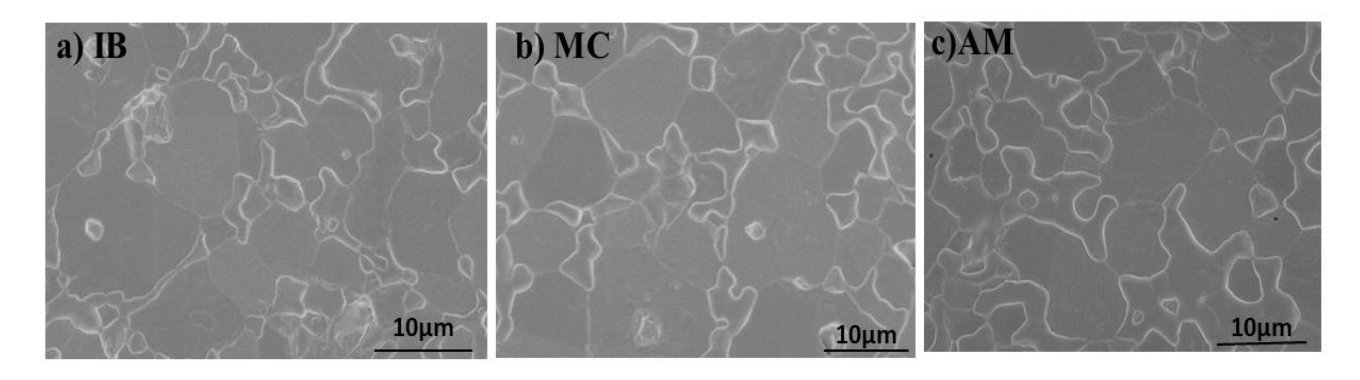


Fig.3.16. (a-c) show micrographs recorded in BSTO specimens fabricated by IB, MC and AM gelling systems respectively, after polishing and thermal etching.

Dielectric properties

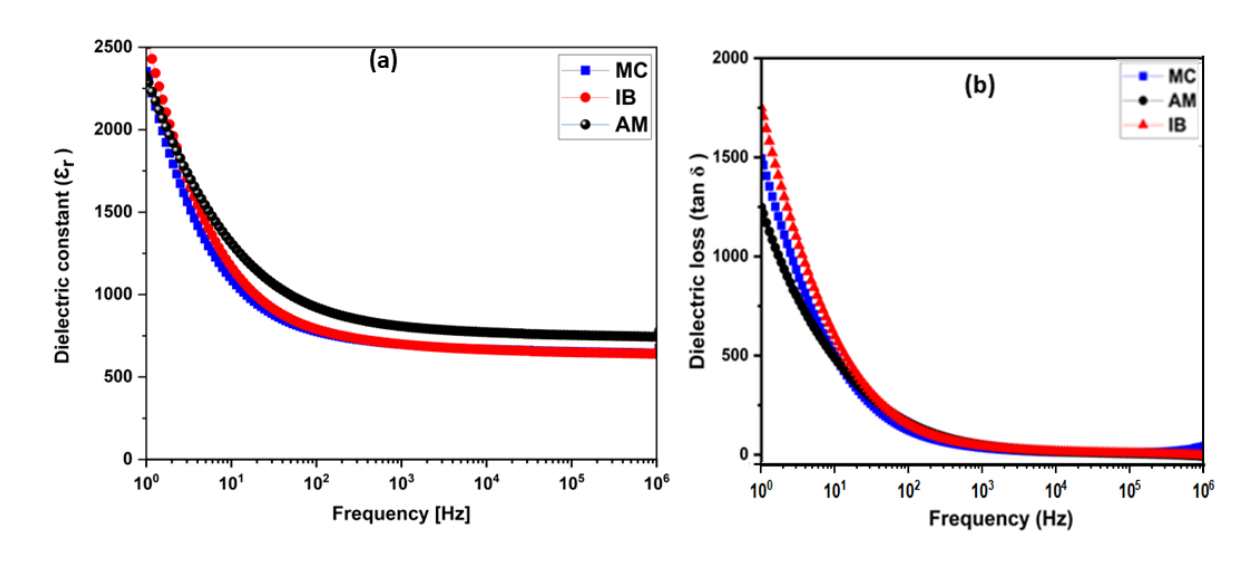


Fig.3.17. (a) Dielectric constant (\mathcal{E}_r) and b) Dielectric loss (tan δ), as a function of frequency up to 1 MHz, measured at room temperature.

The dielectric constant (\mathcal{E}_r) and dielectric loss (tan δ) were determined using a Novocontrol dielectric spectrometer. This measurement was conducted on pellets

with a diameter of 1 cm. Prior to the measurement, the surfaces of the pellets were coated with Ag paint and then subjected to annealing at a temperature of 200 to create electrodes. Figure 3.17 displays the frequency dependence of the dielectric characteristics up to 1MHz at room temperature for BSTO components manufactured using AM, IB, and MC gelcasting processes.

Table 3.2 compares the dielectric characteristics of BSTO components produced using three different gelling systems in relation to those described in the literature utilizing various synthesis methods. The research indicates that the sintering temperature significantly influences the dielectric behavior of BSTO samples. At elevated sintering temperatures, when there is a possibility of grain development, the values of \mathcal{E}_r are observed to be reduced.

The dielectric constant of BSTO components produced using AM gelcasting is around 800, somewhat higher than those manufactured by IB and MC gelling techniques in the frequency range of 1 kHz to 1 MHz, as indicated in Table 3. 2. In addition, the BSTO components have little dielectric loss across

the whole frequency range, which makes them promising options for applications that demand dependable and energy-efficient electrical properties.

Table 3.2 compares the dielectric constants and dielectric losses for barium strontium titanate using various gelcasting processes acquired in this study and the values reported in the literature for barium strontium titanate ceramics.

Method	Ceramics	Sintering	Sinterin	$\mathbf{\epsilon_r}$	$\mathcal{E}_{\mathbf{r}}$	tan δ	tan δ	Ref.
		Temp. (°C)	g Time	(1kHz)	(1MHz)	(1kHz)	(1MHz)	
			(hours)					
SSR	$Ba_{0.5}Sr_{0.5}TiO_3$	1260	2	928	-	0.91	-	25
SSR	$Ba_{0.5}Sr_{0.5}(Sn_{0.12}Ti_{0.88})$	1300	3	850		0.014		26
	O_3							
SSR	$Ba_{0.5}Sr_{0.5}TiO_3$	1230	2	1000	-	0.93	-	27
SCM	Ba _{0.5} Sr _{0.5} (Sn _{0.20} Ti _{0.80})	1350	2	179	167	0.06	0.011	20
	O_3							
SCM	$Ba_{0.5}Sr_{0.5}(Sn_{0.10}Ti_{0.90})$	1350	2	392	395	0.030	0.006	20
	O_3							
SCM	$Ba_{0.5}Sr_{0.5}(Sn_{0.05}Ti_{0.95})$	1350	2	502	483	0.029	0.005	20
	O_3							
Gelcasting(AM)	$Ba_{0.5}Sr_{0.5}TiO_3$	1350	2	854	800	0.003	0.003	PW
Gelcasting(IB)	$Ba_{0.5}Sr_{0.5}TiO_3$	1350	2	764	736	0.003	0.002	PW
Gelcasting(MC)	Ba _{0.5} Sr _{0.5} TiO ₃	1350	2	756	730	0.002	0.004	PW

Conclusions

This work discusses the near-net-shaping method used to fabricate dense BSTO components, with a focus on environmentally friendly organics for gelcasting process. The quest for low-toxicity gelling agents was fruitful, as the IB and MC were shown to be competitive with the process using AM monomers (toxic) reported in literature. To accomplish this, it was necessary to optimize many processing parameters related to the preparation of ceramic slurries, mold fabrication, drying, and processing conditions, as outlined in this work.

Complex-shaped BSTO ceramic components were fabricated using gelcasting and rapid prototyping techniques, using RP-GC process. The molds were designed using SolidWorks, a CAD software. The free-flowing slurries of suspended ceramic powders were cast into 3D printed ABS molds and 3D profile cut EPS molds to fabricate BSTO components of required shapes. Demolding was accomplished by soaking the mold material in acetone for around 60 minutes for ABS molds and 30 to 60 seconds for EPS molds. We have created molds with a small thickness of 0.3 mm (easily dissolvable) for ABS molds which provides with an advantage of easy dissolution. Another contribution is development of easily dissolvable EPS molds with a coating that renders the interior

of the mold non-porous and also avoids interaction of green body with the soaking medium. Additionally, a reliable de-airing process was implemented prior to casting, to remove the entrapped air.

Using a slurry with a solid loading of 50 vol%, the resultant BSTO components exhibited a density of 98%. The dielectric properties of the components obtained using the three different gelling systems are comparable and are in the range reported in literature [5,42, 43,44] on BSTO samples sintered at similar temperatures. The products fabricated in the present work by the non-toxic gelling systems are pore-free and have comparable microstructures and dielelctric behaviour as those fabricated by the methacrylamide-based gelling system. Gelcasting has a potential to move closer to realising industrial applications with RP-GC process, owing to the non-toxic gelling agents, as brought out in this work.

REFERENCES:

- 1. <u>Davis, Karen</u>, Material Review: Alumina (Al₂O₃). International Journal of Advance Research and Innovative Ideas in Education. 2010; 2: 109-114.
- 2. A. M. Abyzov; Aluminum Oxide And Alumina Ceramics (Review). Part 1. Properties Of Al₂O₃ And Commercial Production Of Dispersed Al₂O₃; Scientific Research And Development. 2019; 60: 16-23.
- 3. BoseS, Vahabzadeh S, Bandyopadhyay A. Bonetissue engineer ing using 3D printing. Mat Tod. 2013;16:496–4504.
- 4. Carolina Tallon ^a, Monika Limacher ^{a b}, George V. Franks. Effect of particle size of shaping of ceramics by slip casting. Journal of European ceramic society. 2010;30: 2819-2826.
- 5. WangS,MirandaAG,ShihC.Astudyof investment casting with plastic patterns. Mat Man Proc. 2010;25:1482–88.
- 6.T. Rajasekharan, P.M. Swaroop Raju, Rakesh Kumar Pandey, V. Seshu Bai, R. Pradyumna, M.A.H. Baig, "Complex-shaped alumina products through rapid prototyping" Met, Mater. Process. 19 (2007) 41–46.
- 7. ZoccaA,GomesCM,BernardoE,MüllerR,GünsterJ,Colombo P. LAS glass— ceramic scaffolds by three-dimensional printing. J Eur Ceram Soc. 2013;33:1525–33.
- 8. Lin T, Liu S, Ji Z, Shao H, Hao J. Vitrified bond diamond grind ing wheelpreparedbygel-casting with 3Dprinting molds. Diam Relat Mater. 2020;108:1–7.
- 9. Zhangwei Chen, Ziyong Li, Junjie Li, Chengbo Liu, Changshi Lao, Yuelong Fu, Changyong Liu, Yang Li, Pei Wang, Yi He, 3D printing of ceramics: A review. Journal of the European Ceramic Society 39 (2019) 661–687.
- 10. Janney MA, Omatete OO, Walls CA, Nunn SD, Ogle RJ, Westmoreland G. Development of low-toxicity gelcasting sys tems. J AmCeramSoc. 1998;81:581–91.

- 11. Ndinisa SS, Whitefield DJ, Sigalas I. Fabrication of complex shaped aluminaparts bygelcasting on 3Dprinted molds. Ceram Int. 2020;46:3177–82.
- 12. Liua G, Attallah MM, Jiang Y, Button TW. Rheological charac terization and shape controlingel-casting of nano-sized zirconia powders. Ceram Int. 2014;40:14405–12.
- 13. Pin-Chuan Chen, Ching Chan Chou Chung Hsuan Chian, Systematically Studying Dissolution Process of 3D Printed Acrylonitrile Butadiene Styrene (ABS) Mold for Creation of Complex and Fully Transparent Polydimethylsiloxane (PDMS) Fluidic Devices. BioChip Journal. 2021. 15:144–151.
- 14. Liu K, Zhou C, Chen F, Sun H, Zhang K. Fabrication of com plicated ceramic parts by gelcasting based on additive manufac tured acetone-soluble plastic mold. Ceram Int. 2020;46:25220 29.
- 15. Standard Test Method for Flexural Strength of Advanced Ceramics at Ambient Temperature. Available from: https://doi.org/10.1520/C1161-13. Accessed 19 January 2014.
- 16.Standard Test Methods for Determination of Fracture Toughness of Advanced Ceramics at Ambient Temperature. Available from: https://doi.org/10.1520/C1421-10. Accessed 19 January 2014.
- 17. M. Liu, J. Zhao, S. Shimai, J. Zhang, H. Chen, H. Chen, D. Han, J. Liu, S. Wang, A Polishing-Free Etching Method for Microstructure Observation of Fine-Grained Ceramics; J. Ceram. Sci. Technol., 12 [1] 59-62 (2021)
- 18. R.A. York, Tuneable Dielectrics for RF Circuits, Scitech Publishing, 2009, pp. 1–54.
- 19. G. Subramanyam, M.W. Cole, N.X. Sun, T.S. Kalkur, N.M. Sbrockey, G.S. Tompa, X. Guo, C. Chen, S.P. Alpay, G.A. Rossetti, K. Dayal, L.Q. Chen, D.G. Schlom, Challenges and opportunities for multi-functional oxide thin films for voltage tunable radio frequency/microwave components, J. Appl. Phys. 114 (2013) 1–37, https://doi.org/10.1063/1.4827019.
- 20. I.A. Souza, L.S. Cavalcante, J.C. Sczancoski, F. Moura, C.O. Paiva-Santos, J. A. Varela, A.Z. Sim~oes, E. Longo, Structural and dielectric properties of Ba 0.5 Sr 0.5 (Sn x Ti 1-x)O 3 ceramics obtained by the soft chemical method, J. Alloys Compd. 477 (2009) 877–882, https://doi.org/10.1016/j.jallcom.2008.11.042.
- 21. Laura Montanaro, Bartolomeo Coppola, Paola Palmero, Jean-Marc Tulliani, A Review on Aqueous Gelcasting:a versatile and low-toxic technique to shape ceramics, Ceram. Int. 45 (2019) 9653–9673, https://doi.org/10.1016/j. ceramint.2018.12.079.
- 22. M.A. Janney, O.O. Omatete, C.A. Walls, S.D. Nunn, R.J. Ogle, G. Westmoreland, Development of low-toxicity gelcasting systems, J. Am. Ceram. Soc. 81 (1998) 581–591, https://doi.org/10.1111/j.1151-2916.1998.tb02377.x.
- 23. P. Jeevankumar, P. Rose, A. Rajanikanth, T. Rajasekharan, V. Seshu Bai, Net-shaping of advanced ceramic composites by gelcasting into precision molds made by rapid-prototyping, Int. J. Appl. Ceram. Technol. Int J Appl Ceram Technol.2024;21:664–674.
- 24. L. Peng, L. Ran, H. Chen, H. Zhang, J.A. Kong, T.M. Grzegorczyk, Experimental observation of left-handed behavior in an array of standard dielectric resonators, Phys. Rev. Lett. 98 (2007) 1–4, https://doi.org/10.1103/PhysRevLett.98.157403.

- 25 H.V. Alexandru, C. Berbecaru, A. Ioachim, M.I. Toacsen, M.G. Banciu, L. Nedelcu, D. Ghetu, Oxides ferroelectric (Ba, Sr)TiO3 for microwave devices, in: Mater Sci Eng B Solid State Mater Adv Technol, 2004, pp. 152–159, https://doi.org/ 10.1016/j.mseb.2003.10.034.
- 26. S.N. Yun, X.L. Wang, X.L. Sun, J. Mater. Eng. 9 (2006) 49–52.
- 27. H.V. Alexandru, C. Berbecaru, A. Ioachim, L. Nedelcu, A. Dutu, BST solid solutions, temperature evolution of the ferroelectric transitions, Appl. Surf. Sci. 253 (2006) 354–357, https://doi.org/10.1016/j.apsusc.2006.06.011.

Chapter IV

Alumina - α alumina platelet composites

The work discusses novel alumina composites with single crystalline alpha-alumina platelets as reinforcement fabricated by integrating gelcasting with rapid prototyping [1,3]. Different amounts of platelet alumina (ranging from 0, 1, 2, 3, 4, 5, 15, and 25 wt%) are coated with monazite (LaPO₄) using a chemical method and are introduced into alumina matrix to enhance its mechanical properties [4]. The alumina platelets have a uniform thickness of approximately 150 ± 25 nm [5]. The gelcasting process was used to mix the monazite-coated alpha-alumina platelets in the alumina matrix uniformly and create a free-flowing ceramic slurry with a 50 vol% solid loading. The slurry was cast and gelled in disposable expanded polystyrene (EPS) molds machined as per the computer-aided design (CAD) [1,3]. The green bodies are dried, debindered, and sintered to obtain compacts of characterized alumina composites. The composite with 4 wt% platelet content exhibited a notable 80% enhancement in fracture toughness when compared to monolithic alumina. Microstructural studies reveal deflection, bridging, and branching of the cracks caused by the coated platelets, providing evidence for their contribution to improved fracture toughness. The composites of optimised composition possess superior mechanical properties and have the potential for applications at high temperatures and in the biomedical sector.

4.1.1 Synthesis of α – alumina platelets

A solution combustion method demonstrated a novel route for obtaining crystalline Al₂O₃ platelets [5]. Briefly, aluminum nitrate (Al(NO₃)₃) was initially dissolved in distilled water, forming a transparent solution. We then added urea (CO(NH₂)), which initiated a complexation reaction with the aluminum ions. When we heat the solution to boiling point, the urea-aluminium complex undergoes rapid exothermic decomposition, leading to significant forming and gas evolution. This self-propagating

combustion effect means that much heat is released into the solution, which speeds up the change of the precursors into α -Al₂O₃ platelets. The reaction involved seen in figure 4.1 is

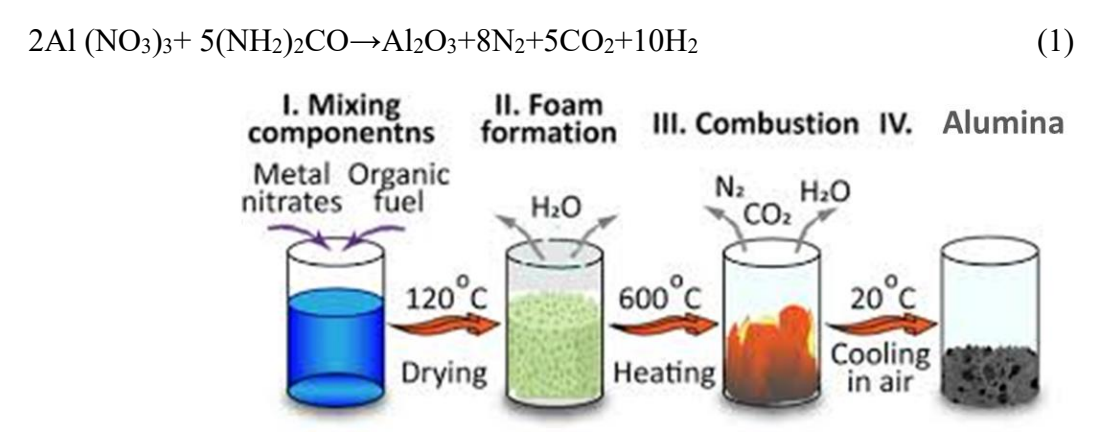


Fig. 4.1 Steps in Solution combustion process

The resulting powder crushed and was subsequently calcined at 800° C in an air atmosphere to promote complete crystallization and phase stabilization. X-ray diffraction (XRD) analysis revealed the successful formation of the α -phase with its characteristic hexagonal crystal structure. Figure 4.2a shows the indexed XRD pattern of the synthesized α -Al₂O₃, phase confirmed by JCPDS data reference code 98-008-5137. The FESEM image shown in Figure 2b shows the platelet morphology of α -alumina which has an average thickness of 150 ± 25 nm.

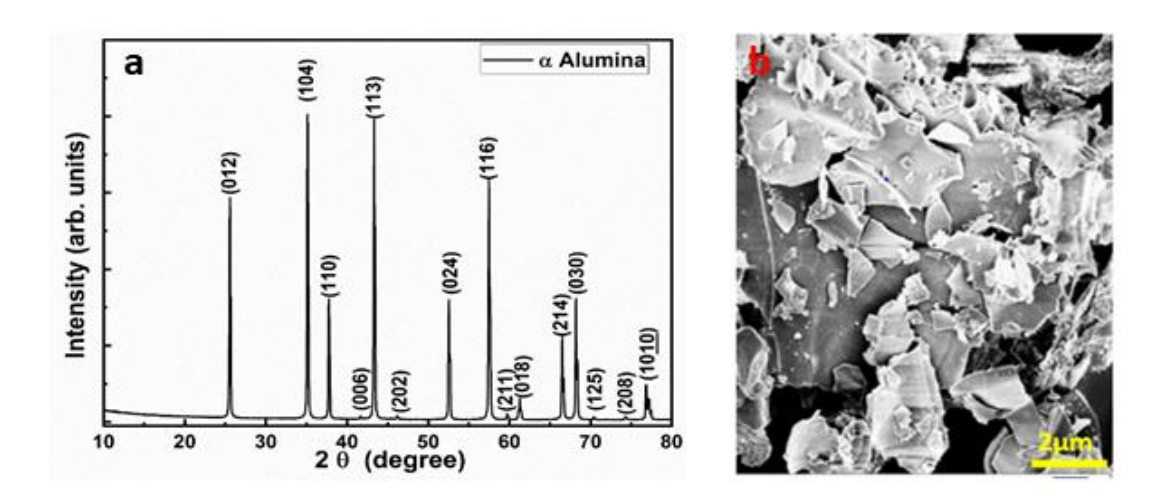


Fig. 4.2 a). Indexed XRD pattern of Al_2O_3 prepared by solution combustion method, confirms formation of hexagonal phase of α -Alumina. b) FESEM micrograph of milled α -alumina platelets.

4.1.2. LaPO₄ coating on α – alumina platelets

LaPO₄ is a suitable interphase for ceramic composites. Alumina platelets were coated with lanthanum phosphate (LaPO₄). In this process, the platelets were immersed in a solution containing dispersed

lanthanum phosphate hydrate in water, supplemented with 1 mL of dispersant. The mixture was maintained at 80°C for 24 hours. Afterward, the platelets were dried and heat treated at 900 °C for 2 hours to ensure proper adherence of the coating.

Figure 4.3a shows the alumina platelet morphology, 4.3b shows the LaPO₄ needle shaped morphology and 4.3c shows LaPO₄ needle coated on alumina platelets. The TEM microstructural analysis showed that the LaPO₄ needles were successfully deposited on the alumina platelets. The needles exhibited a distinct morphology and dispersed themselves evenly on the alumina platelets' surface. This coating on the alumina platelets creates a surface modification that may affect the fracture mechanics of the resulting composites.

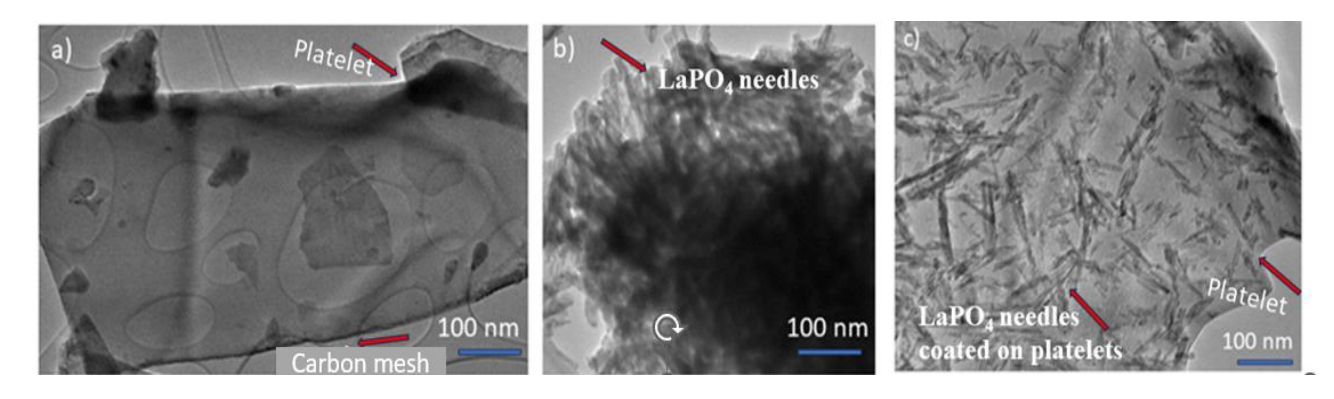


Fig. 4.3. TEM images of a) alpha alumina platelets, b) nano LaPO₄ needles and c) LaPO₄ needles coated on alpha-alumina platelets

4.1.3. Second phase addition and preparation of the composite suspensions

To achieve a free-flowing suspension with a solid loading ranging from 50% to 55%, the required alumina powder (or a powder mix containing secondary phases) is computed and added to a measured amount of an organic premix solution. This solution is prepared by dissolving the monomer (MAM) and cross-linker (MBAM) in deionized water (deionized water:MAM: MBAM = 33:6:1, by weight), with the addition of Darvan 821-A used as a dispersant (1–2 wt% based on solid loading). The resulting ceramic slurry undergoes a 24-hour tumbling process at 15 rpm, utilizing alumina balls as mixing media to achieve uniformity. Subsequently, the slurry is de-aired in a vacuum desiccator to eliminate any trapped air before the casting process [6].

4.1.4 Viscosity of composite slurries

The ceramic slurry's viscosity rises with increasing solid loading during the gelcasting process. The slurry's viscosity can be managed by varying the amount of water and binder material added. The shape and surface properties of the platelets also play a role in determining viscosity, as smooth and rounded particles tend to decrease the viscosity in comparison with irregular, sharp-edged platelets. Figure 4.4

shows the shear rate dependence of viscosities measured for the slurries at 50 vol. % loading, respectively.

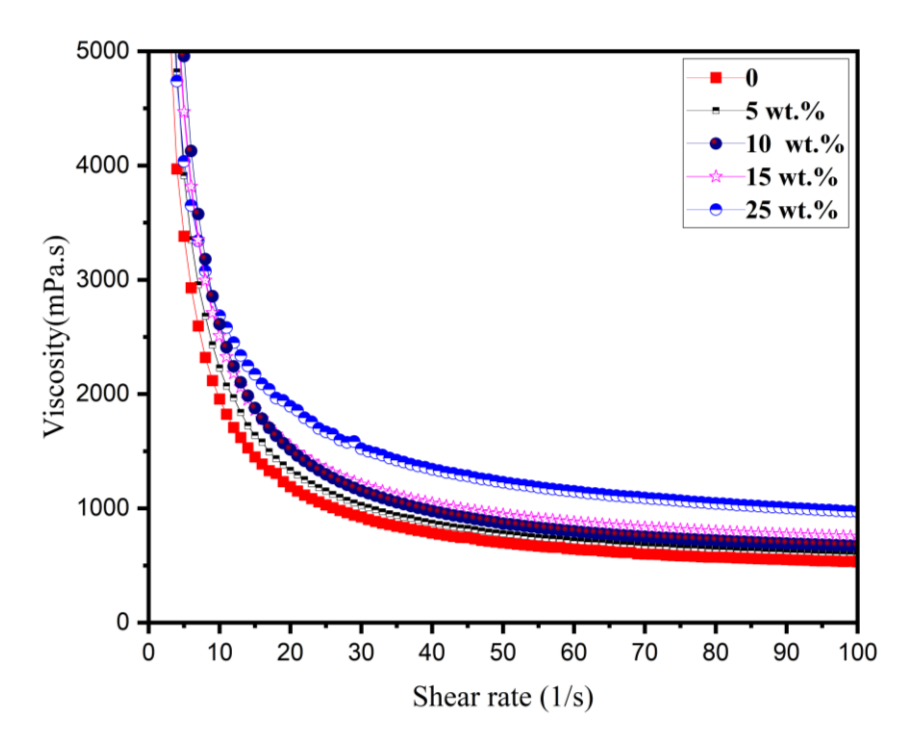


Fig. 4.4. Shear rate dependence of Viscosity of alumina- platelet alumina slurries at 50% solid loading for composites with different alumina content.

A suspension's solid loading is critical, low viscosity must allow easy pouring into molds to produce highly dense products. It is essential to optimise the viscosity and binder contents. In the gelcasting process, achieving viscosities around 1 Pa.s. is considered optimal for obtaining the best properties in the resulting sintered parts. In our study, we measured the viscosity of alumina slurries optimized for 50% solid loading. As shown in Figure 4.4, it has been found that when loaded to 50%, alumina slurries and composites with α-alumina platelet inclusions become less viscous than pure alumina. Additional solid loading produced a thick slurry that hindered deairing and did not flow readily. This would cause flaws in the finished product, such as voids, which would impair its mechanical properties [6]. Therefore, we chose slurries with a 50% solid loading optimal for casting.

4.1.5 Casting, drying, debindering and sintering of composites

The slurry, which exhibited free-flowing characteristics, was cast into EPS molds and underwent polymerization through heating at 60°C in an oven for a duration of 6 hours. Upon the completion of the gelling process, the solid green bodies were extracted by dissolving the molds in acetone. The green bodies were subjected to drying in an environmental chamber at 90% relative humidity and a temperature of 50°C for a period of four days. Following this, the binders in the dried green bodies were removed by heating them to 900°C for 2 hours in a tube furnace. The resulting debindered ceramic parts

were then sintered in air at 1675°C for 2 hours, followed by furnace cooling, to achieve the final aluminaalumina composite structures shown in Figure 4.5.



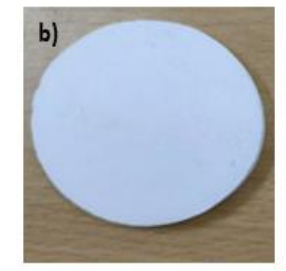


Fig. 4.5 Compacts of alumina-alumina composites with inclusion of 4 wt%% alumina platelets, prepared by the RPGC process. The dimensions of the components in the figure are (a) $70 \times 35 \times 10$ mm and (b) 30 mm diameter and 10 mm height.

4.1.6 Mechanical properties, microstructural and fractography analysis of composites

a) Density

Density and porosity have a considerable impact on the mechanical properties of ceramics and its composites. Materials that have a greater density and a smaller amount of pores typically demonstrate superior mechanical characteristics. We assessed the densities of the sintered samples using Archimedes' principle, employing glycerine as the immersion liquid.

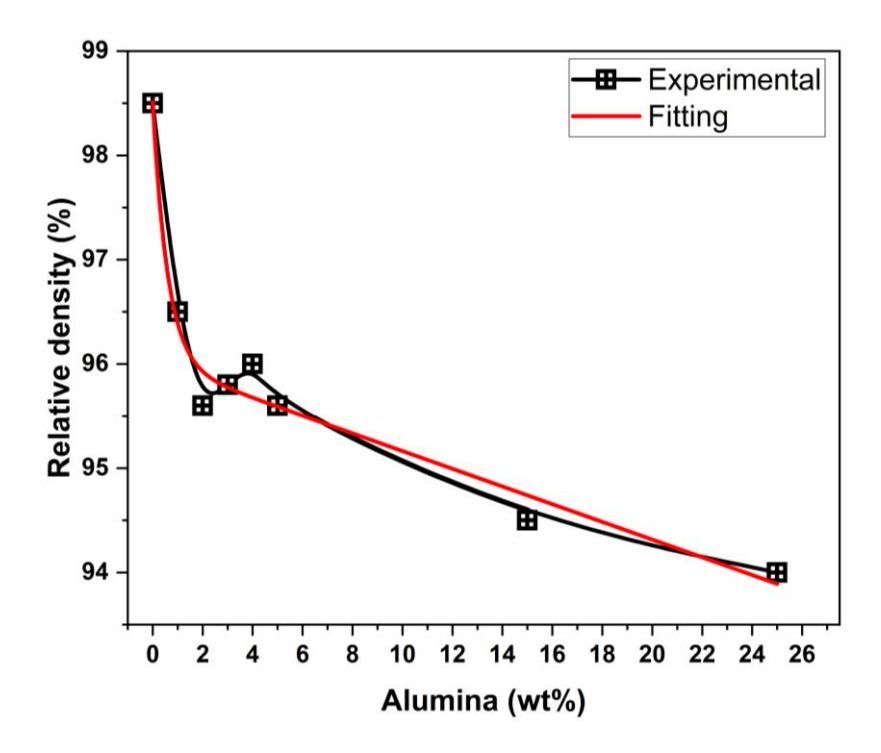


Fig.4.6. Relative density (%), calculated by comparing the measured density to the theoretical density values, for the composite samples sintered at 1675°C for 2 hours. The trend in the variation shows an exponential curve.

Relative density is computed as a percentage of the theoretical density estimated for the composites from the known densities of alumina and α -alumina. Pure alumina sample has a relative density of 98.5%, which is higher than all the composites. As shown in Figure 4.6, the composites with 1-5 wt% alumina have a relative density of nearly 96%. When 15 and 25% α -alumina is added, the relative density drops to 94%. This is because alumina particles have a platelet morphology affecting the extent of packing and this effect is more pronounced at higher platelet concentrations, resulting in a reduction in relative density. Fit of the data to an exponential function shows a trend in the variation.

b) Hardness of the composites

The specimens were evaluated for hardness using the Vickers indentation method. Indentations were formed by applying a 20 kgf load for 15 seconds. The hardness value was obtained by calculating the average of the diagonals measured across the indentations, with five indentations conducted at different locations.

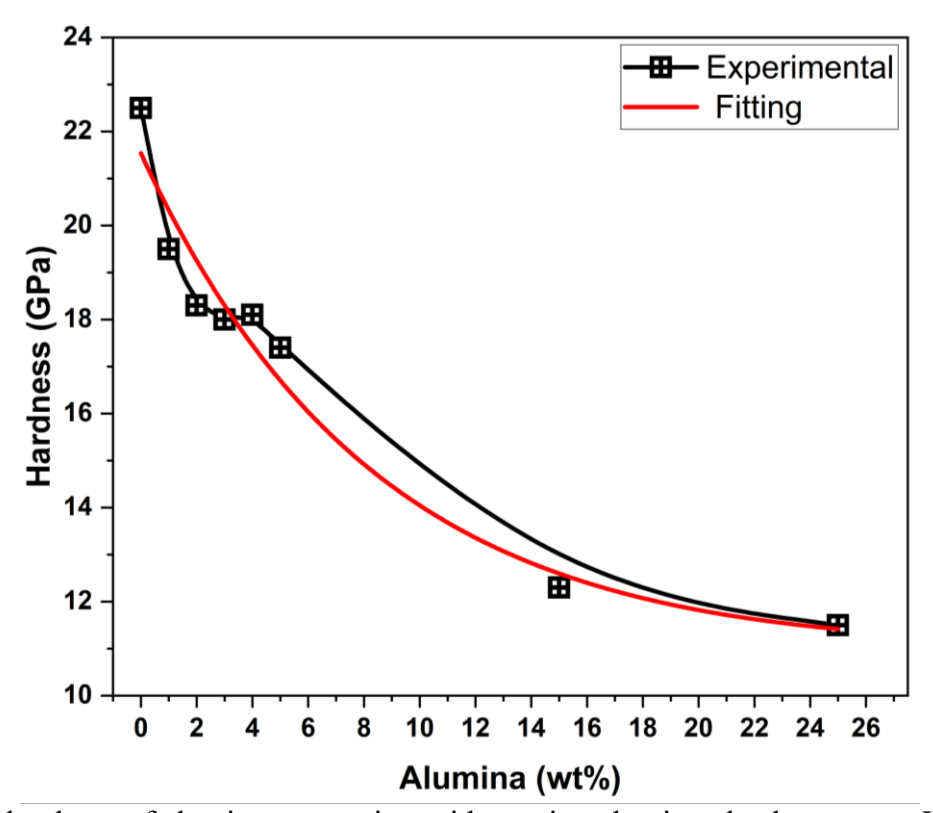


Fig 4.7. Microhardness of alumina composites with varying alumina platelet content. Variation in the data shows an exponential fit.

Figure 4.7 shows the microhardness of alumina composites that have different amounts of Al₂O₃ platelets. The microhardness (HV) is 22.5 GPa in pure alumina with a relative density of 98.5%. It goes down as the amount of Al₂O₃ platelets increasing. The link between microhardness and density shows that microhardness decreases as platelet alumina content increases. The higher platelet content leads to the chance of increasing porosity in the composites.

c) Flexural Strength and Fracture Toughness

Reasonable values of flexural strength (σ) and fracture toughness (K_{Ic}) are essential for a ceramic material to find many applications. We determined the flexural strength using a 3-point bend test on a specimen cut to $3.0 \times 4.0 \times 45.0$ mm dimensions, as per ASTM C1161–13 standard [7] and fracture toughness measurement was conducted using the direct crack method as per ASTM C1421–10 standard [8] discussed in detail in section 2.8, chapter 2.

Pure alumina with no platelet addition, after sintering at 1675° C for 2hrs had shown flexural strength and fracture toughness of 389 MPa and 3.01 MPa \sqrt{m} , respectively.

The flexural strength and fracture toughness values of the composites as a function of wt% of alumina platelets determined from 3-point bend test are presented in Figure 4. 8 a) and b).

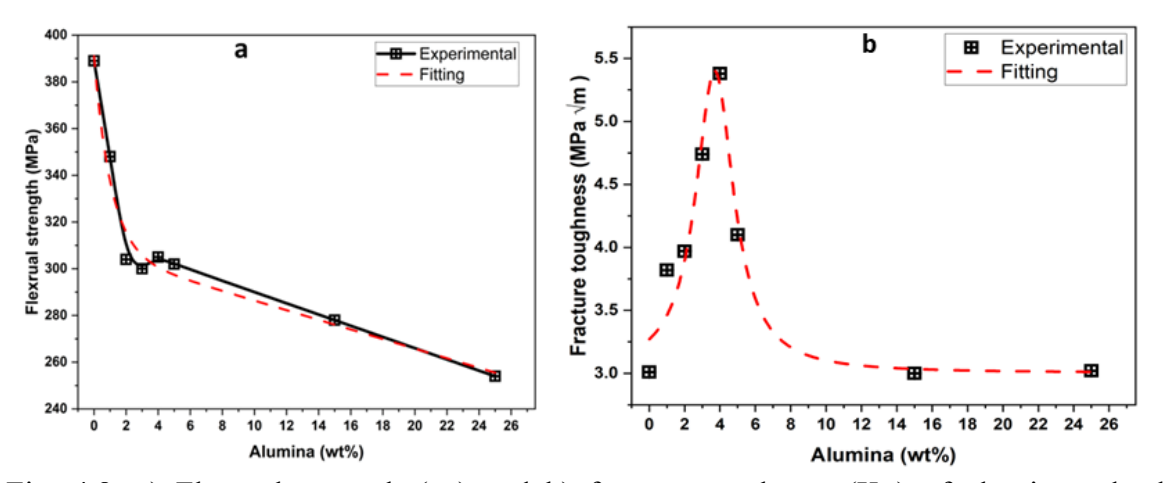


Fig. 4.8. a) Flexural strength (σ_f) and b) fracture toughness (K_{Ic}) of alumina-platelet alumina composites with different wt% of platelets.

Remarkable improvement in fracture toughness was observed in alumina reinforced with Al₂O₃ platelets (4 wt%), resulting in a significant increase from 3 to 5.4 MPa √m. Additionally, the material's flexural strength was measured to be 310 MPa. Alumina platelet composites with varying weight percentages (1 to 5wt%) showed an improvement in fracture toughness, although there was a decrease in flexural strength. It is worth mentioning that the relative density of composites in this range is approximately 96%. The strength and fracture toughness of the alumina (15 and 25 wt%) platelet composite is decreased, while the relative density is approximately 94%. The packing of alumina platelets in the matrix causes a decrease in density and an increase in porosity in higher concentrations of platelet-reinforced composites.

d) Microstructural studies and fractography analysis

The inclusion of Al₂O₃ platelets as a secondary phase in the alumina matrix was expected to result in alterations to the microstructure, which in turn will affect the mechanical properties and crack propagation. Extensive microstructure analysis was conducted to understand better the connection between these platelets and the observed enhancement in fracture toughness in the current composites.

FESEM images were recorded in polished composites after thermal etching at 1350°C for 2 hrs [9] and are shown in Figure 4. 9 (a &b). Figure 4. 9 (a) shows the pure alumina. Figure 4. 9 (b) shows the distribution of alumina (5 wt%) platelets in the alumina matrix, and pores are not present.

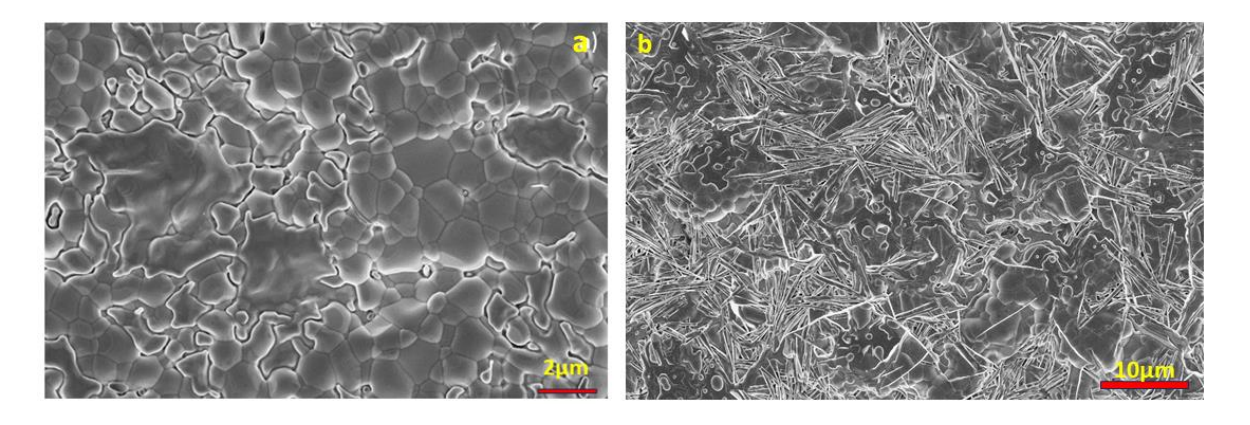


Fig. 4.9. FESEM microstructures of polished and thermally etched pure alumina and Al_2O_3 -5 wt% platelet Al_2O_3 composites.

Platelets are a barrier to prevent trans-granular cracks in composites containing 4 wt% alumina, as shown in Figure 4. 10 a). Platelets can reduce the stress concentration at the tip of a crack, preventing the break from spreading further. We explore how platelets act as a barrier between materials and cracks, stopping cracks from spreading further. We aim to understand how effective platelets are in preventing crack propagation. Figure 4. 10(b-d) illustrate the presence of fracture bridging and crack deflection resulting from the inclusion of platelets in a composite material with a 4 wt% platelet alumina content. Platelets can serve as connectors between particles, increasing the quantity of tie lines and thereby enhancing the fracture toughness of composites. The observations above provide empirical support for the notion that platelets are efficacious in impeding crack propagation and enhancing the material's overall fracture toughness.

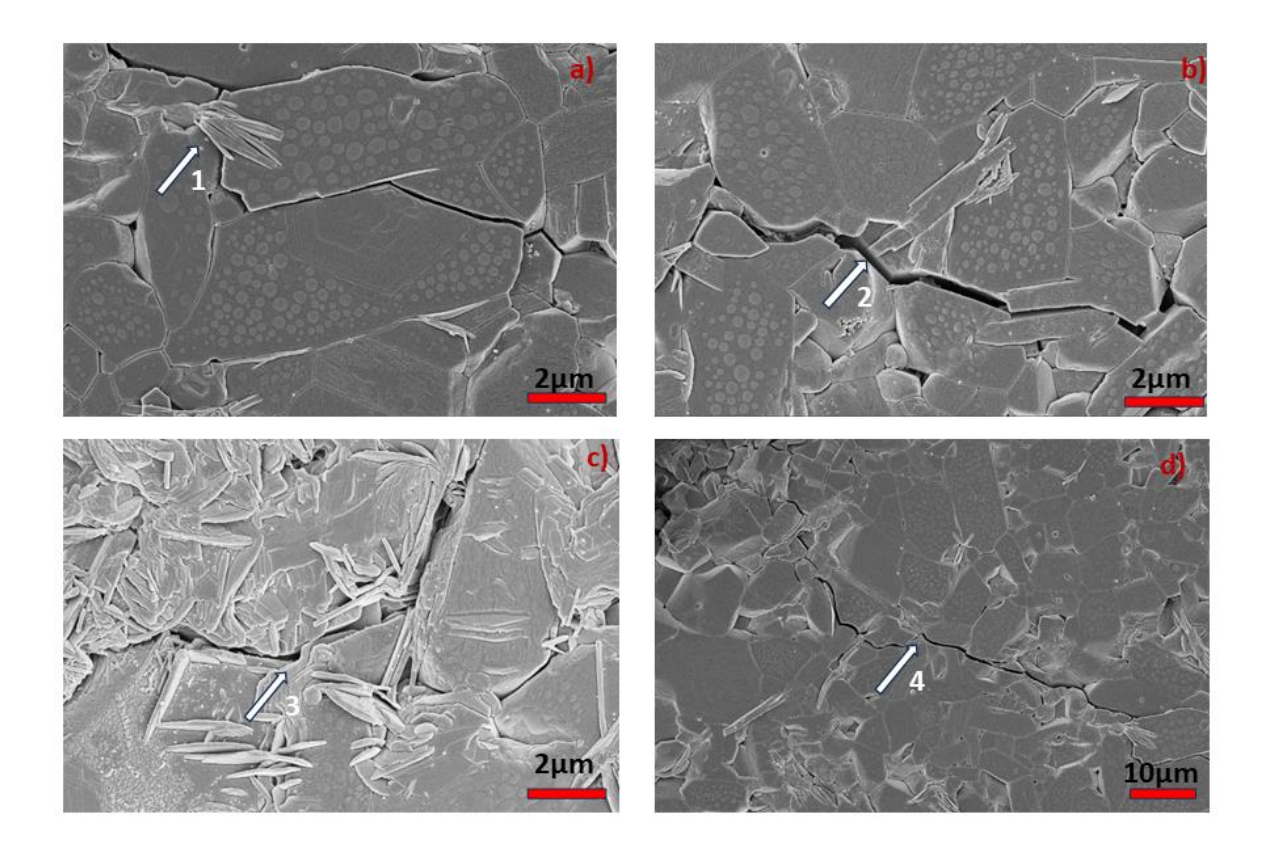


Fig. 4.10. FESEM microstructures of polished and thermally etched alumina-alumina composites, after crack initiation by indentation, with: (a) & (b) 4 wt% and (c) & (d) 3 wt% % alumina platelets. All figures show distribution of platelets among alumina grains (typical platelets marked at 1). Evidence is seen for arresting of cracks (at 1), deflection of the cracks (at 2, 3 & 4).

Summary

In the present work, we chose to investigate the possibility of improving the properties of alumina, reinforced with alumina platelets which are given an interface coating of LaPO₄. The α -alumina platelets synthesized by the combustion route are of nanometric thickness, have large aspect ratio and are single crystalline. The process of gelcasting free flowing slurries enables uniform distribution of second phases and provides an easy, scalable, and cost-effective method of shape forming ceramic components.

Microstructures recorded in those composites showed no substantial porosity or cracking. FESEM images (Figure. 4.10) of polished specimen (thermally etched after indentation) provide clear evidence for arresting of crack propagation, deflection and bridging of the cracks, by the presence of platelets, shown typically in the composites with 3 and 4 wt%% platelet alumina. The concept of crack bridging by platelets is also observed as one of the toughening mechanisms in these composites. The platelets form a bridge between two separated crack faces and creates an obstruction that slows down the crack

propagation. The large surface of the platelets provides many crack-stopping sites and increases the amount of energy required for the material to fail. Our results on the alumina- alumina composites thus obtained show that addition of 3 to 4 wt% platelet alumina results in an improvement in mechanical properties yielding substantial flexural strength (310 MPa) as well as fracture toughness (5.4 MPa \sqrt{m}), simultaneously.

The combination of these effects has caused a significant increase in the fracture toughness of the composites with optimal composition (alumina with 3 and 4 wt%% platelets), making them potential candidates as dental implants and as high temperature components in aerospace and automobile applications. The possibility of casting the slurries of the above compositions into molds fabricated by rapid prototyping and geleasting (RPGC) process makes many niche applications accessible in medical and defence fields.

References:

- 1. Rajasekharan T, Swaroop Raju PM, Pandey RK, Seshu Bai V, Pradyumna R, Baig MAH. Complex-shaped alumina products through rapid prototyping. Met Mat and Proc. 2007; 19:41–46.
- 2. P. Jeevankumar, P. Rose, A. Rajanikanth, T. Rajasekharan, V. Seshu Bai, Netshaping of advanced ceramic composites by gelcasting into precision molds made by rapid-prototyping, Int. J. Appl. Ceram. Technol. (2023) 1–11, https://doi.org/10.1111/ijac.14568.
- 3. P.Jeevankumar, Poly Rose, Pawan Kumar Verma , Seshu Bai Vummethala, Rajasekharan Thankappan Pillai, Fabrication of Ba_{0.5} Sr_{0.5} TiO₃ components combining rapid prototyping with gelcasting using different gelling systems; Open Ceramics 17 (2024) 100512
- 4. J.B. Davis, D.B. Marshall, P.E.D. Morgan, Monazite-containing oxide/oxide composites; Journal of the European Ceramic Society 20 (2000) 583±587
- 5. J.J. Kingsley And K.C. Patil, A Novel Combustion Process For The Synthesis Of Fine Particle A-Alumina And Related Oxide Materials; Materials Letters, Volume 6, Number I 1,12,1998
- 6. Emad Mohamed M. Ewais, Rhoological properties of concentrated alumina slurries: influence of pH and dispersant agent, TESCE, Vol. 30, No.2,2004
- 7 Standard Test Method for Flexural Strength of Advanced Ceramics at Ambient Temperature. Available from: https://doi.org/10. 1520/C1161-13. Accessed 19 January 2014.
- 8 Standard Test Methods for Determination of Fracture Toughness of Advanced Ceramics at Ambient Temperature. Available from: https://doi.org/10.1520/C1421-10. Accessed 19 January 2014.
- 9 M. Liu, J. Zhao, S. Shimai, J. Zhang, H. Chen, H. Chen, D. Han, J. Liu, S. Wang, A Polishing-Free Etching Method for Microstructure Observation of Fine-Grained Ceramics; J. Ceram. Sci. Technol., 12 [1] 59-62 (2021)

Chapter V

Yttria stabilized zirconia (3Y-PSZ) – α alumina platelet composites

Introduction

Dental prostheses and implants utilize ceramics because of their biocompatibility and chemical stability [1-3]. The aerospace and power generating industries want composites that possess both low density and exceptional damage tolerance [4,5]. Oxide/oxide composites are well-suited for hightemperature applications due to their inherent oxidation resistance. Additionally, they are more costeffective compared to other composites. Zirconium dioxide (ZrO₂) is a highly important ceramic material because it has a diverse variety of uses. Zirconium dioxide (ZrO₂) is found in three different crystalline structures under normal atmospheric pressure: monoclinic (m), tetragonal (t), and cubic (c). The monoclinic phase is thermodynamically stable at room temperature and undergoes a phase transition to the tetragonal phase at around 1170 °C. The tetragonal phase is thermodynamically stable until a temperature of 2370 °C, at which time it undergoes a transformation to the cubic phase. The cubic phase remains stable until it reaches the melting point at 2680 °C [7]. At ambient temperature, the high-temperature phases of ZrO2 can be made stable by incorporating oxides such as Y₂O₃, MgO, CeO₂, or CaO. Y₂O₃ is the predominant stabilizer in widespread usage. Zirconia ceramics can be classified into two types according to their crystal structure: fully stabilized zirconia (FSZ) and partially stabilized zirconia (PSZ) [8]. Zirconia ceramics that have been stabilized with a Y₂O₃ content ranging from 3 to 6.5 mol% are commonly referred to as PSZ. These ceramics provide advantageous qualities [9]. Additionally, zirconia that has been stabilized with 8 to 10 mol% is also known. You are referred to as FSZ. Zirconia ceramics with less than 3 mol% of Y₂O₃ are utilized in the fields of biomedicine and structural engineering due to their remarkable strength and resistance to fracture. The ceramics mentioned are classified as toughened zirconia ceramics [10].

5.1 Fabrication of yttria stabilized zirconia (YSZ) - α alumina composites

The present work has focused on variation in the mechanical and physical characteristics of α -alumina platelet toughened zirconia composites. Solution combustion synthesis was used to obtain single crystalline α - alumina platelets of high hardness, large aspect ratio and about 150 nm thickness. Dense ceramic components were fabricated by gelcasting free flowing slurries of the composites into expandable polystyrene (EPS) molds, and by further processing. The addition of LaPO₄-coated platelets to the partially stabilised zirconia (3Y-PSZ) matrix resulted in a significant enhancement of fracture toughness in the composites. The 3Y-PSZ composites, with 5 to 15 wt% platelets, had a

relative density of approximately 93-95%. These composites also demonstrated a significant flexural strength of around 600 MPa, along with an excellent fracture toughness of approximately 8.8 MPa√m. Microstructural studies provided clear evidence for the role of platelets in resisting the crack propagation, deflecting and bridging the cracks. Owing to superior properties, the PSZ- alumina platelet composites with optimal composition show promise as dental implants and as high temperature components in aerospace and automobile applications. These 3Y-PSZ composites have an edge over continuous fibre reinforced composites due to their higher strength and prospects to be fabricated in large complex shapes by combining rapid prototyping and gelcasting (RPGC) techniques [11-13].

5.1.1. Second phase addition and preparation of composite suspensions

To prepare a free-flowing slurry of requisite composition, 3 mol% YSZ powder (with an average particle size of 200- 800 nm) was mixed with different weight percentages (x = 0, 1, 5, 10, 15 and 25 wt. %) of LaPO₄ coated alumina platelets and was tumbled in a turbo-mixer for 12 hours. A premix solution was prepared by dissolving monomer MAM and cross-linker MBAM in deionized water. The ratio of deionized water to MAM to MBAM was 33:6:1 by weight. Additionally, DARVAN - CN was added as a dispersant (1-2 wt% based on the solid loading). Subsequently, suspensions were prepared by combining the ceramic slurry with the organic premix gelling medium. A ceramic slurry with a solid loading of 50% was obtained by adding a calculated amount of mixed powder (3Y-PSZ + different wt% of LaPO₄ coated α-platelets [14,15]) to measured amount of premix solution, allowed for mixing. The ceramic slurry obtained was tumbled for 24 hours at a speed of 15 rpm using zirconia balls as the mixing medium. Subsequently, the slurry was subjected to vacuum de-airing in a desiccator before being cast into EPS molds [16]. The loading level is optimized to achieve a viscosity of approximately 1 Pa. s to ensure that the slurry flows freely. Ammonium persulfate was used as an initiator and TEMED was used as a catalyst.

5.1.2 Viscosity of composite slurries

In the gelcasting process, the viscosity of the ceramic slurry increases as the solid loading increases. The viscosity of the slurry can be controlled by varying the amount of water and binder material in the premix. In addition to powder particle size and shape, the surface characteristics of the particle also affect the viscosity; smooth, rounded particles tend to have a lower viscosity than irregular, sharpedged platelets. The shear rate dependency of viscosities recorded for the slurries at 55 and 50 vol% loading, respectively, is shown in Figure 5. 1(a and b). Higher viscosity values made it difficult for the slurries with 55 vol% volume loading to flow freely, as shown in Figure 5.1(a). Since slurries usually have lower viscosity, we handled them by pouring them into molds with 50 vol% solid loading. As we

added more alumina platelets, the viscosity increased systematically (Figure 5.1(b)). Also, we adjusted the amount of dispersant to ensure the slurry flows well.

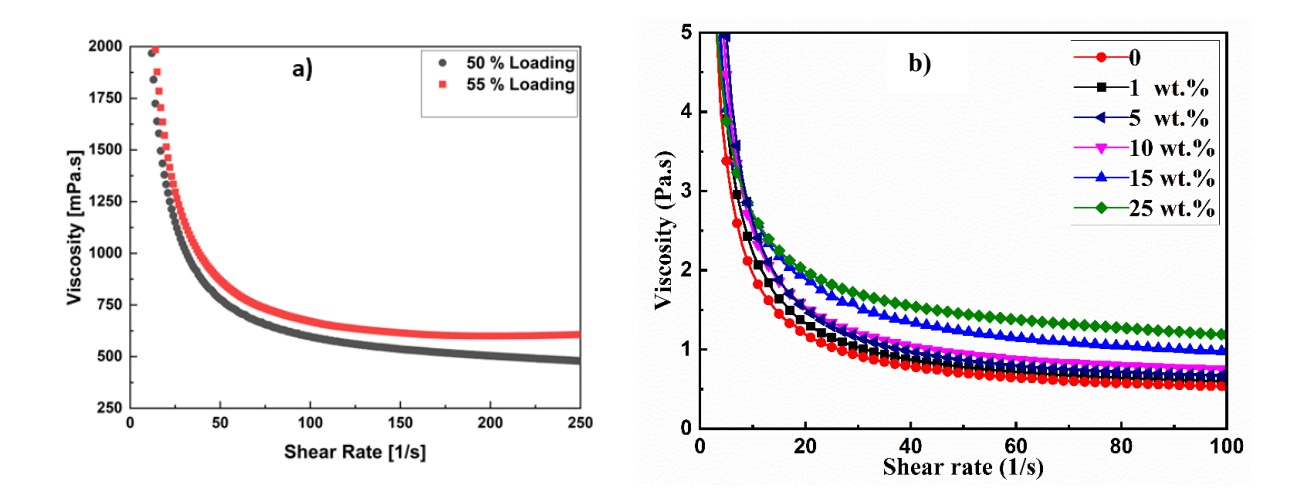


Fig.5 1. Shear rate dependence of Viscosity of PSZ- platelet alumina slurries: a) at 55% solid loading and b) at 50% solid loading for composites with different alumina platelet content.

5.1.3 Casting, drying, debindering and sintering of composites

The composites, consisting of 3Y-PSZ/α-Al₂O₃ (LaPO₄-coated) platelets, were fabricated using gelcasting and rapid prototyping (RPGC) process. The slurries are cast into EPS molds and kept at a temperature of 65°C for 5-6 hours to allow for polymerization and completion of the gelling process. The solid green bodies were removed from the mold by dissolving the mold with acetone. They were then dried in a humidity-controlled oven for a week. The green bodies underwent debindering at a temperature of 900°C and were subjected to a soak time of 2 hours to eliminate the organic binders. Subsequently, the material was subjected to a sintering 1550 °C at a rate of heat is 1°C per minute for 3 hours and furnace cooled. Figure 5.2 the compacts of the 3Y-PSZ composite, fabricated with 5 wt% of alumina platelets. Usage of small amounts of (10 to 15 wt%) organic binders in the RPGC process enables higher densities to be achieved after sintering, compared to competing slurry-based techniques.



Fig. 5.2. Compacts of YSZ-alumina composites with inclusion of 5 wt.% alumina platelets, prepared by the GC-RPT process. The dimensions of the components in the figure are a) 70 x 30 x 10 mm, and b) 30 mm diameter and 10 mm height.

5.1.4 Mechanical properties, microstructural and fractography analysis of composites

a) Density of composites

The mechanical characteristics of ceramics are significantly influenced by density and porosity. Materials with higher density and minimum porosity demonstrate superior mechanical performance. In order to establish a relationship between the characteristics of the current composites, the densities of the sintered samples were determined using Archimedes' principle, with glycerine as used for immersion medium. The percentage of relative density, calculated by comparing the measured density to the theoretical density values, is shown in Figure 5.3 for the composite samples sintered at a temperature of 1550 °C for 3 hours.

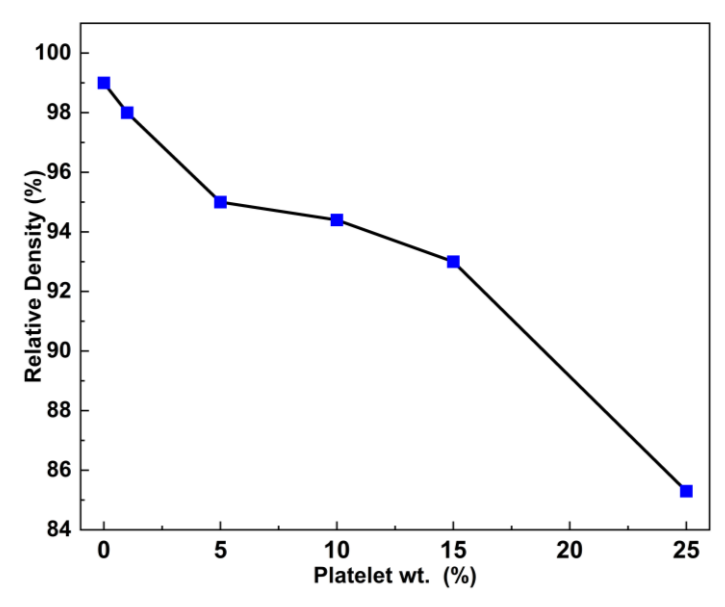


Fig. 5.3. Relative Density of YSZ-Alumina composites having different wt. % of alumina platelets.

Relative density is computed as a percentage of the theoretical density estimated for the composites from the known densities of PSZ and α -alumina. Pure YSZ sample has a relative density of 99%, which is higher compared to all the composites. The composites with 5-15 wt. % alumina has a relative density of nearly 94%. When 25% α -alumina is added, the relative density drops significantly to 85%. The platelet morphology of alumina particles influences their packing efficiency. This effect becomes more significant at higher alumina concentrations, leading to a notable reduction in relative density, specifically at the 25 wt% alumina content.

b) Hardness of the composites

The specimens were evaluated for hardness using the Vickers indentation method. Indentations were formed by applying a 20 kgf load for 15 seconds. The hardness value was obtained by calculating the average of the diagonals measured across the indentations, with five indentations conducted at different locations

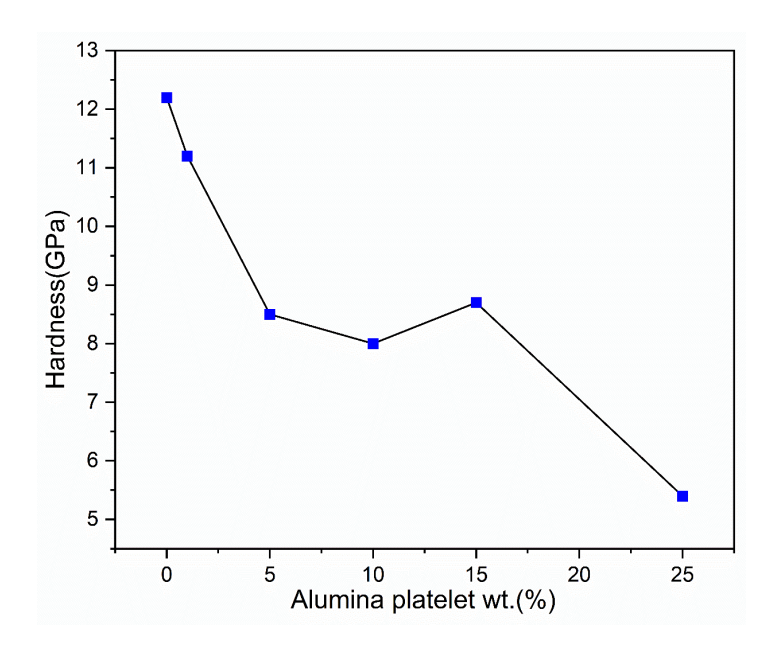


Fig. 5.4. Microhardness of 3Y-PSZ composites with varying alumina platelet content.

Figure 5.4 illustrates the microhardness of 3Y-PSZ composites with different levels of Al2O3 platelet content. The figure demonstrates that pure PSZ with 99% relative density achieved a microhardness (HV) of 12.3 GPa. However, when the content of Al₂O₃ platelets increased, the microhardness decreased. The decrease in hardness values correlates with the drop in density as platelet concentration increases. Consequently, there exists noticeable correlation between microhardness and the increasing porosity resulting from higher platelet alumina content.

c) Flexural Strength and Fracture Toughness

Reasonable values of flexural strength (σ) and fracture toughness (K_{Ic}) are essential for a ceramic material to find many applications. We determined the flexural strength using a 3-point bend test on a specimen cut to $3.0 \times 4.0 \times 45.0$ mm dimensions, as per ASTM C1161–13 [17] standard and Fracture toughness is measured by the direct crack method as per ASTM C1421–10 [18], as discussed in detail in section 2.8, chapter 2.

Pure YSZ (x = 0) compact with no alumina addition, after sintering at 1550°C for 3hrs had shown considerably high flexural strength and fracture toughness of ~1029 MPa and ~4.97 MPa \sqrt{m} , respectively.

The flexural strength and fracture toughness values of the composites as a function of wt% of alumina platelets (x = 0, 1, 5, 10, 15 and 25 wt%) determined from 3-point bend test are presented in Figure 5.5 (as A: present work) along with the corresponding data reported in literature on PSZ and fully stabilised zirconia (FSZ) composites with varying alumina particulate [20-22] or platelet [19] addition.

The data from literature [19,22] available in mol% of alumina inclusion in YSZ is converted to wt% to enable comparison.

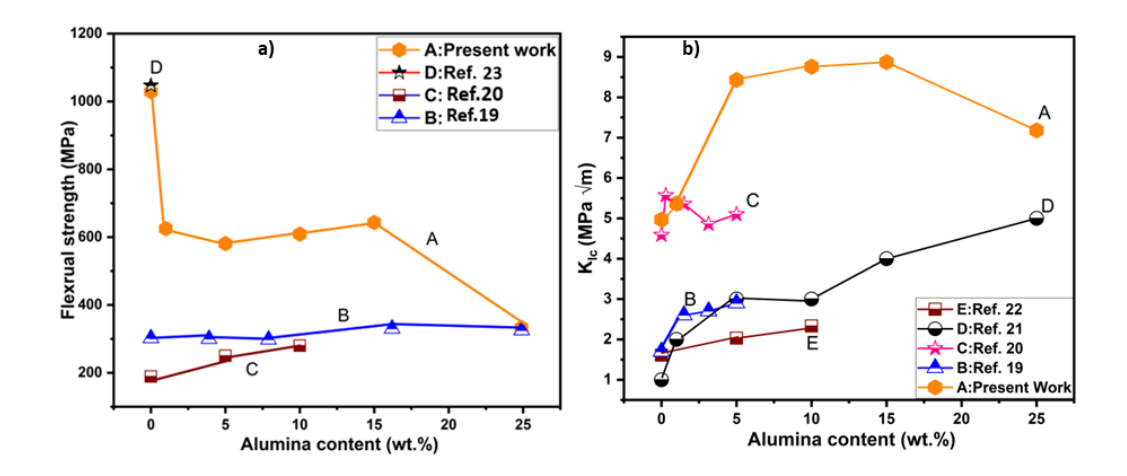


Fig. 5.5 a) Flexural strength (σ) and b) fracture toughness (K_{IC}) of 3Y - PSZ-Alumina composites with different wt% of alumina platelets. Data of the present work are shown as curve (A). Data reported in literature on 3Y-PSZ composites with alumina content as second phase addition [19, 20-22] are also shown (as B-E) in the figure for comparison.

The composites' flexural strength and fracture toughness were measured using a 3-point bend test. The values of alumina platelets were determined for different weight percentages (wt%) (x = 0, 1, 5, 10, 15, and 25wt. %). The results are shown in Figure 5.5 (labeled as A: present work).

From the figure 5.5 shows 3Y-PSZ composites thus obtained show that addition of 5 to 15 wt. % platelet alumina results in remarkable improvement in mechanical properties yielding high flexural strength (643 MPa) as well as fracture toughness (8.87 MPa \sqrt{m}), simultaneously.

5.1.5. Transformation toughening

An essential mechanism for transformation toughening in PSZ is the tetragonal to monoclinic phase transformation, which creates compressive stresses that prevent crack propagation. When stressed, PSZ transforms from a tetragonal to a monoclinic phase.

When yttria-stabilized tetragonal zirconia is subjected to stress, its crystal structure at the point of stress locally transforms from tetragonal to monoclinic, which increases by around 4 vol%. This phenomenon is known as stress-induced phase transformation. Cracks that are formed experience compressive stress at their tips, which stops them from further propagation [24]. The t m phase transformation induced by stress locally in ZrO₂ is shown to improve materials' strength and fracture toughness of zirconia composites [25]. This transformation results in the creation of compression around cracks, causing them to deflect. The stress is distributed more evenly by deflecting cracks,

preventing further propagation. This phenomenon enhances the material's resistance to crack propagation, contributing to its improved fracture toughness and mechanical properties.

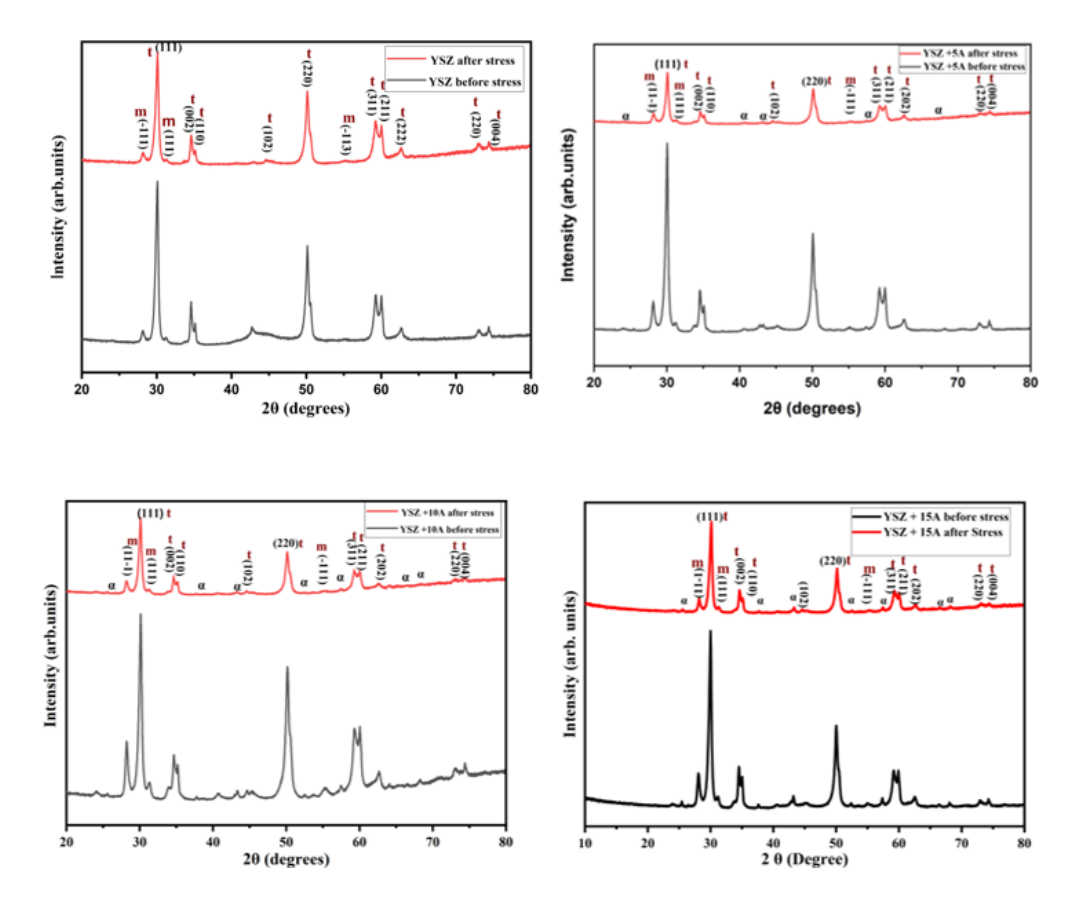


Fig 5.6. Indexed XRD patterns of pure 3Y-PSZ and 3Y-PSZ with 5, 10 & 15 wt. % α-alumina platelet composites before and after stress application, showing tetragonal and monoclinic phases to co-exist.

Table1: Quantitative assessment of phase transformation in pure PSZ and 3Y-PSZ composites with 5, 10 and 15 wt% α -alumina under stress application, from XRD

S.no:	3Y-PSZ	Before stress application		After stress application		
	composites	Monoclinic	Tetragonal Phase(%)	Monoclinic	Tetragonal Phase(%)	
		Phase(%)	` ′	Phase(%)	` ′	
1	PSZ	4.22	95.80	5.02	94.98	
2	PSZ + 5 wt%	8.30	91.7	9.00	91.0	
3	PSZ + 10 wt%	8.90	91.1	9.30	90.7	
4	PSZ+ 15 wt%	9.28	90.70	10.5	89.40	

In order to assess the contribution of transformation toughening to 3Y-PSZ $+ \alpha$ - alumina composites with α -platelets of the present study, XRD patterns are recorded in the composite samples before and after stress application. Samples subjected to stress for fracture toughness measurements were used for this purpose. The XRD data shown in Figure 5.6 for the composites with 5, 10 and 15 wt% platelet content were analyzed to determine the monoclinic phase present before and after stress, and the resulrs are presented in Table 1.

All the 3Y-PSZ composites show a small amount of monoclinic phase to be present, which increases from 4.22 to 9.28%, with a corresponding decrease in the tetragonal phase as the alumina platelet content is increased. On the application of stress, all the composites show nearly the same increase in the monoclinic phase by about 1%, as is seen from Figure 5.7 and Table 1, compared to its content before stress. These observations suggest that stress-induced transformation toughening is minimal and occurs nearly to the same extent in all the composites.

The fact that the 3Y - PSZ composites showed remarkable enhancement in fracture toughness from 5 to ~ 8.5 MPa \sqrt{m} , when the platelet content is in the range 5 to 15 wt%, as seen from Fig. 6, projects the significant role played by single crystalline alumina platelets in causing effective reinforcement.

A possible reason for an increase in the monoclinic phase in the presence of alumina is that Yttria (Y₂O₃), the stabilizer in 3Y-PSZ, and alumina (Al₂O₃) tend to segregate at the grain boundaries [26]. If yttria reacts with alumina, this segregation can form a Y-Al-O phase at the boundaries, which is less effective in stabilizing the tetragonal phase than yttria alone [27]. This reduces the overall stability of the tetragonal phase and promotes the transformation to the monoclinic phase.

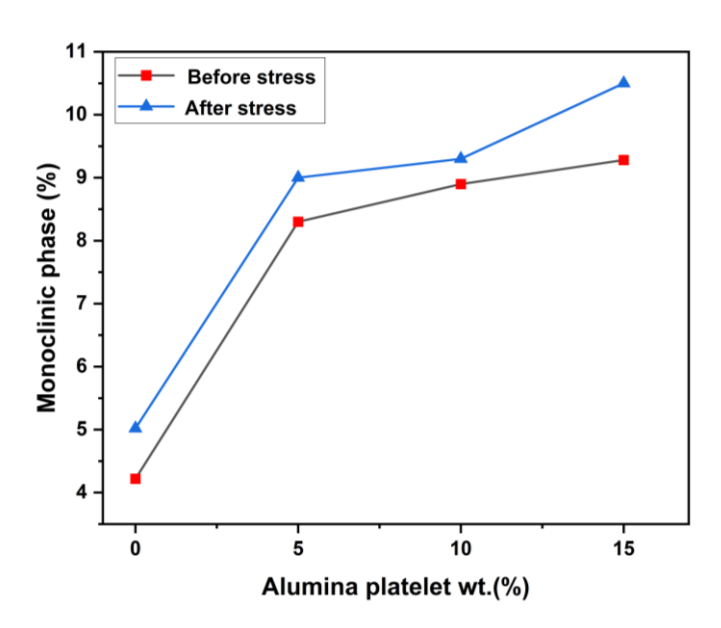


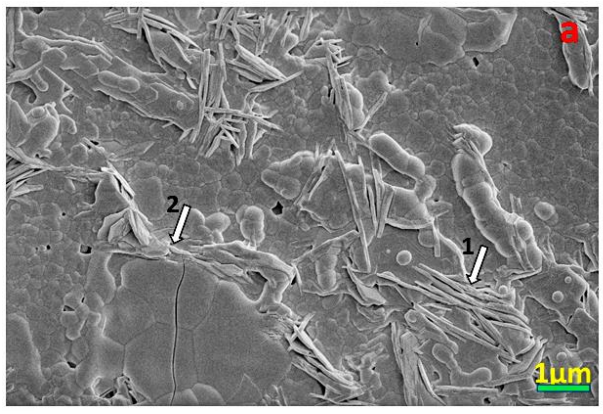
Fig. 5.7. Monoclinic phase (%) varying with alumina platelet content, before and after stress application.

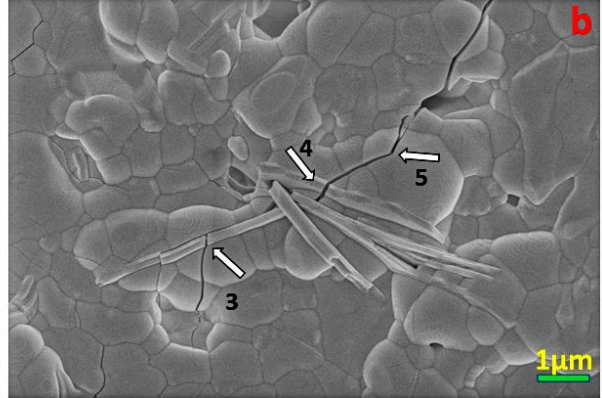
5.1.6 Microstructural Studies

Inclusion of Al₂O₃ platelets in YSZ matrix as the second phase would bring about a change in the microstructures and have an impact on the crack propagation and mechanical properties. To have an insight into the role of platelets on the observed enhancement in the fracture toughness of the present composites, detailed microstructural investigations were carried out.

FESEM images were recorded in polished composites after thermal etching at 1250°C for 3 hrs [28] and are shown in Figure 5.8(a -d). Figure 5.8(a) shows distribution of alumina platelets in YSZ matrix. Arresting of trans-granular cracks by the platelets can be clearly seen in Figure 5.8(b) in 3Y-PSZ with 10 wt. % alumina. The platelets can reduce the stress concentration at the crack tip, and thus suppress the crack propagation. The platelets can be seen to form a barrier between the matrix and the crack, preventing it from spreading further. Figure 5.8(c-d) depict the occurrence of crack bridging and crack deflection by the presence of platelets shown typically in the composite with 15 wt% alumina. Platelets can serve as bridges between particles, increasing the number of tie lines and thus improve the fracture toughness of the composites [29]. The above observations give evidence that platelets are effective in providing resistance to crack propagation and thus lead to the material's overall fracture toughness.

Figure 5.8(e) shows an image recorded in fractured surface of 3Y-PSZ composite with 15 wt.% platelets, after thermal etching; it shows that debonding of the platelets is one of the operative mechanisms, which dissipates energy and thus resists failure. Occurrence of platelet pull-out suggests the presence of strong interfacial bonding and thus accounts for increased fracture toughness of the YSZ-platelet alumina composites. The larger surface area of the platelets, compared to alumina particulates, has an advantage in enhancing the interfacial bonding. Figure 5.8(f) shows the microstructure of the polished and etched composite with 25 wt.% alumina. Agglomeration of platelets, and voids occurring due to those agglomerates, can be seen this polished and etched composite, which accounts for its lower density and reduction in its observed fracture toughness.





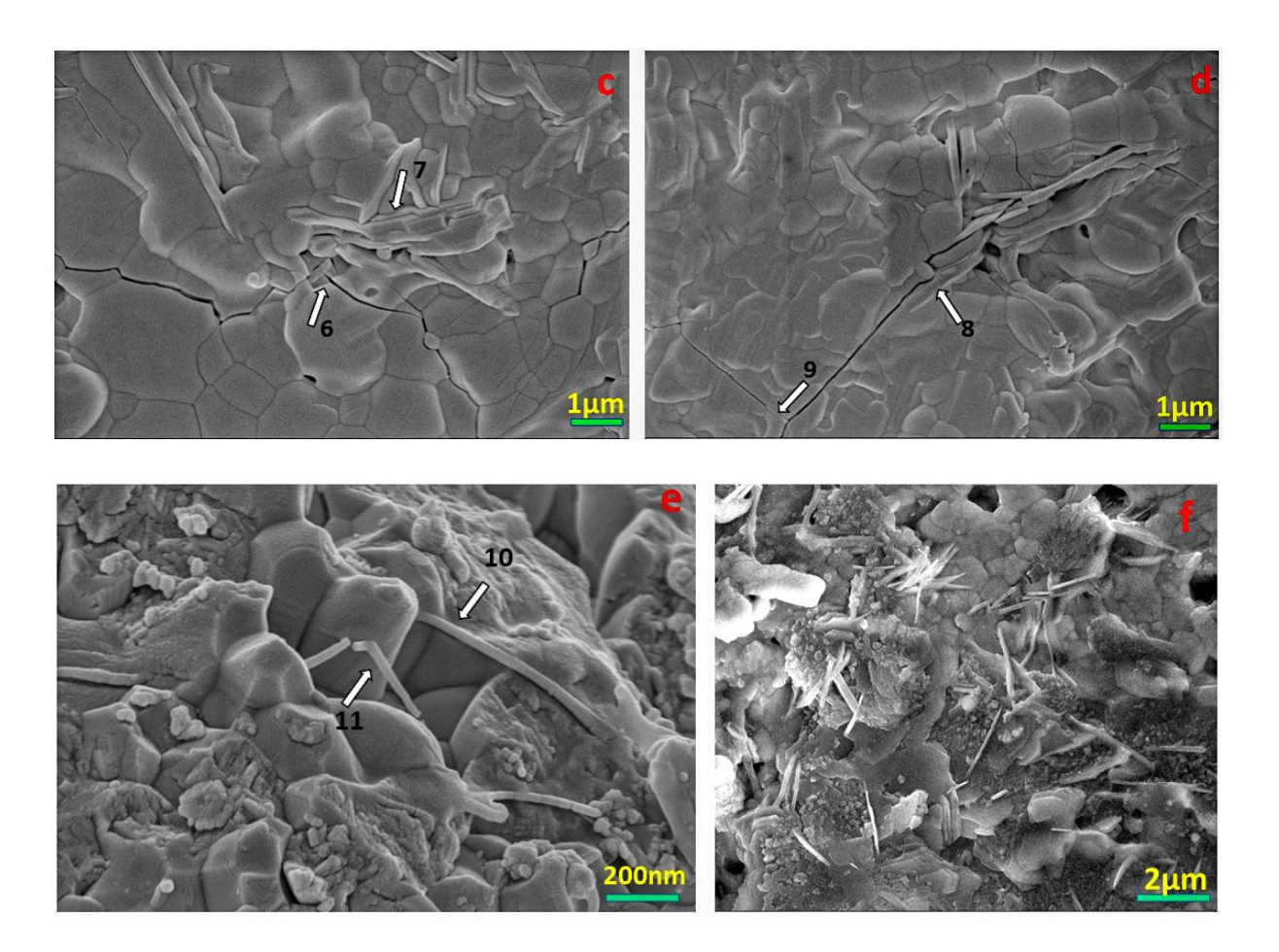


Fig. 5.8. FESEM microstructures of polished and thermally etched ATZ composites, after crack initiation by indentation, with: (a) & (b) 10 wt% and (c) & (d) 15 wt% alumina platelets. All figures show distribution of platelets among YSZ grains (typical platelets marked at 1). Evidence is seen for arresting of cracks (at 2, 3, 4 & 6), deflection of the cracks (at 5, 7 & 8), crack bridging (at 9). (e) shows debonding of platelets (at 10 & 11) in the fractured and thermally etched composite with 15 wt% platelets; and (f) shows agglomeration of platelets and associated voids in polished and etched composite with 25 wt% platelets.

Summary

In the present work, we chose to investigate the possibility of improving the properties of 3Y-PSZ, reinforced with alumina platelets which are given an interface coating of LaPO₄. The α-alumina platelets synthesized by the combustion route are of nanometric thickness, have large aspect ratio and are single crystalline. The process of gelcasting free flowing slurries into 3D profile-cut EPS molds enables uniform distribution of second phases and provides an easy, scalable, and cost-effective method of shape forming ceramic components.

Our results of composites thus obtained show that addition of 5 to 15 wt% platelet alumina results in remarkable improvement in mechanical properties yielding high flexural strength (643 MPa) as well as fracture toughness (8.87 MPa \sqrt{m}), simultaneously.

We gather from the above literature that improvement of fracture toughness with fibre reinforcement occurs at the expense of flexural strength, and that LaPO₄ coating increases K_{IC} substantially. Moreover, the process involved in the fabrication of fibre reinforced components into complex shapes is expensive and involved. Hence, in the present work, we chose to investigate the possibility of improving the properties of 3Y-PSZ, reinforced with alumina platelets which are given an interface coating of LaPO₄. The α -alumina platelets synthesized by the combustion route are of nanometric thickness, have large aspect ratio and are single crystalline. The process of gelcasting free flowing slurries into 3D profile-cut EPS molds enables uniform distribution of second phases and provides an easy, scalable, and cost-effective method of shape forming ceramic components.

Our results on the 3Y-PSZ composites thus obtained show that addition of 5 to 15 wt% platelet alumina results in remarkable improvement in mechanical properties yielding high flexural strength (643 MPa) as well as fracture toughness (8.87 MPa \sqrt{m}) simultaneously.

Microstructures recorded in those composites showed no substantial porosity or cracking. FESEM images (Fig.5. 8) of polished specimen (thermally etched after indentation) provide clear evidence for arresting of crack propagation, deflection and bridging of the cracks, by the presence of platelets, shown typically in the composites with 10 and 15 wt% platelet alumina. The concept of crack bridging by platelets is also observed as one of the toughening mechanisms in these composites. The platelets form a bridge between two separated crack faces and creates an obstruction that slows down the crack propagation. The large surface of the platelets provides many crack-stopping sites and increases the amount of energy required for the material to fail. It also provides strong interface bonding, as suggested by the observed platelet pull-out.

Based on the XRD observations, it was found that 3Y-PSZ composites with and without platelet addition exhibit similar increase in the monoclinic phase by \sim 1% on stress application, indicating minimal contribution from transformation toughening to the observed enhanced fracture toughness.

The significant increase in the fracture toughness of the composites with optimal composition (3Y-PSZ with 5 to 15 wt% platelets), makes them potential candidates for use as dental implants and as components in high temperature aerospace and automobile applications. The possibility of casting the slurries of the above compositions into molds fabricated by rapid prototyping makes many niche applications accessible in medical and defence fields.

References:

[1] P.Y. Lee, T. Yano, Influence of alumina powder size on mechanical properties of in-situ coated alumina fiber-reinforced alumina composites, J Eur Ceram Soc. 24 (2004) 3359–3365. https://doi.org/10.1016/j.jeurceramsoc.2003.10.023.

- [2] D.B. Marshall, J.B. Davis, Fiber reinforced oxide composites, Cur Opi Sol Ste Mat Sci. 5 (2001) 283–289. https://doi.org/10.1016/S1359-0286(01)00017-1.
- [3] X.W. Yin, L.F. Cheng, L.T. Zhang, N. Travitzky, P. Greil, Fibre-reinforced multifunctional SiC matrix composite materials, Int Mat Rev. 62 (2017) 117–172. https://doi.org/10.1080/09506608.2016.1213939.
- [4] F.W. Zok, Developments in oxide fiber composites, J Ame Cera Soc. 89 (2006) 3309–3324. https://doi.org/10.1111/j.1551-2916.2006.01342.x.
- [5] C.G. Levi, J.Y. Yang, B.J. Dalgleish, F.W. Zok, A.G. Evans, Processing and Performance of an All-Oxide Ceramic Composite, J Ame Ceram Soc. 81 (1998) 2077–86. https://doi.org/10.1111/j.1151-2916.1998.tb02590.xsss
- [6] E. Mouchon, P. Colomban, Oxide ceramic matrix/oxide fibre woven fabric composites exhibiting dissipative fracture behaviour, Composites 26 (1995) 175-182. https://doi.org/10.1016/0010-4361(95)91380-N.
- [7] X. Luo, W. Zhou, S. V. Ushakov, A. Navrotsky and A. A. Demkov, Monocline to tetragonal transformations in hafnia and zirconia: A combined calorimetric and density functional study, Physical Review B 80 (2009) 134119-12. https://doi.org/10.1103/PhysRevB.80.134119.
- [8] J. Chevalier and L. Gremillard, The tetragonal-monoclinic transformation in zirconia: Lessons learned and future trends, Journal of the American Ceramic Society 92 (2009) 1901-1920. https://doi.org/10.1111/j.1551-2916.2009.03278.x.
- [9] Marek Bonieckia, Tomasz Sadowski, Przemysław Gołębiewski, Helena Węglarz, Anna Piątkowska, Magdalena Romaniec, Konrad Krzyżak, Kamil Łosiewicz, Mechanical properties of alumina/zirconia composites, Ceramics International. 46 (2020) 1033-1039. https://doi.org/10.1016/j.ceramint.2019.09.068.
- [10] Harushige Tsubakino and Ryoichi Nozato. Effect of Alumina Addition on the Tetragonal-to-Monoclinic Phase Transformation in Zirconia-3 mol% Yttria, J Am Cerum SOC. 74 (1991) 440-43. 10.1111/j.1151-2916.1991.tb06905.x
- [11] Rajasekharan T, Swaroop Raju PM, Pandey RK, Seshu Bai V, Pradyumna R, Baig MAH. Complex-shaped alumina products through rapid prototyping. Met Mat and Proc. 2007; 19:41–46.
- [12] P. Jeevankumar, P. Rose, A. Rajanikanth, T. Rajasekharan, V. Seshu Bai, Netshaping of advanced ceramic composites by gelcasting into precision molds made by rapid-prototyping, Int. J. Appl. Ceram. Technol. (2023) 1–11, https://doi.org/10.1111/ijac.14568.
- [13] P.Jeevankumar, Poly Rose, Pawan Kumar Verma , Seshu Bai Vummethala, Rajasekharan Thankappan Pillai, Fabrication of $Ba_{0.5}$ $Sr_{0.5}$ TiO_3 components combining rapid prototyping with gelcasting using different gelling systems; Open Ceramics 17 (2024) 100512.
- [14]. J.J. Kingsley And K.C. Patil, A Novel Combustion Process For The Synthesis Of Fine Particle A-Alumina And Related Oxide Materials; Materials Letters, Volume 6, Number I 1,12,1998.
- [15] J.B. Davis, D.B. Marshall, P.E.D. Morgan, Monazite-containing oxide/oxide composites; Journal of the European Ceramic Society 20 (2000) 583±587
- [16] Emad Mohamed M. Ewais, Rhoological properties of concentrated alumina slurries: influence of pH and dispersant agent, TESCE, Vol. 30, No.2,2004

- [17] Standard Test Method for Flexural Strength of Advanced Ceramics at Ambient Temperature. Available from: https://doi.org/10. 1520/C1161-13. Accessed 19 January 2014.
- [18] Standard Test Methods for Determination of Fracture Toughness of Advanced Ceramics at Ambient Temperature. Available from: https://doi.org/10.1520/C1421-10. Accessed 19 January 2014. [19] N.P. Bansal, D. Zhu, Thermal conductivity of zirconia-alumina composites, Ceram Int. 31 (2005) 911–916. https://doi.org/10.1016/j.ceramint.2004.09.018.
- [20] A.H. Pakseresht, S.M. Mousavi, M. Saremi, E. Ghasali, H. Rajaei, Microstructure and mechanical properties of YSZ-alumina composites designed for thermal barrier coatings, Materials at High Temperatures. 38 (2021) 23–30. https://doi.org/10.1080/09603409.2020.1837414.
- [21] R.H.L. Garcia, V. Ussui, N.B. de Lima, E.N.S. Muccillo, D.R.R. Lazar, Physical properties of alumina/yttria-stabilized zirconia composites with improved microstructure, J Alloys Compd. 486 (2009) 747–753. https://doi.org/10.1016/j.jallcom.2009.06.204.
- [22] J. Chłędowska, J. Wyrwa, M. Rękas, T. Brylewski, Effects of Aluminum Oxide Addition on Electrical and Mechanical Properties of 3 mol% Yttria-Stabilized Tetragonal Zirconia Electrolyte for IT-SOFCs, Materials. 15 (2022). https://doi.org/10.3390/ma15062101.
- [23] X. Li, X. Fan, N. Ni, X. Zhao, C. Li, P. Xiao, Continuous alumina fiber-reinforced yttria-stabilized zirconia composites with high density and toughness, J Eur Ceram Soc. 40 (2020) 1539–1548. https://doi.org/10.1016/j.jeurceramsoc.2019.12.041.
- [24] Swain MV, Rose LRF, Strength limitations of transformation-toughened zirconia alloys, J Am Ceram Soc. 1986;69:511–518.
- [25] Richard H. J. Hannink, Patrick M. Kelly, Barry C. Muddle, Transformation Toughening in Zirconia-Containing Ceramics, J. Am. Ceram. Soc., 83 (2000) 461–87. https://doi.org/10.1111/j.1151-2916.2000.tb01221.x.
- [26] F. Zhanga, K. Vanmeensel, M. Inokoshi, M. Batuk, J. Hadermann, B. Van Meerbeek, I. Naert, J. Vleugels, Critical influence of alumina content on the low temperature degradation of 2–3 mol% yttria-stabilized TZP for dental restorations, J Eur Ceram Soci.35 (2015) 741–750. http://dx.doi.org/10.1016/j.jeurceramsoc.2014.09.018.
- [27] A.A. Nogiwa-Valdez, W.M. Rainforth, P. Zeng, I.M. Ross, Deceleration of hydrothermal degradation of 3Y-TZP by alumina and lanthana co-doping, Acta Biomaterialia 9 (2013) 6226–6235. http://dx.doi.org/10.1016/j.actbio.2012.11.027.
- [28] M. Liu, J. Zhao, S. Shimai, J. Zhang, H. Chen, D. Han, J. Liu, S. Wang, A Polishing-Free Etching Method for Microstructure Observation of Fine-Grained Ceramics, J. Ceram. Sci. Technol. (2021) 12–13. https://doi.org/10.4416/JCST2020-00024.
- [29] S. Sequeira, M.H. Fernandes, N. Neves, M.M. Almeida, Development and characterization of zirconia–alumina composites for orthopedic implants, Ceram Int. 43 (2017) 693–703. https://doi.org/10.1016/j.ceramint.2016.09.216.

CHAPTER VI

Yttria stabilized zirconia (3Y-PSZ) composites with short carbon fibre reinforcement

Introduction

Reinforcing monolithic ceramics with continuous fibers is an efficient way to get composites with superior mechanical properties. The commonly used continuous fibers include carbon, alumina, and zirconia [1]. With the addition of unidirectional carbon fibre into zirconia composites, an improved fracture toughness of 15.4 MPa√m and flexural strength of 588.0 MPa were observed parallel to the fiber direction [2]. Even though continuous fiber is an effective method for reinforcement, it is difficult to make such composites in complex shapes, which limits its use in practical applications. On the other hand, it is interesting to explore the efficacy of short fibre reinforcement, which can be combined with the RPGC process to make complex shapes of composites with improved mechanical properties.

6.1 Fabrication

This study focuses on the fabrication of YSZ composites reinforced with short carbon fibres. We have used the RPGC process [3 - 5], which involves fabricating suitable mold which is a replica of the actual product desired, and setting a concentrated slurry of the required ceramic powders in the mold. This process allows complex shapes to be fabricated with a uniform dispersion of any second phase added [6]. We have chosen short carbon fibres as reinforcement in this work for improving mechanical properties. Weak interfaces were generated between the fibre and the 3Y-PSZ matrix by coating second phases by sol-gel techniques [7], so as to allow fibre pullout to enhance fracture toughness [8-10]. The sintered products were evaluated by measuring density, microstructure and mechanical properties. The current process of fabrication is generic and allows uniform dispersion of various second-phase particles to complex-shaped parts, to suit a chosen application.

6.1.1. Monazite (LaPO₄) coating on short carbon fibre

To create 0.1 molar concentration solutions of La(NO₃)₃ and H₃PO₄, dissolve 3.24 g of La(NO₃)₃ and 0.98 g of 85% phosphoric acid (H₃PO₄) in 100 ml of distilled water in separate beakers at room temperature. After dissolving, ensure a 1:1 molar ratio of La to P. Stir the solutions and heat to 60°C to speed up the reaction. Finally, obtain a white-colored wet gel.

$$La(NO_3)_3 + H_3PO_4 = LaPO_4 + 3HNO_3$$

Once the gel has formed, add the pre-prepared short carbon (diameter 6 µm) fibers (figure 6.1 shows the short carbon fiber) and mix for 2 hours. Repeat the coating process three times to obtain uniform

coating and allow for drying. To ensure the monazite coating, heated in an argon atmosphere at 800 °C for 2 hours to ensure adherence of the coating on them. Figure 6.2 a shows the short carbon fiber without coating and figure 6.2 (b & c) show LaPO₄ coated short carbon fiber used as reinforcement.



Fig.6. 1. Short carbon fibre

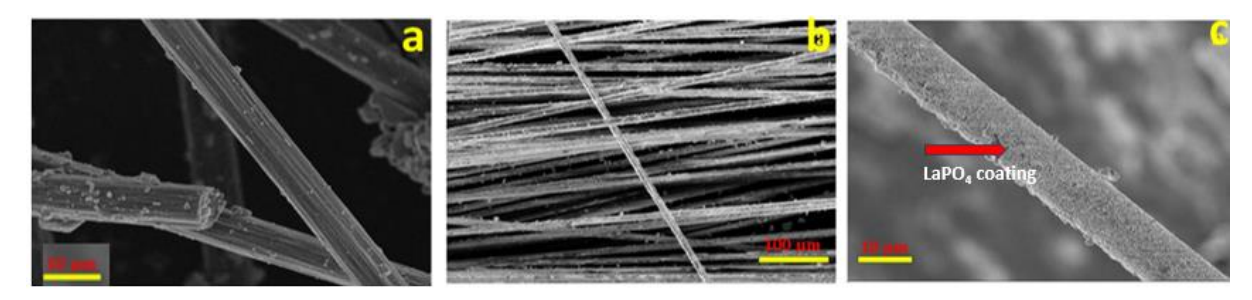


Fig.6. 2. (a) Carbon fibre diameter of 6 µm and (b & c) Carbon fibre coated with LaPO₄

6.1.2. Second phase addition and prepare the composite's suspensions

To attain a free-flowing suspension with a solid loading ranging from 50 vol% the required quantity of PSZ powder (or a powder mix containing reinforcement of short fiber) is calculated and added into a measured amount of an organic premix solution. This solution is prepared by dissolving the monomer (MAM) and cross-linker (MBAM) in deionized water (deionized water: MAM: MBAM = 33:6:1, by weight), with the addition of Darvan - CN used as a dispersant (1–2 wt% based on solid loading) [11]. The resulting ceramic slurry undergoes a 24-hour tumbling process at 15 rpm, utilizing zirconia balls as mixing media to achieve uniformity. Subsequently, the slurry is de-aired in a vacuum desiccator to eliminate any trapped air before the casting process.

In the RPGC process, a suitable mold material is chosen which does not interact with the slurry of the ceramic material. A Computer-Aided Design (CAD) file generates the negative of the final shape required, to be printed by Additive manufacturing. The mold is printed layer by layer by additive or subtractive manufacturing depending on the mold material. For the former, we used ABS plastic and for the latter, we used Expanded Polystyrene (EPS) [4,5]. Both materials can be dissolved off in acetone after the slurry has been set in the mold.

Slurry of YSZ containing 5 wt% amount of carbon fibres were prepared and optimised viscosity (<1 Pa.s) for casting. Then cast into EPS mold and allowed to set in the mold by polymerisation. The mold

was then removed without damaging the green body. It was then dried in a controlled fashion, debindered at about 900 °C and then sintered. The parts were sintered at 1550°C for 3hrs in argon atmosphere. Test specimens were cut out of the samples and were characterized as follows. Figure 6.3(a) shows, an EPS mold of rectangular cross section and figure 6.3(b) shows the fabricated 3Y-PSZ - carbon fibre composite after pre-sintering.





Fig. 6.3(a). Expanded polystyrene (EPS) mold of rectangular cross section and (b) short carbon fiber reinforced 3Y–PSZ composite.

6.1.4 Mechanical properties, microstructural and fractography analysis of composites

Reasonable values of flexural strength (σ) and fracture toughness (K_{Ic}) are essential for a ceramic material to find many applications. We determined the flexural strength using a 3-point bend test on a specimen cut to $3.0 \times 4.0 \times 45.0$ mm dimensions, as per ASTM C1161–13 [12] standard and fracture toughness was measured by the direct crack method as per ASTM C1421–10 standard [13] as discussed in section 2.8 in chapter 2.

3Y- PSZ composite with 5 wt% short carbon fiber addition, after sintering at 1550°C for 3 h in argon atmosphere had shown considerably high flexural strength and fracture toughness which are \sim 431 MPa and \sim 9.1 MPa \sqrt{m} , respectively.

These purpose of LaPO₄ coating on carbon fibers is to lead to weak interfaces between the fiber and the YSZ (Yttria-Stabilized Zirconia) matrix that can debond easily absorbing energy and suppressing crack propagation. The weak interaction results in fiber pullout under stress applications and plays a critical factor in improving fracture toughness. The YSZ composite's fracture toughness and flexural strength are measured to be 9.1 MPa√m and 431 MPa, respectively. These properties indicate the material's ability to resist crack propagation and tolerate bending stresses, indicating its potential for use in challenging environments that require superior mechanical performance.

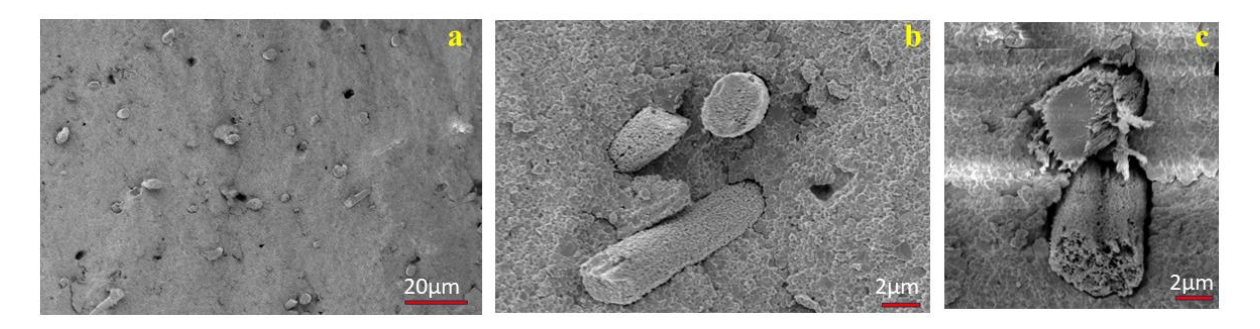


Fig. 6.4. (a, b & c) show microstructures of cracked beam and carbon fibre pull out.

The fractured surfaces were systematically studied at the microscopic level. The primary toughening mechanism for enhancing toughness in ceramic matrix composites is the feature of fiber pullout, which is evidenced in the microstructures shown in Figure 6.4. When stress initiates the crack propagation process, the fibers separate from the matrix and slide out, requiring additional energy. Thus, fiber pullout mechanism contributes to fracture toughness by absorbing energy and restricting the propagation of cracks.

Summary

The successful net-shaping of 3Y-PSZ composites with short carbon fibers has been demonstrated by combining Rapid Prototyping Technology with Gelcasting (RPGC) process. This process with reinforcements allowed fabrication of complex-shaped ceramic composites with highly enhanced properties. Weak interfaces between the fiber and the YSZ matrix were created by LaPO₄ coating on the carbon fiber. From microstructures, fiber pullout was observed, which is known to cause enhancement in fracture toughness. The YSZ composite with 5 wt% short carbon fiber exhibited a fracture toughness of 9.1 MPa√m and a flexural strength of 431 MPa. The present approach is economical and reproducible, and it can be extended to fabricate different complex shapes of composite systems.

References:

- [1] Xuewu Li, Xiaohui Fan, Na Ni, Xiaofeng Zhao, Chuanwei Li, Ping Xiao, Continuous alumina fiber-reinforced yttria-stabilized zirconia composites with high density and toughness, Journal of the European Ceramic Society. https://doi.org/10.1016/j.jeurceramsoc.2019.12.041.
- [2] G.H. Zhou, S.W. Wang, J.K. Guo, Z. Zhang, The preparation and mechanical properties of the unidirectional carbon fiber reinforced zirconia composite, Journal of the European Ceramic Society. https://doi.org/10.1016/j.jeurceramsoc.2007.07.005.
- [3] Rajasekharan T, Swaroop Raju PM, Pandey RK, Seshu Bai V, Pradyumna R, Baig MAH. Complex-shaped alumina products through rapid prototyping. Met Mat and Proc. 2007; 19:41–46.

- [4] P. Jeevankumar, P. Rose, A. Rajanikanth, T. Rajasekharan, V. Seshu Bai, Netshaping of advanced ceramic composites by gelcasting into precision molds made by rapid-prototyping, Int. J. Appl. Ceram. Technol. (2023) 1–11, https://doi.org/10.1111/ijac.14568.
- [5] P.Jeevankumar, Poly Rose, Pawan Kumar Verma, Seshu Bai Vummethala, Rajasekharan Thankappan Pillai, Fabrication of Ba_{0.5} Sr_{0.5} TiO₃ components combining rapid prototyping with gelcasting using different gelling systems; Open Ceramics 17 (2024) 100512.
- [6] A. Herzog, G. Woetting, U.F. Vog, Short-fibre-reinforced reaction-bonded silicon nitride (RBSN) by precursor route: Processing and properties. Journal of the European Ceramic Society 27 (2007) 3561–3572.
- [7] K.K. Chawlaa, H. Liub, J. Janczak-Ruschc, S. Sambasivand, Microstructure and properties of monazite (LaPO4) coated saphikon ®ber/alumina matrix composites. Journal of the European Ceramic Society 20 (2000) 551-559.
- [8] D.T. Di Salvoa, E.E. Sackett a, R.E. Johnstona, D. Thompsonb, P. Andrews c, M.R. Bachea, Mechanical characterisation of a fibre reinforced oxide/oxide ceramic matrix composite. Journal of the European Ceramic Society 35 (2015) 4513–4520.
- [9] X. Li, X. Fan, N. Ni, X. Zhao, C. Li, P. Xiao, Continuous alumina fiber-reinforced yttria-stabilized zirconia composites with high density and toughness, J Eur Ceram Soc. 40 (2020) 1539–1548.
- [10] J.B. Davis, D.B. Marshall, P.E.D. Morgan, Monazite-containing oxide/oxide composites, J Eur Ceram Soci.5(2000) 583-586, https://doi.org/10.1016/S0955-2219(99)00256-3
- [11] Janney MA, Omatete OO, Walls CA, Nunn SD, Ogle RJ, Westmoreland G. Development of low-toxicity gelcasting sys tems. J AmCeramSoc. 1998;81:581–9.
- [12] Standard Test Method for Flexural Strength of Advanced Ceramics at Ambient Temperature. Available from: https://doi.org/10. 1520/C1161-13. Accessed 19 January 2014.
- [13] Standard Test Methods for Determination of Fracture Toughness of Advanced Ceramics at Ambient Temperature. Available from: https://doi.org/10.1520/C1421-10. Accessed 19 January 2014.

CHAPTER VII

Summary and conclusions

Ceramics find applications in several areas because of their high strength, hardness, resistance to oxidation at high temperature, resistance to corrosion, low density, chemical stability, erosion resistance and relatively of low cost [1]. However, advancements in ceramic technology require to address two broad technical aspects, namely, selecting suitable reinforcements for a given system and develop innovative and inexpensive methods for shape forming it into compacts.

Because of their high melting pointing and difficulty in machining ceramics into final components, fabricating them into required shapes is an involved process. The conventional method of shaping ceramics using colloidal processing techniques into molds is widely recognized [2]. These methods include die-casting, slip-casting, and injection molding, each have their own advantages and disadvantages, which are discussed in detail in Chapter1.

With regard to oxide ceramics, like alumina and zirconia, improvements in their prospective applications require i) identification of suitable reinforcements that would enhance their mechanical properties, ii) extending their capability for operation to high temperatures, iii) development of methods to distribute second phases uniformly without agglomeration in the matrix, for homogeneity of the properties across the dimensions of the product, iv) adapting modern techniques to net shape the components of the composites reproducibly at low cost, using bio-compatible organics, avoiding toxic chemicals.

The present thesis addresses the above issues by employing RPGC process [3] that combines the rapid prototyping and geleasting techniques to fabricate complex shaped ceramic components. Products of complex shapes were fabricated from free-flowing alumina slurry cast into 3D printed ABS molds by additive manufacturing and 3D profile cut expanded polystyrene (EPS) molds by subtractive manufacturing. The EPS and thin-walled molds make the demolding process quick avoiding unwanted interaction of green body with mold removal solvents. EPS mold has added advantage of low cost and fast fabrication. The final products were of density close to 99% [4].

Monolithic ceramics

Initially the process was developed and optimized to consolidate various monolithic ceramics like alumina, barium strontium titanate (BSTO) and zirconia partially stabilized with 3 wt% yttria. The products were characterized with regard to their density, microstructure and mechanical properties. By using RPGC process, mechanical properties of final components of alumina exhibited flexural strength of 388MPa and fracture toughness of 3 MPa√m. From figure 7.1 shows the various complex geometries of alumina ceramics fabricated by RPGC process.



Fig. 7.1. Various alumina components fabricated by RPGC process.

Traditional geleasting system uses toxic acrylamide-based organics as binders which is demerit of the process [5]. As an alternative isobam and methyl cellulose as binders makes the process environmentally friendly. BSTO ceramic shapes were fabricated using three gelling agents such as AM, IB and MC and compared the results. The different shapes of BSTO components prepared by RPGC process were shown in Fig.3.14 of chapter 3 [6].

The products fabricated by the non-toxic gelling systems are pore-free and have comparable microstructures and dielectric behaviour as those fabricated by the methacrylamide-based gelling system. Gelcasting has a potential to move closer to realizing industrial applications with RPGC process, owing to the non-toxic gelling agents.

Monolithic ceramics are prone to brittle fracture at high stress levels and limited fracture toughness limits its use in practical applications. Low thermal shock resistance is also a drawback. This can be overcome by reinforcing ceramic with second phases such as particulates, platelets, whiskers, short and long fibres [7]. Though fiber reinforced ceramic matrix composites have high fracture toughness of 15.93 MPa √m; its flexural strength reported is low and is < 300 MPa [8]; and it is difficult to process them to attain complex shapes. Moreover, alumina fibers undergo structural phase transformation above 1150 °C, rendering them unsuitable for applications at higher temperatures.

The CMC systems taken up for the present study are composites of i) alumina and ii) zirconia choosing single crystalline α -alumina platelets of nanometric thickness as a reinforcement. The α -alumina platelets have an advantage that they are structurally stable at high temperatures. The platelets were fabricated by combustion synthesis and were coated with monazite (LaPO₄) to provide weak interface between the platelets used as reinforcement and the matrix. The coating is stable to 1600 °C. To

distribute the chosen second phase uniformly into the matrix. Solcasting method [9] was used where the reinforcements were distributed and polymerized in the matrix phase. Subsequent heat treatments remove the organics and result in a composite.

Composites of Alumina

Compacts of alumina composites of different concentrations of α-alumina platelets, ranging from 0, 1, 2, 3, 4, 5, 15, and 25 wt% were added to the alumina matrix (using solcasting method) were fabricated by RPGC process and the resultant composites were characterized.

To assess the fracture toughness (K_{IC}) of the two-phase composites, direct crack method was used as per ASTM C1421–10 standard, by making a pb notch, rather than estimating K_{IC} from hardness measurements. Composites obtained with 3 to 4 wt% platelet alumina exhibited a flexural strength of 310 MPa and fracture toughness of 5.4 MPa \sqrt{m} . Remarkable improvement in K_{IC} by about 80 %, with substantial flexural strength project these composites for various potential applications. Microstructural studies revealed that crack deflection, crack bridging contributed to toughening mechanisms. The density and mechanical properties of alumina-alumina platelet composites are summarized in table 7.1.

Table 1: Density and mechanical properties of alumina- α alumina platelet composites.

S.no:	Matrix	Reinforcement:	Sintering	Relative	Hardness	Flexrual	Fracture
	phase:	α- alumina	temp.(°C)	Density	(GPa)	strength	toughness
	Alumina	platelets with	@ 2 hr	(%)		(MPa)	(MPa.√m)
		LaPO ₄ coating					
1	Al ₂ O ₃	No addition	1675	98.5	22.5	389	3.01
2	Al ₂ O ₃	1 wt%	1675	96.5	19.5	348	3.82
3	Al ₂ O ₃	2 wt%	1675	95.6	18.3	304	3.97
4	Al ₂ O ₃	3 wt%	1675	95.8	18	300	4.74
5	Al ₂ O ₃	4 wt%	1675	96	18.1	305	5.38
6	Al ₂ O ₃	5 wt%	1675	95.6	17.4	302	4.1
7	Al ₂ O ₃	15 wt%	1675	94.5	12.3	278	3.0
8	Al ₂ O ₃	25 wt%	1675	94	11.5	254	3.02

Composites of Zirconia (3Y-PSZ)

Composites of zirconia reinforced with LaPO₄ coated α- alumina platelets were introduced into zirconia, partially stabilized with 3 mol% yttria, (3Y-PSZ) matrix. Using RPGC process, 3Y-PSZ composites with the addition of 0 to 25 wt% platelet alumina as reinforcement were fabricated and characterized. Notable enhancement in the mechanical properties was observed for composites with 5 to 15 wt% platelet content, recording flexural strength of 643 MPa) and fracture toughness of 8.87 MPa√m, simultaneously. From the microstructures recorded in the composites, evidenced arresting of

crack propagation, deflection and bridging by platelet presence in the matrix. The density and mechanical properties of 3Y-PSZ compotes with α alumina platelet reinforcement are summarized in table 7.2.

Since PSZ is known to have a contribution from structural transformation to toughening, detailed XRD analysis was carried out to estimate the percentage rise in monoclinic phase on stress application and its contribution to K_{IC} . Based on the XRD analysis, it was found that 3Y - PSZ composites exhibit similar increase in the monoclinic phase by only $\sim 1\%$, with and without platelet addition, on stress application. The observations indicate the contribution from transformation toughening to the observed enhanced fracture toughness to be minimal and that the significant enhancement in K_{IC} arises from platelet reinforcements.

Table 7.2 Shows the mechanical properties of alumina-zirconia composites.

S.no:	Matrix	Reinforcement:	Sintering	Relative	Hardness	Flexrual	Fracture
	phase:	α- alumina	temp.(°C)	Density	(GPa)	strength	toughness
	3Y	platelets with	@ 3 hr	(%)		(MPa)	(MPa.√m)
	PSZ	LaPO ₄ coating					
1	PSZ	No addition	1550	99.0	12.3	1029	4.97
2	PSZ	1 wt%	1550	97.6	11.2	625	5.37
3	PSZ	5 wt%	1550	95.0	8.4	581	8.43
4	PSZ	10 wt%	1550	94.3	8.0	609	8.76
5	PSZ	15 wt%	1550	93.6	8.5	643	8.87
6	PSZ	25 wt%	1550	85.2	5.4	333	7.18

Considering the disadvantage of continuous fibre reinforced composites in their inability to be made it into complex shapes, the present work explored the possibility of fabricating 3Y-PSZ

composites with short carbon fibres coated with monazite as reinforcements. 3Y-PSZ composites reinforced with coated short carbon fibre showed considerably improved K_{IC} compared to 3Y-PSZ with no addition. Weak interfaces generated between the fiber and the 3Y-PSZ matrix by coating is found to allow fiber pullout to occur on stress, causing enhanced fracture toughness. 3Y- PSZ composite fabricated with 5 wt% short carbon fiber using RPGC process had a relative density of ~97% and flexural strength of 431 MPa and fracture toughness of 9.1 MPa√m. This result is interesting because components of monolithic 3Y-PSZ ceramic with short fibres with superior properties can be shaped into complex geometries by RPGC process, to suit chosen applications. The process also enables uniform distribution of second phases and provides an easy, scalable, and cost-effective method of shape forming ceramic composites.

Advantage of the current process is the ability to modify molds to address shrinkage during debindering and sintering. Using slurry-based processes, this technique is versatile, easily replicable, inexpensive, and adaptable to fabricate intricately shaped components from ceramic and metal powders. The RPGC method is aptly suited for the net-shaping of large and complex-shaped components.

The process advancements made in this work in mold fabrication, and the ceramic composites of optimum compositions identified open up the scope for designing and fabricating high-value components for medical, automotive, and aerospace applications.

References:

- 1. <u>Davis, Karen</u>, Material Review: Alumina (Al₂O₃). International Journal of Advance Research and Innovative Ideas in Education. 2010; 2: 109-114.
- 2. Jurgen Stampfl J, Liu H-C, Woo Nam S, Sakamoto K, Tsuru H, Kang S, et al. Rapid prototyping and manufacturing by gelcasting of metallic and ceramic slurries. Mat Sci Eng. 2002; 334:187–92.
- 3. Rajasekharan T, Swaroop Raju PM, Pandey RK, Seshu Bai V, Pradyumna R, Baig MAH. Complex-shaped alumina products through rapid prototyping. Met Mat and Proc. 2007; 19:41–46.
- 4. P. Jeevankumar, P. Rose, A. Rajanikanth, T. Rajasekharan, V. Seshu Bai, Net-shaping of advanced ceramic composites by gelcasting into precision molds made by rapid-prototyping, Int. J. Appl. Ceram. Technol. Int J Appl Ceram Technol.2024;21:664–674.
- 5. M.A. Janney, O.O. Omatete, C.A. Walls, S.D. Nunn, R.J. Ogle, G. Westmoreland, Development of low-toxicity gelcasting systems, J. Am. Ceram. Soc. 1998; 81: 581–591.
- 6. P. Jeevankumar, Poly Rose, Pawan Kumar Verma, Seshu Bai Vummethala, Rajasekharan Thankappan Pillai, Fabrication of Ba_{0.5} Sr_{0.5} TiO₃ components combining rapid prototyping with gelcasting using different gelling systems; Open Ceramics 17 (2024) 100512.
- 7. I. W. DONALD, P. W. McMI LLAN, Review Ceramic-matrix composites. J. Mate. Sci. 1976;11: 949-972.
- 8. Xuewu Lia, Xiaohui Fana, *, Na Nib,c, *, Xiaofeng Zhaoa, Chuanwei Lid, Ping Xiao, Continuous alumina fiber-reinforced yttria-stabilized zirconia composites with high density and toughness. J. Euro Ceram Soci. 2020;40: 1539-1548
- 9. P. Missak Swarup Raju , V. Seshubai , T. Rajasekharan , A generic process to introduce nanoparticles into powder preforms and its application to Infiltration Growth processing of REBa2Cu3O7 superconductor. Materials Chemistry and Physics 161 (2015) 59-64.

Titles of Patents applied:

- 1. A Method for Fabricating a Component with Complex Geometry.
- 2. A Method Preparing Ceramic Components Comprising Alpha Alumina Platelets.

Publications in Journals and Presentations at Conferences

- 1. **P. Jeevankumar**, Poly Rose, Rajanikanth A, Rajasekharan T, V.Seshu Bai Net-shaping of advanced ceramic composites bygelcasting into precision molds made by rapid-prototyping. Int J Appl Ceram Technol.2024;21:664–74.https ACerS. https://doi.org/10.1111/ijac.14568. (Editor's Choice The Editor-in-Chief recommends this outstanding article.)
- 2. **P. Jeevankumar**, Poly Rose, Pawan kumar Verma, V. Seshu Bai. Rajashekharan. T, Fabrication of Ba0.5Sr0.5TiO3 components combining rapid prototyping with gelcasting using different gelling systems, Open Ceramics 17 (2024) ECerS. https://doi.org/10.1016/j.oceram.2023.100512.
- 3. Poly Rose, **P. Jeevan Kumar** and V. Seshu Bai* Properties of porous Magnesia-stabilized zirconia ceramics fabricated by slurry infiltration into polyurethane foam, International Journal of Applied Ceramic Technology, ACerS, 2024 (under review)
- 4.**P. Jeevankumar**, Polyrose, T. Rajasekharan, I. Srikanth, V. Seshu Bai 1"Fabrication of carbon fibre reinforced YSZ composites by gelcasting into expendable moulds fabricated by rapid prototyping" Indian Conference on Carbon Materials (ICCM-2023) during 30th November to 2nd December, 2023 at DAE convention Centre, BARC, INDIA
- 5. **P. Jeevankumar**, Pawankumar Verma, Polyrose, Rajasekharan T, Seshu Bai. V, "BSTO components using Rapid prototyping and different Gelcasting systems" The XVIIIth Conference of the European Ceramic Society, 2nd -6th July 2023,Lyon, FRANCE.
- 6. **P. Jeevankumar**, Pawankumar Verma, Polyrose, Rajasekharan T, Seshu Bai. V, "Shape forming alumina composites using EPS moulds" FRONTIERS IN PHYSICS 2023, School of Physics, University of Hydebad, 3rd-4th March,2023,INDIA.
- 7. P. Jeevan Kumar, Pawan Kumar Verma, Poly Rose, T. Rajasekharan, V. Seshu Bai, 1-3 dielectric composites using rapid prototyping technique, 83rd Annual Technical Session of the Indian Ceramic Society scheduled NIIST, Thiruvananthapuram during December 11th-12th, 2019, INDIA.

Awards:

- 1.Best Poster Award sponsored by American Chemical Society at the Indian Conference on Carbon Materials, held at BARC-2023, Title of the paper "Fabrication of carbon fibre reinforced YSZ composites by gelcasting into expendable moulds fabricated by rapid prototyping".
- 2.European Ceramic Society (ECerS) YCN representative for Indian Ceramic Society (InCerS) for the period of January 2024 August 2025.
- 3. Selected for the JECS Trust Summer School travel grant at INSA Lyon, France.

Process innovations for netshaping of oxide ceramic composites and property enhancement by reinforcements

by Jeevan Kumar

Submission date: 27-May-2024 11:53AM (UTC+0530)

Submission ID: 2389040618

File name: Jeevankumar_Thesis-1.pdf (9.29M)

Word count: 34264

Character count: 191700

Process innovations for net-shaping of oxide ceramic composites and property enhancement by reinforcements

ORIGINALITY REPORT

INTERNET SOURCES

STUDENT PAPERS

PRIMARY SOURCES

Pallagani Jeevan Kumar, Poly Rose, Pawan Kumar Verma, Seshu Bai Vummethala, Rajasekharan Thankappan Pillai. "Fabrication of Ba0.5Sr0.5TiO3 components combining rapid prototyping with gelcasting using School of Physics different gelling systems", Open Ceramics University of Hyderabad 2023

Publication

Pallagani Jeevankumar, Poly Rose, Pawan Kumar Verma, Seshu Bai Vummethala, Rajasekharan Thankappan Pillai, "Fabrication of Ba0.5Sr0.5TiO3 components combining different gelling systems", Open Ceramics, University of Hyderabad

Publication

Tassilo Moritz, Saeed Maleksaeedi. "Additive 3 manufacturing of ceramic components", Elsevier BV, 2018

Publication

Prof. V. Seshu Bai School of Physics



UNIVERSITY OF HYDERABAD

CENTRAL UNIVERSITY P.O. GACHIBOWLI, HYDERABAD – 500 046

Plagiarism-free statement

This is to certify that the thesis entitled "Process innovations for net-shaping of oxide ceramic composites and property enhancement by reinforcements" authored by Jeevankumar Pallagani has been screened by the Turnitin software at the Indira Gandhi Memorial Library of the University of Hyderabad. The software shows 18% similarity index, out of which 9% came from candidate's own two research articles related to this thesis, which are already published and available online. The effective similarity index excluding his research articles is 18% -9% = 9%, which is in accordance with university guidelines. Hence the thesis is free from plagiarism.

V. Seshie Bai

V. Seshu Bai

Date 27th May 2024u Bai School of Physics University of Hyderabad

Phone: 9440176443, E-mail: seshubai@uohyd.ac.in, seshubai@gmail.com